ABSTRACT

ZHANG, LIWEN. Aligned Carbon Nanotubes for High-Performance Films and Composites. (Under the direction of Professor Yuntian Zhu).

Carbon nanotubes (CNTs) with extraordinary properties and thus many potential applications have been predicted to be the best reinforcements for the next-generation multifunctional composite materials. Difficulties exist in transferring the most use of the unprecedented properties of individual CNTs to macroscopic forms of CNT assemblies. Therefore, this thesis focuses on two main goals: 1) discussing the issues that influence the performance of bulk CNT products, and 2) fabricating high-performance dry CNT films and composite films with an understanding of the fundamental structure-property relationship in these materials.

Dry CNT films were fabricated by a winding process using CNT arrays with heights of 230 μm, 300 μm and 360 μm. The structures of the as-produced films, as well as their mechanical and electrical properties were examined in order to find out the effects of different CNT lengths. It was found that the shorter CNTs synthesized by shorter time in the CVD furnace exhibited less structural defects and amorphous carbon, resulting in more compact packing and better nanotube alignment when made into dry films, thus, having better mechanical and electrical performance.

A novel microcombing approach was developed to mitigate the CNT waviness and alignment in the dry films, and ultrahigh mechanical properties and exceptional electrical performance were obtained. This method utilized a pair of sharp surgical blades with microsized features at the blade edges as micro-combs to, for the first time, disentangle and straighten the wavy CNTs in the dry-drawn CNT sheet at single-layer level. The as-combed CNT sheet exhibited high level of nanotube alignment and straightness, reduced structural

defects, and enhanced nanotube packing density. The dry CNT films produced by microcombing had a very high Young's modulus of 172 GPa, excellent tensile strength of 3.2 GPa, and unprecedented electrical conductivity of 1.8×10^5 S/m, which were records for CNT films or buckypapers. This novel technique could construct CNT films with reproducible properties, which also had the potential to be scale-up for industrial mass production.

Based on the microcombing approach, dispersion issue of the long, straight, and highly aligned CNTs was investigated by adding PVA matrix into the microcombed CNT sheets. It was found although microcombing promoted the formation of agglomerated strands of the long, straight, and aligned CNTs, this was not an adverse problem in impairing the composite performance. When matrix was added, those agglomerated strands were wrapped together which maintained a more stable and better contact between nanotubes than those in the dry films. The as-produced CNT/PVA composite films exhibit an electrical conductivity of 1.84×10^5 S/m, Young's modulus of 119 GPa, tensile strength of 2.9 GPa, and toughness of 52.4 J/cm^3, which represent improvements over those of uncombed samples by 300%, 100%, 120%, and 200%, respectively, demonstrating the effectiveness and reliability of microcombing in producing high-performance CNT/polymer composite films.

Aligned Carbon Nanotubes for High-Performance Films and Composites

by
Liwen Zhang

A dissertation submitted to the Graduate Faculty of
North Carolina State University
in partial fulfillment of the
requirements for the degree of
Doctor of Philosophy

Materials Science and Engineering

Raleigh, North Carolina

2017

APPROVED BY:

Yuntian Zhu Committee Chair Materials Science and Engineering	Ronald Scattergood Materials Science and Engineering
Philip Bradford Textile Engineering, Chemistry, and Science	Suveen Mathaudhu Mechanical Engineering University of California, Riverside

DEDICATION

To my dear family

who I love and be loved

who has been a rock of stability in my life

BIOGRAPHY

Liwen Zhang was born in Suzhou, China, November 1st, 1989. She lived with her family in that beautiful city for more than 18 years, where she attended elementary, middle, and high school. During the 18 years, Chinese economic reform made great progress, and China became more and more fertile and prosperous, also, more international. Liwen was exposed to different cultures, which broadened her horizon and mind.

2008 was a big year for China, when Sichuan had a great earthquake, we lost thousands of compatriots; and when Beijing held the 2008 Summer Olympic Games, millions of people were shocked by China. 2008 was also a big year for Liwen, when she was admitted by Donghua University in Shanghai, China, to learn Textile Engineering. She completed her B.S. program in fall 2011 and got a chance to go to North Carolina State University, USA, to continue her Master's degree in Textile Engineering. During her first year in North Carolina State University, she met Dr. Xin Wang in the Department of Materials Science and Engineering, who introduced her to Professor Yuntian Zhu and let her to work in the lab to make carbon nanotube yarns. That was the first time Liwen saw carbon nanotubes and worked with them. In fall 2012, she joined Professor Yuntian Zhu's group to take Ph.D. in Materials Science and Engineering, but continued the Master in Textile Engineering. In December 2012, she received Master of Science in Textile Engineering from North Carolina State University. Under the guidance of Professor Yuntian Zhu for the Ph.D. program, Liwen dedicated herself in producing high-performance carbon nanotube films and composites. She received her Ph.D. degree in Materials Science and Engineering from North Carolina State University in 2016.

ACKNOWLEDGMENTS

First and foremost, I am grateful to my advisor, Professor Yuntian Zhu, for the opportunity and financial support to work in his group and his patience and guidance along the way. I would also like to sincerely thank my committee members, Professor Philip Bradford, Professor Ronald Scattergood, and Professor Suveen Mathaudhu, for their invaluable advice and support in my research.

I would like to express my gratefulness to Dr. Xin Wang who led my way to scientific research and introduced me to Professor Yuntian Zhu.

I thank all of those who contributed to my research and allowed me to use their equipment: Dr. Qingwen Li (in China) and her students for providing drawable CNT arrays, Dr. Philip Bradford for use of the hot press and providing drawable CNT arrays, Dr. Yong Zhu and Mrs. Judy Elson for use of Raman, Dr. Jon-Paul Maria for use of X-ray diffaraction equipment, Dr. Ching-Chang Chung and Xiaoyu Kang for their help in the X-ray diffraction analysis, Dr. Birgit Anderson for her help in the Thermogravimetric Analysis, Dr. Weizong Xu and Xiaolong Ma for their help in use of Transmission Electron Microscope.

I would also like to express my great appreciation to my group mates: Xin Wang, Chris Page, Varun Thiagarajan, Weiwei Jian, Weizong Xu, Orm Piyawit, Zhou Zhou, Fan Wu, Jordan Moreing, Xiaolong Ma, Haotian Deng, David Ho, Dan Song, Xiaotian Fang, Silu Liu, and Yingying Yu. It is wonderful to work with them. And without their help, I could not accomplish this.

Last but not least, I would like to thank my fiancé, Julin, for his accompany from China to the United States and his academic support; thanks to my family, they are my harbor ever.

TABLE OF CONTENTS

LIST OF TABLES

LIST OF FIGURES

Chapter 1

Thesis Introduction

Carbon nanotubes (CNTs) have emerged as new materials with amazing theoretical mechanical, thermal, electrical, chemical, and optical properties, opening a lot of interesting ways of operation in different scientific and technological fields. The remarkable properties of CNTs come from their special structures: strong σ and π bonds in the sp^2 hybrid orbital of carbon atoms; seamless graphitic tube structures; exceptionally high length-to-diameter ratios; and polymer-like low density. The final goal in carbon nanotube research is to find a way for their integration inside existing technologies, in order to fully exploit their tremendous characteristics. A crucial step involves transforming the nano-sized materials into macro-sized products, which can enormously help for the development of widely diffused practical applications. Based on literatures, it has been found the system requirements for obtaining the maximum value of CNT products are: long nanotubes perfectly aligned in one direction with a high degree of nanotube straightness; and when composite are to make, additional requirements are: high CNT fraction, good dispersion, and good interfacial stress transfer. However, it has been a challenge to produce CNT assemblies that meet all the requirements. The objectives of this work are to discuss the issues that render high-performance dry CNT films and CNT composite materials, and develop an innovative solution to meet all the requirements simultaneously.

Firstly, Chapter 2 generally reviews the structures, properties, and applications of CNTs, and discusses the methods of growing CNTs and fabricating CNT products in the literature.

Chapter 3 introduces the common experimental procedures used in this dissertation. In Chapter 4, the length effects of carbon nanotubes on the structure and properties of aligned dry CNT films are investigated. Chapter 5 proposed a microcombing method to effectively enhance the CNT alignment and reduce the CNT waviness in the dry-drawn CNT sheet to fabricate dry CNT films with unprecedented mechanical and electrical properties. Chapter 6 discusses the dispersion issue of long, highly aligned, and straight nanotubes when aligned CNT/polymer composite films are produced by microcombing method. Chapter 7 summarizes the outcomes of the research in this work and discusses the work can be done in the future.

Chapter 2

Literature Review

2.1 Carbon Nanotube Structures

Carbon nanotubes (CNTs) are allotropes of carbon. Rather than the 2-dimensional (2D) planar atom structure of graphite and the 3-dimensional (3D) tetrahedral atom structure of diamond, CNT has a 1-dimensional (1D) hollowed cylindrical structure formed by carbon atoms. The discovery of CNTs has an arguably long history. It was speculated that the first hollow carbon filament was possibly synthesized as early as 1889 in Thomas Alva Edison's era when a light bulb filament was searched for incandescent lamps based on the experimental method and conditions, [1,2]. Their well-known discovery was in 1991, Sumio Iijima got clear transmission electron microscopy (TEM) images and completed the tube structure analysis [3]. From then on, CNTs have attracted tens of thousands of research studies.

The carbon atom has three possible hybridizations: sp^1, sp^2, and sp^3. And different hybridization options lead to different structural arrangements of carbon atoms, forming different materials. CNTs are sheets of graphite that has been rolled into a seamless tube with open ends or capped with a hemisphere of fullerene structure [4,5]. The carbon atoms in CNTs are essentially sp^2 hybridized and bonded trigonally as in graphite. Three outer-shell electrons of each carbon atom occupy the planar sp^2 hybrid orbital to form three in-plane σ bonds, and the other outer-shell electron in the p orbital forms an out-of-plane π bond. This makes a planar hexagonal network, which is very strong. However, different from graphite,

the circular curvature of the CNT causes quantum confinement and σ-π rehybridization in which three σ bonds are slightly out of plane; for compensation, the π orbital is more delocalized outside the tube [6], as shown in Figure 2.1. This makes CNTs mechanically stronger, electrically and thermally more conductive, and chemically and biologically more active than graphite. In addition, they allow topological defects, such as pentagons and heptagons, to be incorporated into the hexagonal network to form capped, bent, toroidal, and helical nanotubes, whereas electrons will be localized in pentagons and heptagons because of redistribution of π electrons.

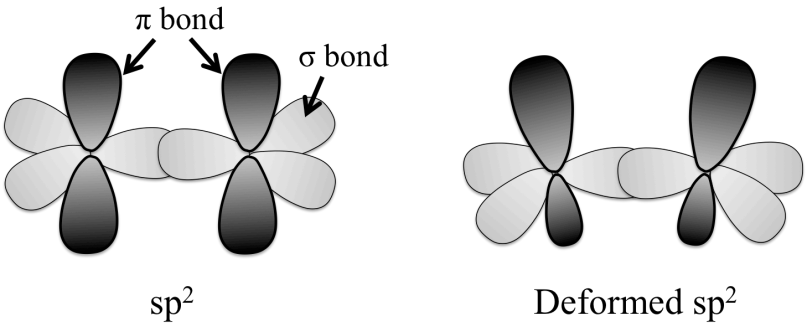

Figure 2.1 Schematic of sp^2 hybridization in graphite and the deformed sp^2 hybridization in CNT structure (drew based on ref.[6]).

Depending on the number of layers of rolled coaxial graphite sheets, CNTs can typically be classified as single-walled carbon nanotubes (SWNTs) and multi-walled carbon nanotubes (MWNTs). MWNTs can be further classified as double-walled (DWNTs), triple-walled (TWNTs), or few-walled carbon nanotubes (FWNTs). The structure of an SWNT can be conceptualized by wrapping a one-atom-thick layer of graphite called graphene into a seamless cylinder [4]. The way the graphene sheet is wrapped is represented by a pair of

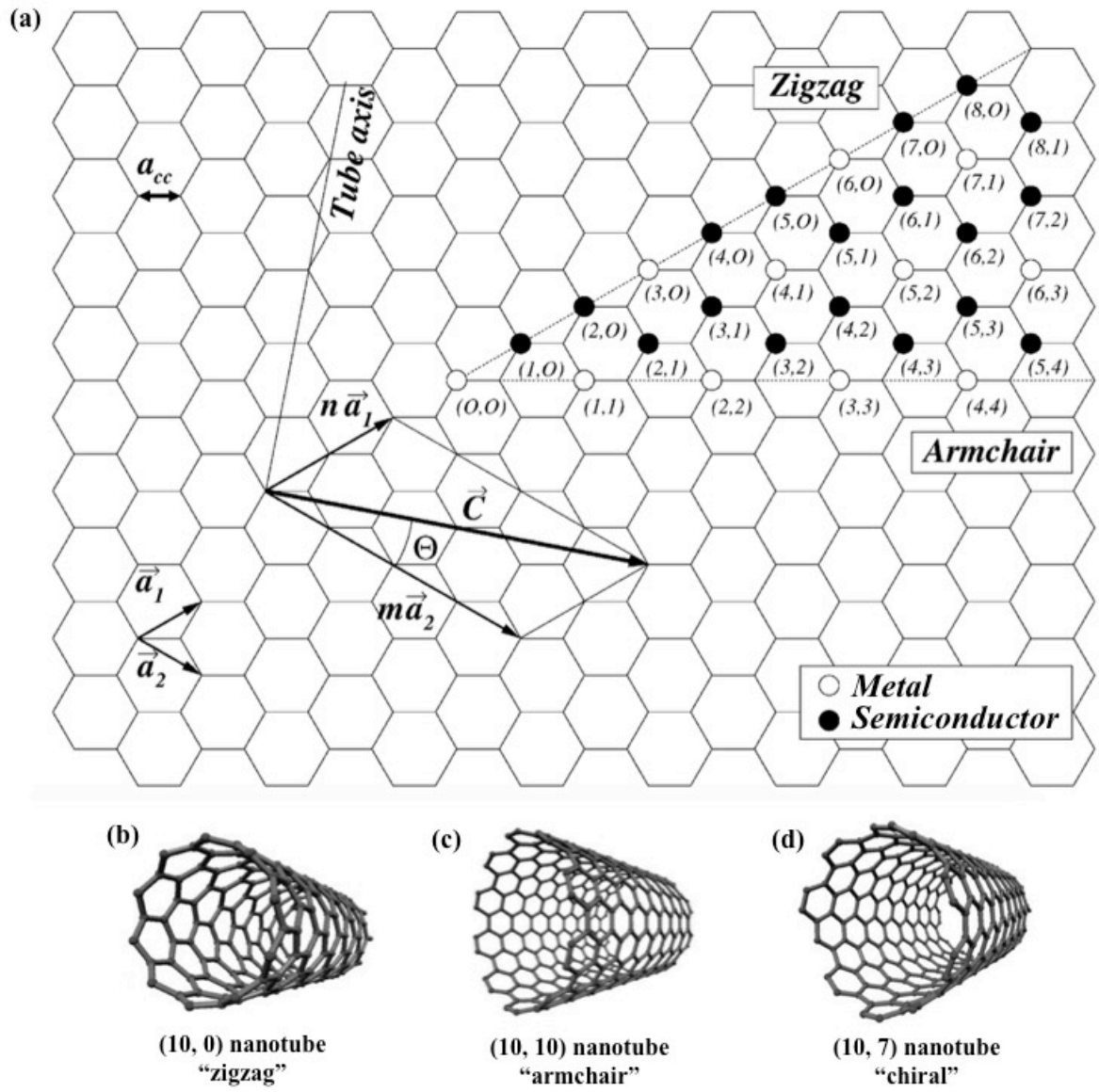

Figure 2.2 (a) A graphene layer with (n, m) nanotube naming scheme describing how a nanotube is rolled up; (b) SWNT of zigzag structure; (c) SWNT of armchair structure; (d) SWNT of chiral structure [4,7].

indices (n, m) called the chiral vector $\vec{C} = n\vec{a}_1 + m\vec{a}_2$ (Figure 2.2). The integers n and m denote the number of unit vectors along two directions in the honeycomb crystal lattice of graphene. If n = m, the nanotubes are called "armchair". If m = 0 and n > 0, the nanotubes

are called “zigzag”. Otherwise, they are called “chiral”. SWNTs have unique electrical properties due to their chirality. When $n-m$ is a multiple of 3, metallic conductance occurs. This suggests that one third of the tubes are metallic and two thirds are semiconducting. Armchair nanotubes are all metallic while zigzag and chiral nanotubes can be either metallic or semiconducting [8–10]. It is hard to identify the chirality of MWNTs because of their nested layers; however, most of them exhibit semiconducting properties.

2.2 Carbon Nanotube Properties and Applications

While the diameter of a CNT ranges from several nanometers to less than a hundred nanometers, the length of a CNT may range from less than a micron to several millimeters or even centimeters, resulting in high aspect ratio of individual CNTs with up to ~10^7 [11–13]. In addition, the hollowed cylindrical structure gives CNTs very low densities. These unique nanostructures result in many extraordinary properties of CNTs, such as high tensile strength, high electrical and thermal conductivities, high ductility, high thermal and chemical stability, which make them suitable for a variety of applications like nanoprobes [5,14–16], displays [17–19], sensors [20], molecular reinforcements in composites [5,6,21–23], molecular electronic devices [24–28], optical devices [29], thermal interface materials [30–32], and electrochemical and chemical storage media [5,19,26,33]. However, because of the high aspect ratios, the properties of CNTs are highly anisotropic.

The superb mechanical properties of CNTs are the major concern for applying them as advanced reinforcements in the composite materials. Their remarkable stiffness and strength come from the strong σ bonds in the sp^2 hybrid orbital. In graphite, the σ bond is 0.14 nm

long and 420 kcal/mol strong in sp^2 orbital. And in diamond, the σ bond is 0.15 nm long and 360 kcal/mol in sp^3 configuration. Therefore, graphite is stronger in-plane than diamond [6]. However, in CNTs, the σ-π rehybridization caused by circular curvature makes the σ bonds even stronger than those in graphite. For SWNTs, the experimentally measured Young's modulus is about 1 to 4 TPa [34,35] and the tensile strength is in the range of 13 to 52 GPa [35] along the tube axis. For MWNTs, the experimentally measured Young's modulus and tensile strength are around 1 TPa [36] and 11 to 63 GPa [37], respectively. These properties are one to two magnitudes higher than the high-performance carbon fibers which are made of planar graphene layers [38,39]. Therefore, CNTs are the desired materials that promise effective reinforcements for composites. In addition, CNT also exhibits a high ductility, i.e. large strain-to-failure, which arises from its strong covalent bonding and seamless tube structure that has less defects and stress concentrations than other graphitic structures. When CNTs are fully strained, their strain-to-failure can reach up to 12% [37] and 16% [40] under tension and bending conditions, respectively. Molecular-dynamics simulations of SWNTs under tensile deformation have revealed that under certain circumstances, the strain-to-failure of the nanotubes can be as large as ~30% [41]. The high ductility of nanotubes adds their advantage when reinforcing composites where energy absorbance is done by deformation but not cracking.

The exceptionally high electrical conductivity is another important feature for CNTs, which comes from the strong σ and π bonds in the atomic structures as well as their chirality. The electrical conductivity of metallic SWNTs can be as high as about 10^7 S/m as reported by Ebbesen et al. in 1996 [42] since the defect-free tube structures allow ballistic electron

transports [43,44]. For metallic MWNTs, the measured electrical conductivity is usually lower than that of metallic SWNTs for mainly two reasons: firstly, there are always both metallic and semiconducting individual tubes in MWNTs according to the statistical probability of their chirality; secondly, the experimental studies have been limited to the bulk measurements where only outmost wall of MWNT is contacted and measured [45]. Nevertheless, both metallic SWNTs and metallic MWNTs can carry high current densities along their tube length [46]. Adding only a small fraction of CNTs into insulating polymers or ceramics can effectively increases their electrical conductivities [47–50]. Such composite materials can dissipate electrostatic charges, having potential applications in electrostatic charge dissipation and electromagnetic interference shielding. When high fraction of CNTs are applied or composing them with conductive materials, the extraordinary electrical properties of CNTs promise their use as electrode materials for energy storage devices, and nanoelectronic devices and circuits [19,24–28,33].

CNTs are also good thermal conductors along their length that the thermal conductivities of both SWNTs and MWNTs are higher than those of natural diamond and the basal plane graphite [51,52], making them good thermal interface materials for heat dissipation [30–32]. And due to their nano-sized tube structures and low densities, CNTs have an extremely large surface area per unit mass, which is chemically reactive [53]. This opens up many likely applications for CNTs such as drug delivery materials, chemical- and bio-sensors, and catalyst supports [54–56]. In addition, the aligned CNTs are good choices as templates to grow other ordered nanostructures [2].

2.3 Carbon Nanotubes Synthesis

2.3.1 Arc Discharge and Laser Ablation Methods

The growth of CNTs is of great importance since it determines the properties of the nanotubes, and then the final performance of CNT products. It has been shown that given the right conditions, CNT synthesis can occur in a wide range of environments. There are mainly three techniques to grow CNTs: arc discharge, laser ablation, and chemical vapor deposition (CVD) [2,26,57,58].

Arc discharge method is the earliest technique that has been discovered to grow CNTs, and is also the first recognized technique for synthesizing both SWNTs and MWNTs. It involves direct current discharging between two arcing graphite electrodes in a helium or argon gas below atmospheric pressure and produces CNTs in the plasma of carbon gas [57–59]. A setup is shown in Figure 2.3. The CNTs produced in this method are usually random but have good crystallinity and very few defects, although the yield is low and the purification procedure is complex [2].

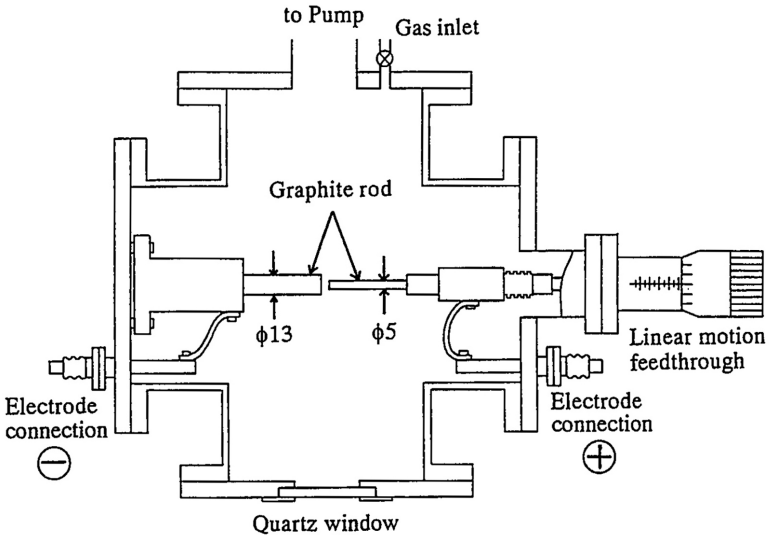

Figure 2.3 Setup of arc discharge technique [59].

Laser ablation is a process of removing materials from a solid surface by irradiating the surface with a laser beam. When synthesizing CNTs, a piece of graphite target is vaporized by laser irradiation under a high temperature in an inert atmosphere [57,58,60]. Similar to the arc discharge method, the CNTs produced by this technique are also powder-like and randomly entangled, and it is also not suitable for large-scale production of nanotubes. Figure 2.4 illustrates the growth apparatus of laser ablation method. SWNTs can be formed from a composite block of graphite and metal catalyst particles [61], whereas MWNTs are found when a pure graphite target is used [62]. The quality and yield of the products are highly dependent on the growth temperature that the best quality is obtained at 1200°C according to literatures. At lower temperatures, the structural quality of CNTs decreases that they present more defects. However, laser ablation method produces CNTs with higher purity than arc discharge method.

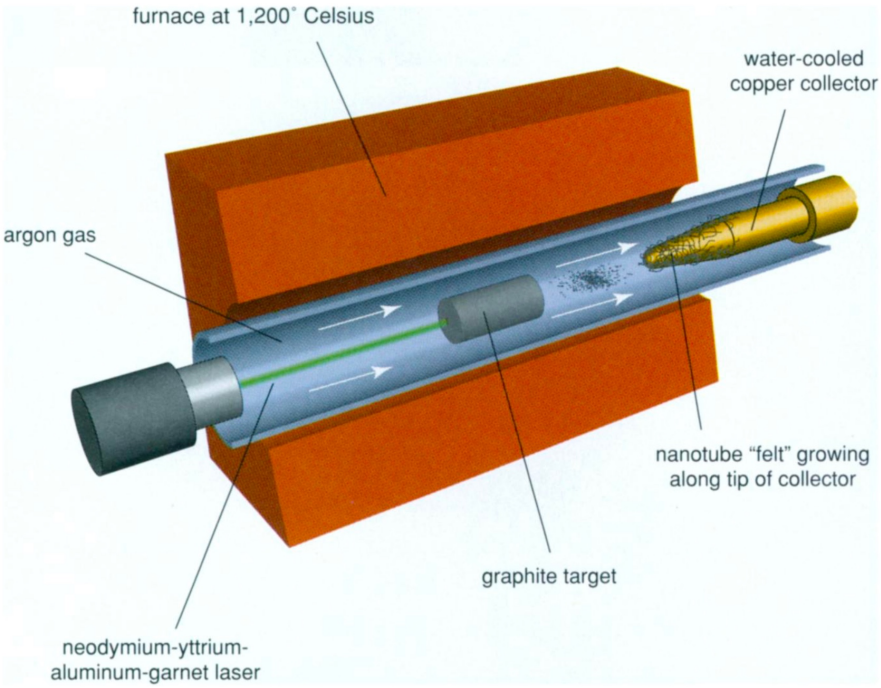

Figure 2.4 Apparatus of laser ablation method for producing CNTs [60].

2.3.2 Chemical Vapor Deposition Method

Chemical vapor deposition is a chemical process that deposits a solid on a heated surface from a chemical reaction in the vapor phase [58]. It is widely used to produce high-purity and high-performance solid materials. CVD growth of CNTs is the most often used technique nowadays and shows the most promise for industrial production due to its easy setup and operation, easy scale-up at low cost, and capability of growing CNTs directly on a desired substrate [2,6]. This is the technique that used to grow CNTs utilized in this work, therefore, a more detailed literature review is provided.

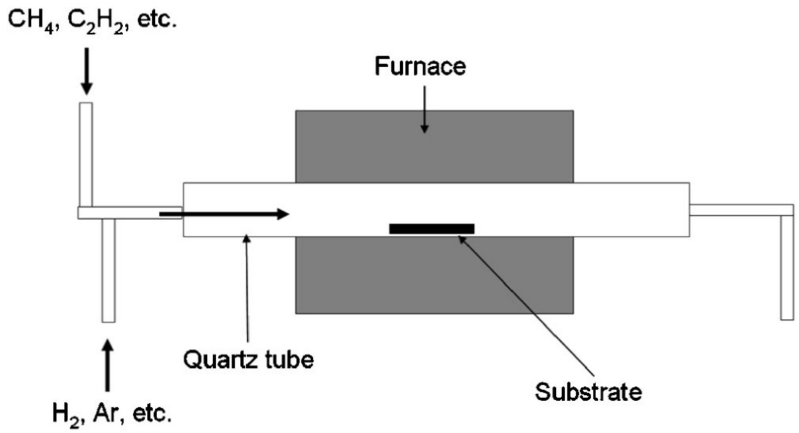

Figure 2.5 Schematic representation of the setup of the CVD method [57].

CVD synthesis of CNTs is usually done at relatively low temperatures (500°C - 1200°C). By imparting energy, a gaseous carbon precursor is "cracked" into reactive atomic carbon and hydrogen by metal catalyst particles, which nucleate CNTs and support their growth on the substrate. A schematic of the CVD process is presented in Figure 2.5. In CVD process, the growth of CNTs occurs in three main steps [63]: (i) decomposition/pyrolysis of the carbonaceous gas molecules; (ii) diffusion of the resultant carbon atoms through the catalytic

particle from the particle/gas interface toward the particle/nanotube interface due to the concentration gradient; (iii) precipitation of carbon atoms at the particle/nanotube interface. In the third step, CNTs grow catalytically and then thicken via a catalyst-free pyrolytic carbon decomposition mechanism.

Carbon-containing gases, such as methane (CH_4), ethylene (C_2H_4), acetylene (C_2H_2), benzene (C_6H_6), toluene (C_7H_8), ethanol (C_2H_5OH), and carbon monoxide (CO), have been used as carbon precursors [2,58]. The carbon precursors affect the quality of CNTs. For example, if the CH concentration is high such as acetylene, many CNTs are enriched by amorphous carbon and carbon nanoparticles, resulting in rough nanotube surfaces [64]. This is due to the over-supply of carbon atoms during the CNT growth. On the other hand, different synthesis temperatures are needed for different carbon precursors in order to break down the C-C or C-H bonds to release carbon atoms for CNT growth, then influencing the CNT structures, purity, and yield accordingly.

Metal catalyst is another key factor for CNT growth in CVD method since they act as the starting points of the tubular structure development [5]. Nickel (Ni), cobalt (Co), iron (Fe), gold (Au), platinum (Pt), stainless steel and their alloys have been successfully used as catalysts for CNT growth [2,15]. The size of catalyst particles determines the diameter of CNTs. The outer diameter of CNTs increases with the increasing of catalyst particle size whereas the inner diameter increases only slightly. Therefore, CNTs cannot grow on catalyst particles with very small diameters. Moreover, the distribution of catalyst particles affects the density of CNTs, and eventually the morphology and quality of the as-grown CNT arrays. The distance between two adjacent nanotubes can be controlled by controlling the spacing

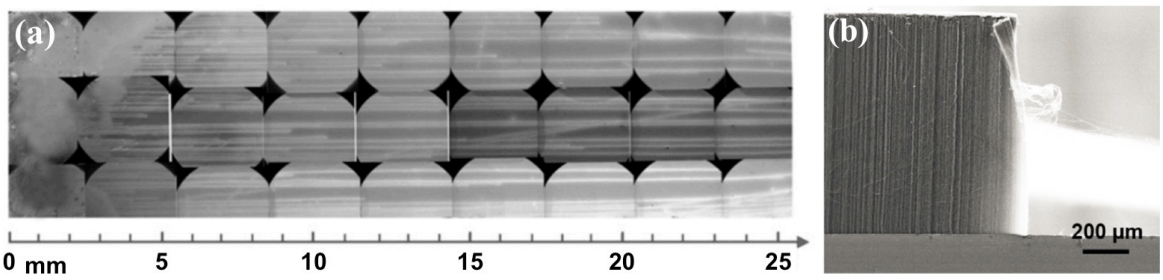

Figure 2.6 (a) Half-meter-long CNTs that buckled and lay down on the substrate [65] ; (b) Vertically aligned millimeter-long CNTs [66].

between catalyst particles. If the catalyst particles are spaced far apart, the growing CNTs are separated too far away to allow van der Waals interactions between neighboring nanotubes, causing CNTs buckle and fall back on to the substrate (Figure 2.6a [65]). If the catalyst particles are spaced closely together, mutual support of the van der Waals forces between adjacent nanotubes enable a continuous growth of vertically aligned CNTs (VACNTs) (Figure 2.6b [66]), which is the most important advantage of CVD method. It has been reported that among all the metal catalysts, transition metal catalysts are the most effective species for CNT growth in CVD process [67–69]. This is because their incomplete d-orbitals make them highly catalytic active in forming meta-stable carbides, breaking down the carbon sources, and dissolving the carbon atoms. The meta-stable carbides are able to release precipitated carbon atoms while continuing to break down and transport carbon from precursor gases [69]. Iron catalyst is the best choice to grow long aligned CNT arrays. Millimeter-long CNTs have been synthesized almost exclusively by iron catalyst [67,68]. The nucleation and growth process of CNTs from iron particles were observed by Yoshida et al. in 2008, and Figure 2.7 shows the images taken during the process [70]. It reveals that

iron particles transform to iron carbides (Fe_3C) during CNT growth, providing a way for carbon atoms to diffuse through rather than migrating on their surfaces. Then, graphite layers form on the iron carbide facets and extend along the facets, forming multiple layers of nanotubes.

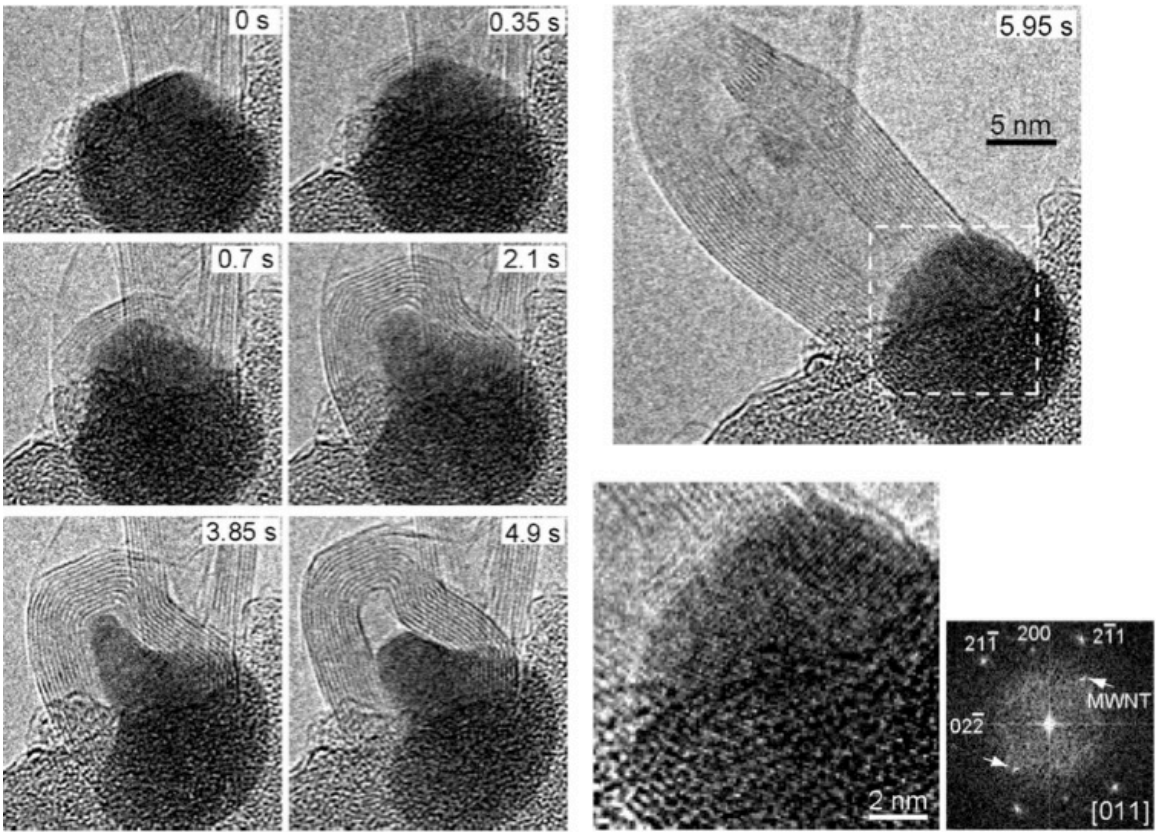

Figure 2.7 Nucleation and growth of a MWNT from an iron catalyst particle [70].

In CVD method, the substrate where CNT array grow on is extremely important, because the metal-support interactions are found to play a determinant role for the CNT growth mechanism [63]. As shown in Figure 2.8, when the metal-support interaction is weak, tip-growth occurs; and when the interaction is strong, base-growth takes place. CNTs can grow

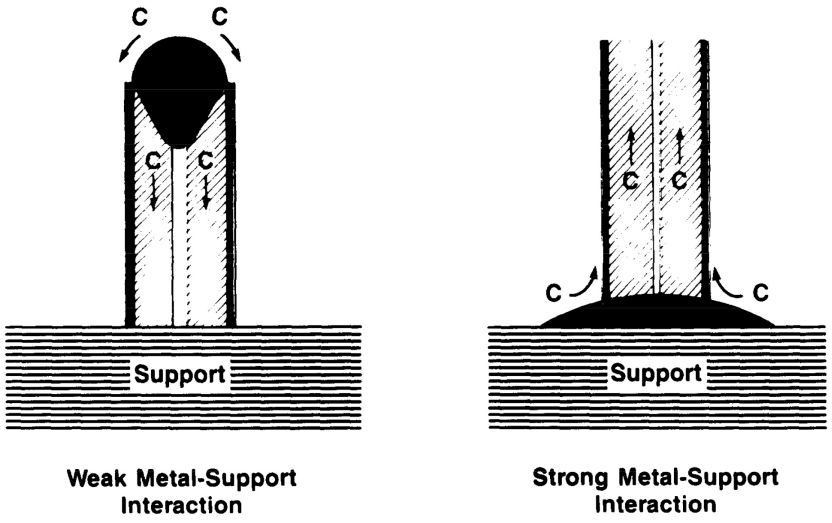

Figure 2.8 Schematic of the influence of the metal-support interaction on the CNT growth mechanism [63].

on substrates such as quartz plates [71], sapphire (α-Al_2O_3) substrates [72], and silicon (Si) wafers [67,69,70,73–75], among which Si wafers are the mostly used due to their low cost, high temperature resistance, and extremely low roughness. When Si wafer is the substrate, a buffer layer is usually needed before the deposition of metal catalyst particles. Many types of metal oxides, such as Al, Al_2O_3, SiO_2, MgO, ZrO_2, Ti, TiN, or TiO_2 can be used as buffer layers to support catalyst [2]. And Al_2O_3 is reported to be the most common and effective buffer material used to increase the aligned CNT length and quality in CVD method through its interaction with Fe catalyst particles [74,75]. It has been proposed that Al_2O_3 and Fe have a strong interaction between each other, which helps restrict the Fe particle size distribution and the diffusion of Fe into the Si substrate [76]. Once a significant amount of catalyst particles diffuse into the substrate, CNT growth terminates. Buffer layer, as well as metal catalyst, can be deposited through a variety of methods, such as thermal evaporation,

magnetron sputtering, pulsed-laser deposition, and ion-beam assisted deposition (IBAD) [2,6]. The thickness, composition, deposition rate and deposition pressure of the buffer layer are of vital importance for determining the final morphology of the catalyst thin film, which in turn influences the CNT growth.

The operating temperature and pressure of CVD process are also critical in influencing the CNT structures, purity, and yield. At low gas pressure, CNTs are completely hollow at low growth temperature and bamboo-like at high growth temperature; while at high gas pressure, all CNTs have bamboo-like structures regardless of the growth temperature [77,78]. And high growth temperature is necessary in synthesizing CNTs with small diameters [79]. However, at high temperatures, the yield of CNTs decreases due to the high dissolving rate of carbon atoms forming amorphous carbon on the CNT surfaces, and the high possibility of chemical reaction between carbon and catalyst forming catalyst carbide causing the catalyst to lose catalytic activity for CNT growth [77]. In this case, CNTs exhibit lower purity at higher growth temperature.

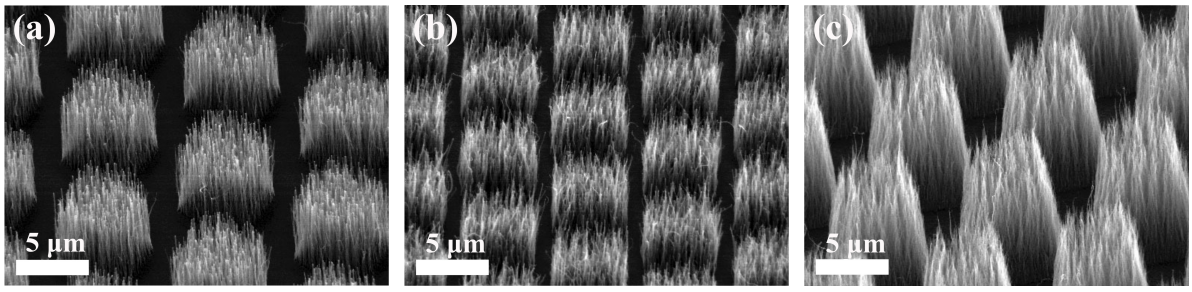

Figure 2.9 Different orientations of the aligned CNTs grown by CVD method [80].

The length of the CNTs synthesized by CVD method can be simply controlled by the growth time. The longest CNTs synthesized by CVD method are about half-meter long as

shown in Figure 2.6 (a), which was reported by Zhang et al. in 2013 [65]. And when an electric field is applied, the orientation of the aligned CNTs can be changed [80], as displayed in Figure 2.9. To summarize, CVD method is able to grow CNTs with high purity, high quality, highly ordered unidirectionally aligned structure, and controlled dimensions. These are all merits of CVD process over arc discharge method and laser ablation method, making them the desired technique for producing CNTs.

2.3.3 Synthesis of Superaligned Carbon Nanotubes

CVD method can grow VACNT arrays, in which CNTs are vertically self-oriented and perpendicular to the substrate. As mentioned in the previous part, the size of catalyst particles determines the diameter of CNTs; and the density of catalyst particles affects the density of CNTs. When the size distribution of catalysts is narrow and the nucleation density for CNTs is high enough, the as-grown CNT array will have a narrow CNT diameter distribution with a high surface density, leading to a high degree of alignment of CNTs in the array which is then called “superaligned” [19,81,82].

Superaligned carbon nanotubes (SACNTs) distinguish themself from ordinary VACNTs by their capability of being drawn out from the array and converted into continuous films and yarns [73,81–84]. They enable easy manipulation of nano-scale CNTs; provide a simple and direct way of making continuous CNT yarns and films at macro-scale, where high fraction of CNTs can be achieve; and show the potential of fully utilizing the superior properties of individual nanotubes, promising for producing high-performance CNT products. Therefore,

SACNTs have been very attractive to academic researchers and industries since they were reported. The SACNT arrays are used as the raw material in this work.

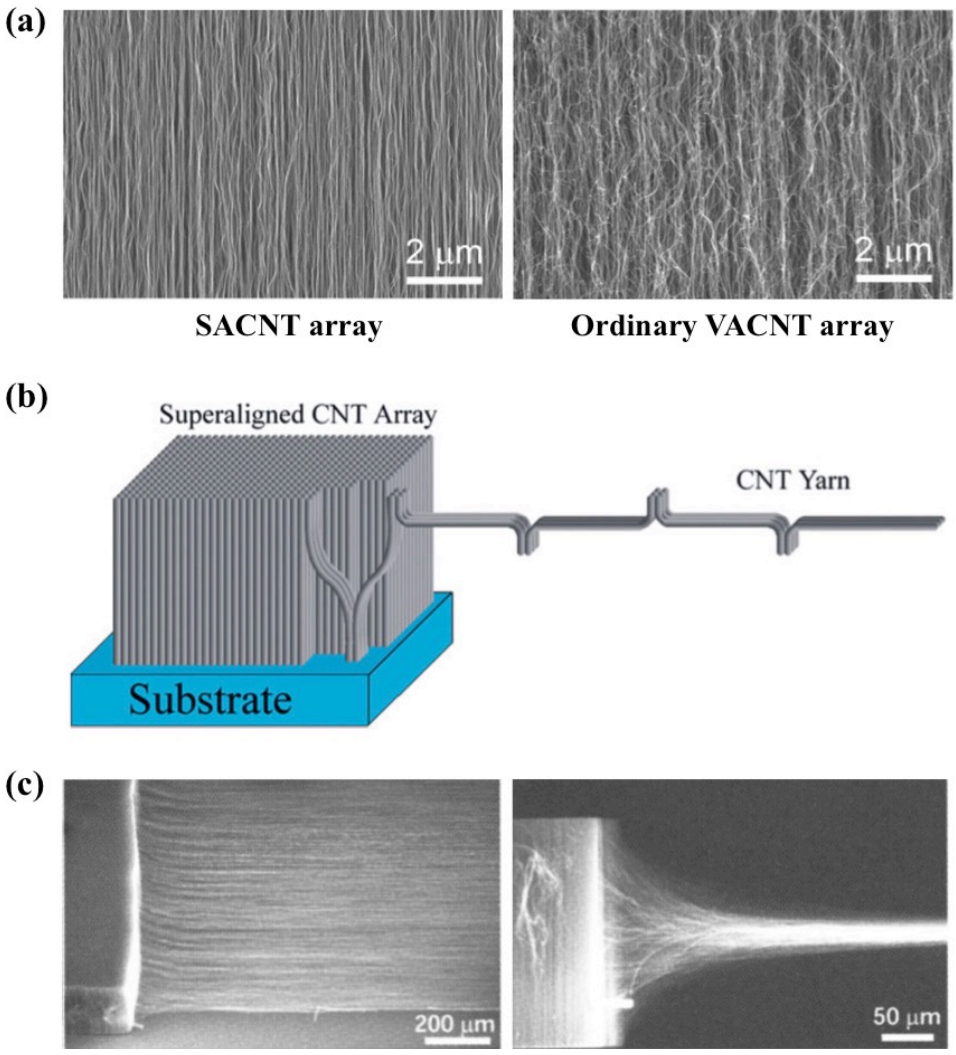

Figure 2.10 (a) Comparison of a SACNT array and an ordinary VACNT array [82]; (b) Schematic illustration of the end-to-end joining model for drawing SACNTs [81]; (c) Images showing the SACNTs being drawn into a sheet [84].

As shown in Figure 2.10 (a), the ordinary VACNTs are not perfectly aligned but have some degree of waviness, whereas the SACNTs have much better alignment and cleaner tube

surfaces. The clean tube surface is also one of the prerequisites for CNTs to be superaligned, because the capability of drawing the CNTs originates from the strong van der Waals interactions between neighboring nanotubes [81,82]. Amorphous carbon on tube surfaces weaken the van der Waals interactions. It is proposed that when SACNTs are being drawn out from the array, the nanotubes come out continuously with their ends joining together by strong van der Waals forces, which process is schematically illustrated in Figure 2.10 (b). Figure 2.10 (c) is the images showing the SACNTs being drawn into a sheet.

To synthesize SACNT arrays, the basic principles are to achieve a narrow size distribution of catalysts, a very high CNT nucleation density, and to keep clean surfaces of CNTs [19,81,82]. The process requires a very precise control of the growth conditions, which is difficult to achieve. Therefore, only a few research groups are capable of synthesizing SACNT arrays so far [73,74,83,85–88]. The SACNT arrays were first successfully synthesized by Fan's group in 2002 [73], and than followed by Baughman's group in 2004 [83]. In their studies, acetylene was used as the carbon precursor gas, and Fe was the catalyst which was deposited on Si wafer by electron-beam evaporation. It was found in their following research [81,82,84] that the high density of catalyst particles and their narrow size distribution could be achieved by controlling the thickness of metal catalyst thin film and the deposition rate for preparing the catalyst film. The CNT nucleation density and growth rate increase with increasing growth temperature and carbon precursor feeding rate; however, on the other hand, high temperature and high feeding rate also give rise to high deposition rate of amorphous carbon on the nanotube surfaces, which renders the CNTs non-drawable. Therefore, growth temperature and feeding rate of carbon precursor need to be carefully

adjusted and combined in order to guarantee high CNT nucleation density and clean surfaces of CNTs. In addition, a polished flat surface of substrate is important since it affects the morphology of deposited metal catalyst thin film. The SACNTs produced in this way are MWNTs of about 3 to 10 walls with a diameter of about 5-15 nm and a length of a few hundred micrometers [81–84].

However, long drawable CNTs are preferred for their better mechanical performance. In 2006, Li et al. [74] modified the above synthesizing process and succeeded in producing 4.7 mm long CNTs with a drawable range of 0.5 to 1.5 mm. Ethylene was used as the carbon precursor and water vapor was added during the growth process. A dense Al_2O_3 buffer layer (10 nm) was deposited in between the substrate and the Fe catalyst thin film (1 nm) by IBAD technique. It was found that the added Al_2O_3 buffer layer helped a more uniform deposition of the Fe film and prevented the interdiffusion between the Fe film and the substrate, leading to a long catalyst life for CNT growth. Additionally, water vapor helped to achieve a high growth rate while maintaining a long catalyst lifetime at high temperature due to its ability to reduce the formation of amorphous carbon at high growth temperature and thus keep the catalyst particles clean.

While the aforementioned SACNT synthesis process involves several steps which all need careful control, an easy and efficient one-step growth method was reported by Inoue et al. in 2008 [85] in which no additional process was required for catalyst preparation. Iron chloride ($FeCl_2$) powder was used as the metal catalyst for growing CNTs, and it was thermally evaporated and deposited on a quartz substrate during the growth procedure. Acetylene was the carbon source. It was reported that $FeCl_2$ had high dehydrogenation

activity on acetylene, which could increase the growth rate of CNTs. The elimination of catalyst predeposition along with the increased growth rate was promised for a significant reduction of the costs for growing CNTs by this chloride mediated CVD method. The drawable CNTs synthesized in this way possess much more walls (> 20) with much larger diameters (~50 nm) than those synthesized by previously mentioned processes, and they are also much longer (millimeter long).

In recent years, other research groups [86–88] have also been able to synthesize drawable SACNT arrays. However, their methods are all based on the above two synthesis systems with only small modifications, such as changing the type and thickness of buffer layer and catalyst thin film, selecting different carbon precursor gases and forming gases, and using different growth temperatures and gas feeding rates, in order to meet certain requirements for the as-grown SACNTs.

2.4 Carbon Nanotube Products

CNTs have extremely small sizes, meanwhile, they are reported to be half dense as aluminum, 20 times strong as high strength steel alloys, have current carrying capacities 1000 times that of copper, and can transmit heat twice as well as pure diamond [89]. With continuous developments in the synthesis and production of CNTs, attempts have been made to assemble these nano-scale materials into macro-scale products which can fully realize those marvelous properties of individual CNTs for real applications. While early attempts failed to take full advantage of the potential of CNTs, emerging new synthesis methods and

novel processing techniques provide the possibilities of fabricating CNT-based materials into different forms with improved performance.

The most common application for random and short CNTs is to incorporate them into ceramic, metallic, or polymeric matrices to build value-added composite materials [5,21,47,48,90–92]. However, usually only a small fraction of CNTs can be added into the matrix, and uniform dispersion and good nanotube/matrix adhesion are critical issues in processing of these nanocomposites. The resulted composites usually show only a slightly improved behavior due to CNT entanglements and poor CNT/matrix interfacial bonding. In this case, additional processes are needed in order to create better CNT dispersion and stronger interfacial bonding [48], which makes the procedure more complicated and less controllable.

Successful growth of aligned CNT arrays by CVD method has opened up a new way of fabricating aligned CNT products. The array itself can be directly used as energy absorbing materials [93], super-hydrophobic surfaces for anti-contamination and self-cleaning [94], and templates to grow other ordered nanostructures [95]. By filling matrices into the gap between the aligned CNTs on the array, composites can also be produced. Infiltration [96], atomic layer deposition [97], and polymerization [98] methods are the common methods used to produce composites from aligned CNT arrays. The resulted composite materials exhibit a higher CNT fraction and better performance than those made from short CNTs because of the long nanotubes and the aligned ordered CNT structure in the array. Nevertheless, the sizes of the composites are limited due to the limitation of the as-grown array dimensions, i.e. large composites cannot be fabricated from CNT arrays since the largest dimension of the array

can be synthesized currently was reported to be only 8 inches [19]. Therefore, they are not suitable for industrial mass production.

The discovery of drawable SACNT arrays and the development of a dry-drawing method in 2002 [73] provide more options for researchers to make CNT products and opportunities to better utilize the superior properties of individual nanotubes. The method is easy to operate and can produce CNT products with either low nanotube fraction or high fraction or even pure CNT products. The CNT yarns or films produced in this way usually have long CNT length, high purity, high quality, high level of nanotube alignment, and highly ordered structure, which results in high-performance of the products. And the product size is not limited by the array dimension. For example, unlike solution spinning of short CNTs where a lot of chemicals are used and complex handling is needed, continuous CNT yarns can be easily produced by drawing and spinning of CNTs from SACNT array using the dry-drawing method, and the yarns present much better properties than those made from short CNTs. Figure 2.11 displays the pulling and twisting of a CNT yarn from a SACNT array [83]. In 2007, Zhang et al. reported the production of pure CNT yarns (Figure 2.12) with a strength of up to 3.3 GPa but very low density of about 0.2 g/cm^3 [99], which specific strength is 5.3 times that of the strongest commercial carbon fiber (T1000) and still remain the highest among CNT-based yarns produced by different methods [90,91,100]. When matrices are added during drawing and spinning process, CNT-based composite yarns can be easily fabricated [101]. The dry-drawing method is also applicable to fabricate CNT sheets/films/buckypapers [84,102,103] or CNT sheet-based composites [66,104–108], which

is going to be discussed later in detail since this is the method used to produce the experimental products in this work.

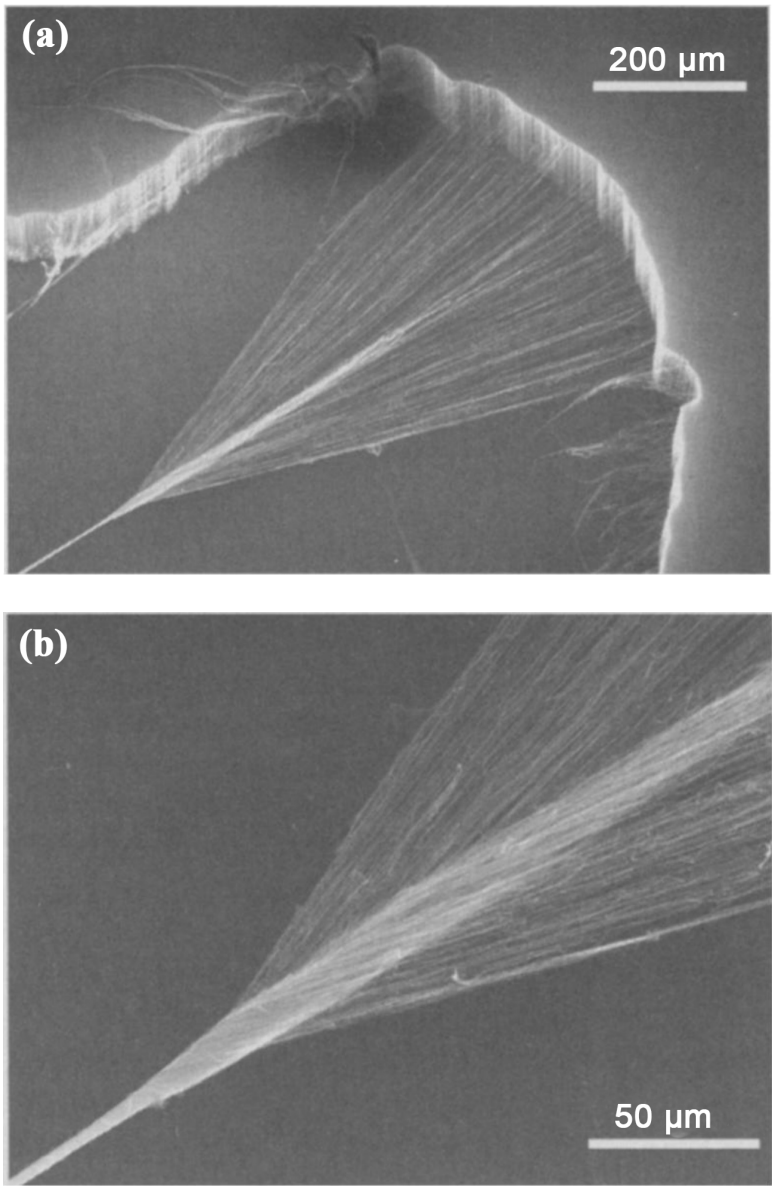

Figure 2.11 A layer of CNT sheet being pulled from a SACNT array and then twisted to form a CNT yarn [83].

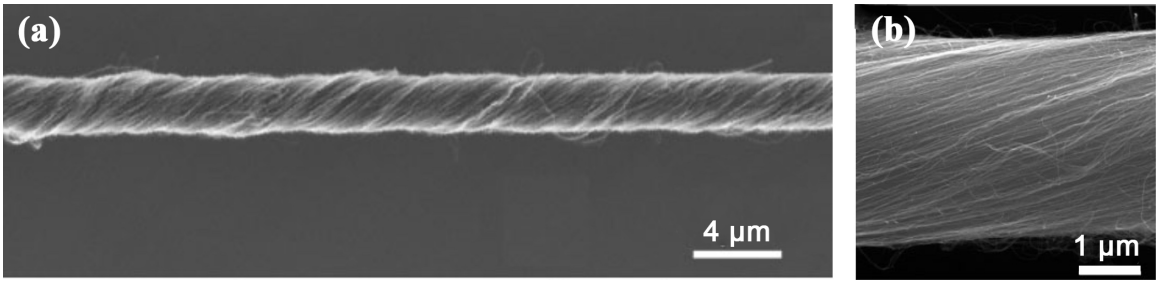

Figure 2.12 Pure CNT yarns spun from a SACNT array by dry-drawing method [99].

2.4.1 Dry Carbon Nanotube Films and Buckypapers

CNTs resemble traditional fibers but possess extraordinary chemical and physical properties, which make them attractive for making paper materials, known as buckypapers. These papers made of CNTs have been widely studied as catalyst supports [109], filters [110,111], structural reinforcements [102,103,112], battery electrodes [113], supercapacitors [114], electrical and thermal interface materials [115], and fire retardant layers [116].

Short CNTs are first made into buckypapers by a general process that is adopted from ancient art of paper-making technique which involves dispersing short CNTs in a solution and then filter the CNT suspension using a fine filter [109–111,113,114,117–119]. Usually, surfactants and high-power sonication are used for helping CNT dispersion. CNTs are almost completely randomly distributed in these buckypapers. The nature of their short lengths, weak interactions among the tubes, and their tendency of crookedness and agglomeration make such CNT sheets very weak and thus diminish CNT potential values [118]. The strength and stiffness for these buckypapers are very low, of only several tens megapascal and several gigapascal, respectively [119]. Figure 2.13 shows the images of typical dispersed short CNT buckypapers, where nanotubes are curved and randomly aligned [117].

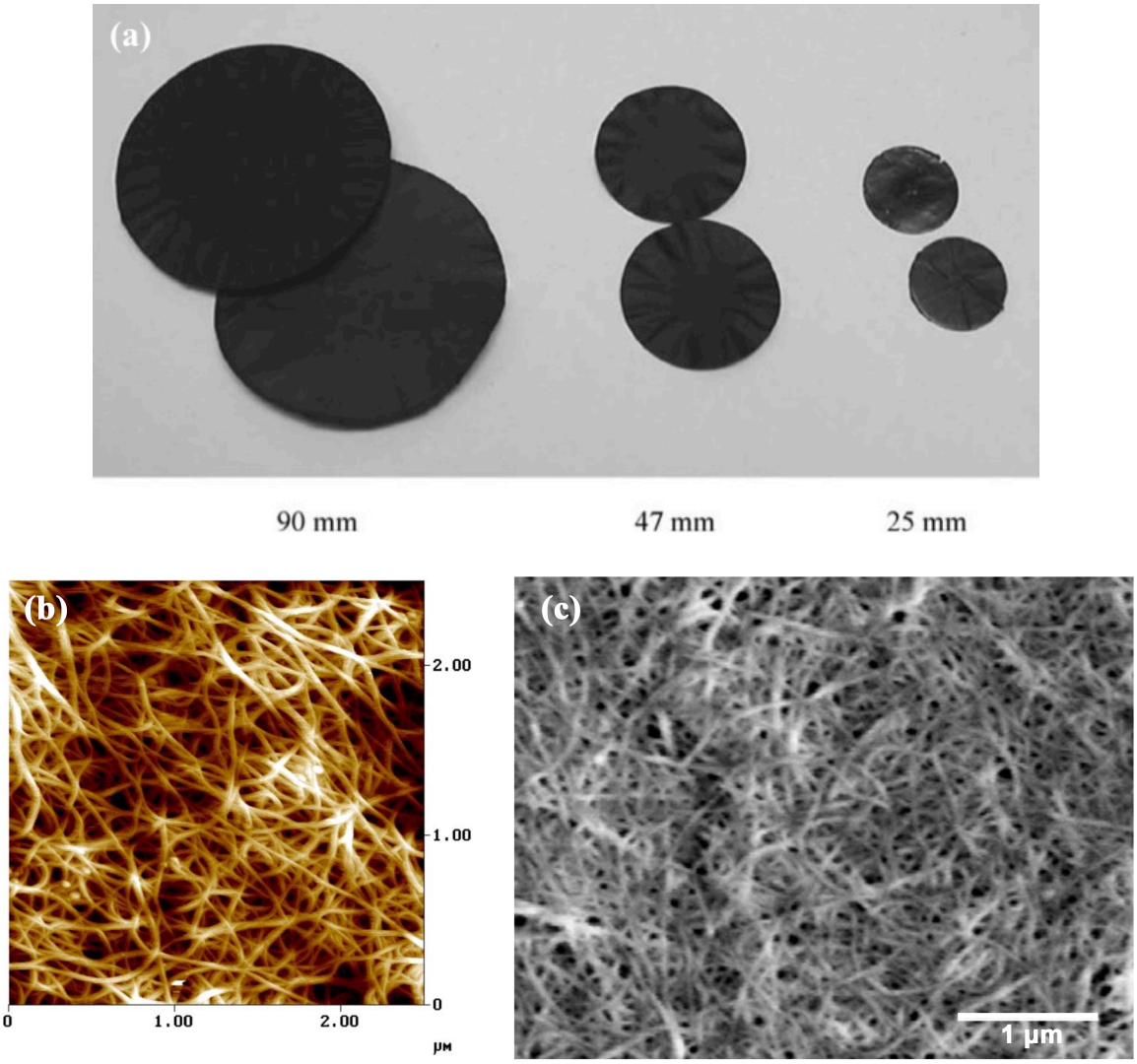

Figure 2.13 (a) Image of SWNT buckypapers; (b) Atomic force microscopy image of the surface of the buckypaper; (c) Scanning electron microscopy image of the buckyppaper [117].

In order to improve their performance, it was proposed that the ideal structure for buckypapers should have long and straight CNTs perfectly aligned and all connected with each other [115]. Growth of CNT arrays by CVD method makes this come true, since the CNTs are long and perfectly aligned in the array. Directly pushing or pressing CNT arrays

into buckypapers can realize highly aligned nanotubes in a planar network. In 2008, Wang et al. developed a "domino pushing" method (Figure 2.14a) to fabricate aligned thick buckypapers, and got an improved thermal conductivity of 331W/(m·K) and good electrical conductivity of 2.0×10^4 S/m along the CNT alignment direction [115]. A similar approach was proposed later by Bradford et al. which was named as "shear pressing" (Figure 2.14b) [112]. They got a high electrical conductivity of 1.18×10^4 S/m for those buckypapers made by millimeter long CNTs.

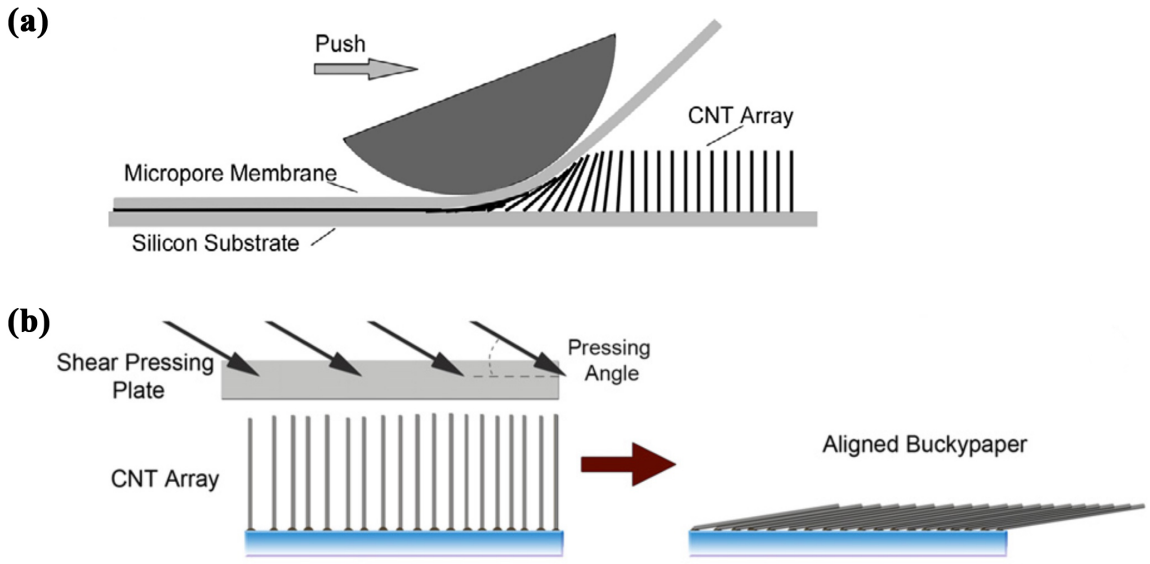

Figure 2.14 (a) Schematic of the "domino pushing" method [115] ; (b) Schematic of the "shear pressing" method [112].

An easier and more efficient approach of making aligned long CNT buckypapers was proposed after finding the drawability of SACNT arrays [84]. When drawing the CNTs in a SACNT array, the vertically aligned long CNTs can be continuously pulled out and converted to a horizontally unidirectionally aligned CNT sheet. Then, buckypapers with

desired thickness can be readily produced by winding the CNT sheet layer by layer [102,120,121]. Since the CNTs are processed in a dry state, the buckypapers made in this way are also referred to as dry CNT films. This dry processing method has the advantage of avoiding complex and time-consuming processes that are typical for solution-based methods of making short CNT buckypapers, and have no limits to the size of buckypapers which is an issue when CNT arrays are pushed or pressed to buckypapers. The dry films made in this way have shown much improved properties than those made by other methods due to a high degree of alignment and dense packing of the long nanotubes in the layered sheets [122]. Di and co-workers reported ultrastrong and flexible dry CNT films with tensile strengths of up to 2 GPa, Young's moduli of up to 90 GPa, and electrical conductivities of about 3.5×10^4 S/m [120]. Figure 2.15 (a) shows the drawing and winding process of making dry CNT films,

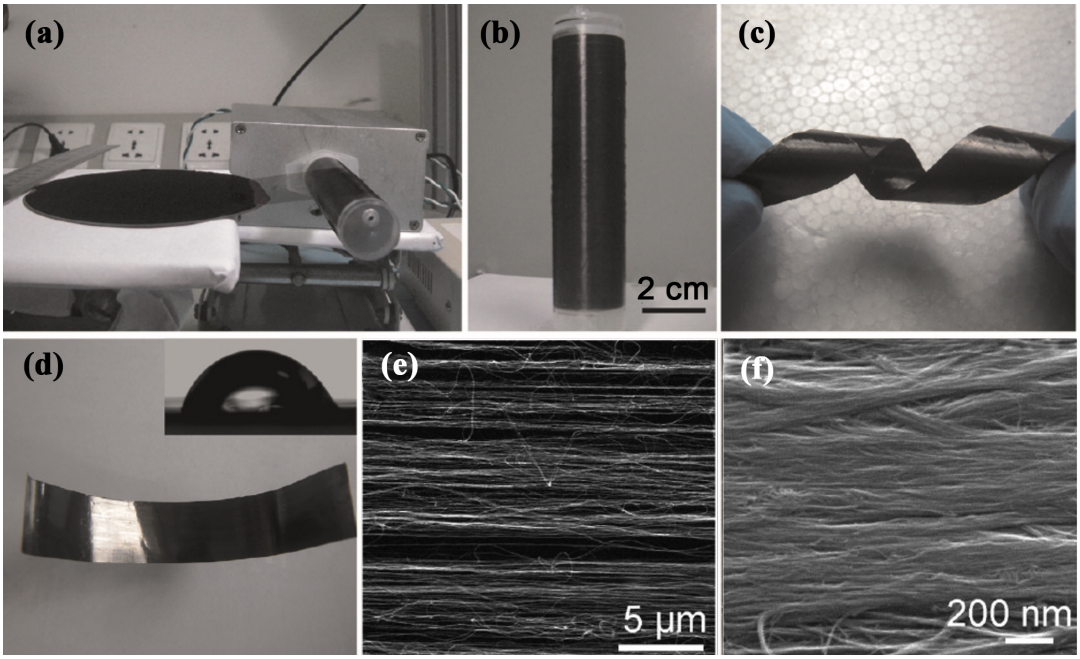

Figure 2.15 (a) Setup of the preparation of a dry CNT film; (b), (c), (d) Appearance of the dry CNT film; (e), (f) Images of the surface morphology of the dry CNT film [120].

and (b)-(f) are the images of the as-produced film revealing the unidirectional alignment and high packing density of the long nanotubes.

2.4.2 Carbon Nanotube Reinforced Polymer Composite Films

Many of modern technologies require materials with unusual combinations of properties that cannot be met by the conventional metal alloys, ceramics, and polymeric materials. This is especially true for materials that are needed for aerospace, under-water, and transportation application. Therefore, composite materials have been developed. Generally speaking, a composite is considered to be any multiphase material that exhibits a significant proportion of the properties of both constituent phases such that a better combination of properties is realized [123]. In most cases, composites have been created to improve combinations of mechanical characteristics, such as stiffness, toughness, and strength.

Usually, composite materials are composed of just two phases: one is termed the matrix, which is continuous and surrounds the other phase, often called the dispersed phase. Composite materials can be classified either by the type of dispersed phase or the type of matrix. In the dispersed phase classification, composite materials consist of three main divisions: particle-reinforced, fiber-reinforced, and structural composites. In the matrix classification, there are also three main subsections: metal-matrix composites (MMCs), polymer-matrix composites (PMCs), and ceramic-matrix composites (CMCs). Among all types of composites, fiber-reinforced polymer-matrix composites are the most important and popular ones because of their ease of fabrication, low cost, great diversity, and large quantities. The main design goal of this kind of composites is high strength and/or stiffness

on a weight basis, i.e. specific strength and specific modulus. Fiber-reinforced polymer-matrix composites with exceptionally high specific strengths and moduli have been produced that utilize low-density but high-performance fibers, such as glass, carbon, and Kevlar. CNTs have unprecedented physical and chemical properties which no other materials exhibit, as well as low densities, making them the most promising candidate for reinforcing composites.

However, mechanical characteristics of a fiber-reinforced composite depend not only on the properties of the fiber, but also on the degree to which an applied load is transmitted to the fibers by the matrix phase [123]. Through intensive attempts to fabricate CNT/polymer composite materials with high performance, it have been found there are four main system requirements for effective reinforcement: a large aspect ratio, good dispersion, alignment, and interfacial stress transfer [22]. Aspect ratio must be large to maximize the load transfer from matrix to nanotubes, which is crucial in order to optimize composite strength and stiffness [123]. More fundamentally, CNTs need to be uniformly dispersed as isolated nanotubes individually coated with polymer matrix, which is imperative to achieve efficient load transfer to nanotube network, and thus results in a more uniform stress distribution and minimizes the presence of stress-concentration centers generated by agglomerated CNTs. Due to the high anisotropic properties of CNTs that come from their unique 1D structure, it is desired to unidirectionally align nanotubes in matrix in order to achieve better utilization of the CNT potential. Good CNT alignment also helps to increase load transfer efficiency [106]. Finally, CNT-matrix interfacial bonding is of great importance which directly determines the interfacial stress transfer. Since CNTs have an atomically smooth surface and few sites for bonding with a matrix, interfacial stress transfer is a critical issue for CNT/polymer

composites. Interfacial shear stress (IFSS) is a parameter that used to control the maximum stress transfer from matrix to nanotubes. It is defined as the shear stress in polymer matrix at CNT-matrix interface. Long nanotubes and strong nanotube-matrix bonding are preferred to fabricate high-performance CNT/polymer composites.

CNT/polymer composites have been processed via a variety of methods, including solution processing [48,90,91], melt processing [96], polymerization processing [98], and dry processing [104–106]. The easiest and most efficient method has turned out to be the dry processing method which uses dry-state drawn of CNT sheets to produce the composite films, where long and pure nanotubes are unidirectionally aligned and uniformed distributed in polymer matrix at a high CNT fraction, resulting in the greatest utilization of the CNT intrinsic properties. Cheng et al. was the first group that tried to fabricate this kind of aligned CNT composites [124,125]. By dry-drawing CNT sheets from a SACNT array and then stacking them together followed by an infiltration process of epoxy resin, they produced CNT/epoxy composite films with 16.5 wt.% CNTs homogeneously dispersed and highly aligned in the epoxy matrix. The Young's modulus and tensile strength of the resulted composite films reached 20.4 GPa and 231.5 MPa, respectively. A breakthrough was made by our group in 2011 by developing a spray-winding process (Figure 2.16), which was a one-step process of fabricating aligned CNT/polymer composite films with high performance [105,106]. By using a winding mandrel and a spray gun, soluble polymer matrix can be sprayed uniformly onto each layer of the continuously drawn CNT sheet while it is being wound on the rotating mandrel. It was found the CNT fraction in the as-produced composite films could be as high as 65 wt.%, and homogeneous integration was achieved between the

nanotubes and the matrix. The best CNT/PVA films produced in this way had a tensile strength of 1.8 GPa, Young's modulus of 45 GPa, toughness of 100J/g, and electrical conductivity of 7.8×10^4 S/m. These results demonstrate the importance of long CNT length, good alignment, high CNT fraction, and uniform CNT-matrix integration for making high-performance CNT composites.

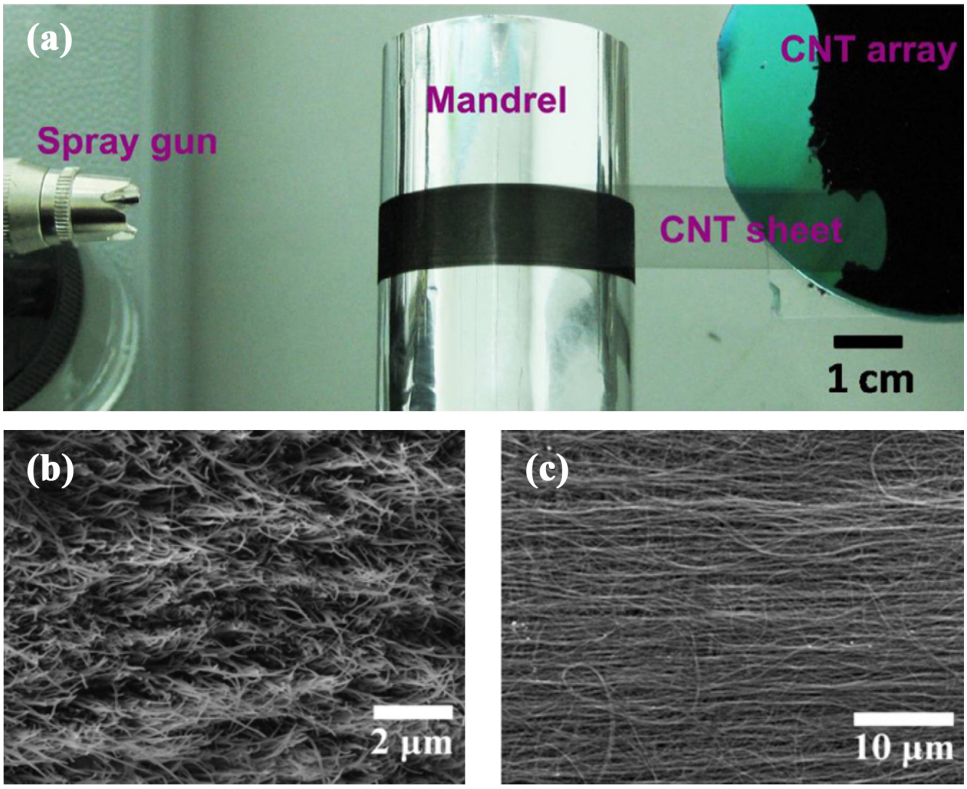

Figure 2.16 (a) Schematic of the spray-winding process [102]; Images showing the fracture surface (b) and surface (c) morphologies of the CNT/PVA composite films produced by spray-winding [106].

While nanotube alignment plays a determinant role in the efficiency of load transfer from matrix to CNTs which influences composite final performance, it has been found that specially for CNTs, the waviness is also a critical issue in limiting the effective CNT

properties. Fisher and co-workers developed a model combining finite element results and micromechanical methods to determine the effective reinforcing modulus (ERM) of a wavy nanotube embedded in polymer matrix [89], as shown in Figure 2.17. They disclosed that even slight nanotube curvature could significantly reduce the effective reinforcement when compared to straight nanotubes. When producing CNT/nylon composite films, Xin et al. tried to stretch the films after fabrication in order to straighten the CNTs in the structure [104]. With a stretch ratio of 7%, the tensile strength, Young's modulus, and electrical conductivity of the composite films improved 190%, 290%, and 300%, respectively, which was quite significant. Figure 2.18 displays the surface morphologies of the CNT/nylon composite films under different stretching rate. In a later study, Xin and co-workers successfully stretched the

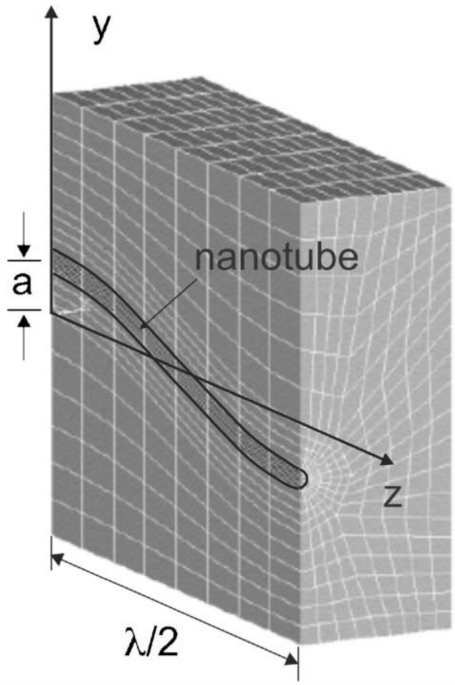

Figure 2.17 Schematic of the finite element cell model of an embedded wavy nanotube [89].

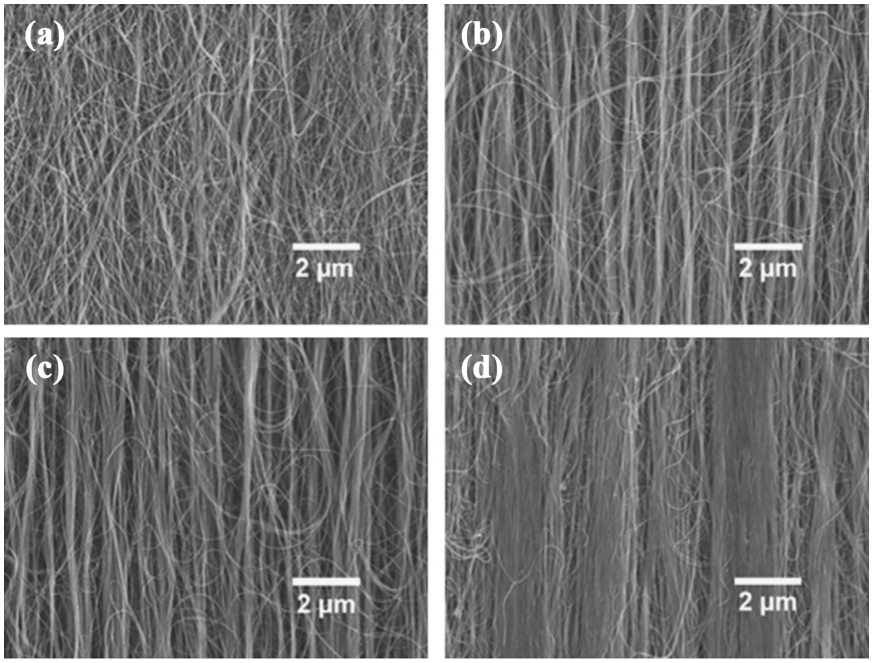

Figure 2.18 Images showing the surface morphologies of CNT/nylon composite films under (a) 0%, (b) 2%, (c) 4%, and (d) 7% stretching rate [104].

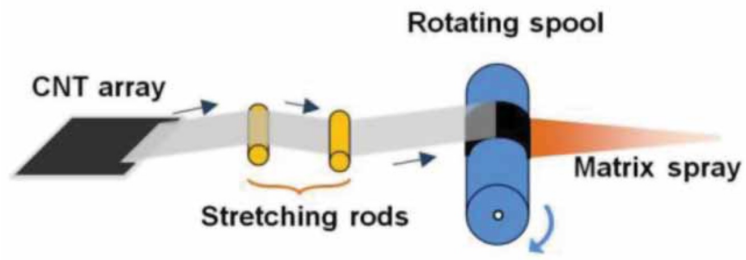

Figure 2.19 Schematic illustration of the concept of straightening CNTs before embedding them in a matrix in a layer-by-layer fashion [107].

dry-drawing CNT sheet before winding it on the mandrel to form a composite [107]. A schematic illustration of the process is shown in Figure 2.19. It was found when the CNT sheet was stretched by 12%, the as-produced CNT/BMI films showed an exceptionally high

tensile strength of up to 3.8 GPa, Young's modulus of up to 293 GPa, electrical conductivity of 1.23×10^5 S/m, and thermal conductivity of 41 W/(m·K).

2.5 Motivations and Research Objectives

Since the discovery of CNTs in early 1990s [3], they have excited scientists and engineers with their wide range of unusual physical and chemical properties, which are direct results of the near-perfect structure of nanotubes. No previous material has displayed the combination of superlative mechanical, thermal, and electrical properties attributed to them. These properties make CNTs ideal, not only for fundamental science but also for a wide range of applications.

As discussed in the previous part, the critical requirements for making high-performance macro-scale CNT assemblies are: long nanotube length, high degree of nanotube alignment, and high CNT straightness, which all maximize load transfer within the structure, promote effective loading, and realize better utilization of the CNT potential. When CNT composite are produced, a high CNT fraction, uniform dispersion, and good CNT-matrix interfacial bonding are also essential. Much progress has been made over the last few years in making CNT buckypapers/dry films and composite films, and their properties are creeping towards which have been predicted by theory. However, there are still many opportunities rising from previous work in achieving improved properties.

One opportunity is to use long-length drawable CNTs to produce dry CNT films. Theoretically, long nanotubes benefit load transfer, which can result in improved mechanical performance of the dry films. This is true when drawable CNTs are made into dry CNT

yarns, that with longer CNT lengths, the yarns exhibit higher tensile strengths [126]. However, this seems not applicable when longer CNTs are made into dry films [102] and composites [66] due to the influence of CNT diameters since CNTs usually exhibit larger diameters when they grow longer. There are very few studies discussing the CNT length effects on the final properties of CNT products, and the mechanism remains unclear. Chapter 4 provides a detailed discussion which focuses on CNT length only, eliminating the effect of CNT diameter.

Another opportunity lies in mitigating CNT waviness. Although stretching the as-formed composite films [104] and stretching the single layer of dry-draw CNT sheet before embedding it into matrix [107] have been proved to be effective in increasing the composite final performance, there are difficulties in the stretching process since the as-formed films are already densely packed that high stretching rate is impossible; while the single-layer of CNT sheet is too brittle to be stretched that careful control of the process and high-quality drawable arrays are needed. In Chapter 5, a novel approach is developed, which can easily and effectively straighten the wavy CNTs in the dry-drawn CNT sheet. This approach takes advantage of the previously reported winding approach [120] which meets all the requirements for making desired high-performance CNT buckypapers, solves the problems existed in the previous stretching process, and meanwhile, realizes enhanced load-bearing efficiency provided by highly straightened and aligned CNTs.

The agglomeration of nanotubes is a big issue when making CNT/polymer composites. And CNT agglomeration happens not only in short CNT dispersed composites, but also in long and aligned CNT composites. When CNTs are too straight and perfectly aligned at a

high fraction, CNTs agglomerate together, causing difficulties for polymer matrix to penetrate, and thus resulting in a non-uniform dispersion. Chapter 6 addresses this issue by infiltrating poly(vinyl alcohol) matrix into the straightened and highly aligned nanotubes. The objective is to develop an understanding of how the mechanical and electrical properties of the as-produced composite films change when a high degree of CNT straightness is achieved.

Chapter 3

General Experimental Procedure

3.1 Growth of Carbon Nanotube Array

The drawable SACNT arrays used in this work were synthesized by CVD method. Electron beam evaporation technique was used to prepare the catalyst to grow CNTs, where a 30 nm-thick SiO_2 layer was first deposited on Si substrate, followed by a 20 nm-thick Al_2O_3 buffer layer, and then a 1 nm-thick layer of Fe catalyst. The thicknesses of Al_2O_3 buffer layer and Fe catalyst layer are very important for they determine the drawability of the CNT arrays.

The SACNT arrays were then grown in a CVD furnace called *EasyTube® 3000* made by *FirstNano®* cooperation (Figure 3.1a). Firstly, the catalyst substrate was put in the load chamber of the furnace, followed by an evacuation of the chamber to below 0.3 Torr. Argon gas was flowed into the load chamber at a rate of 1.5 L/m, meanwhile, the growth chamber was started to heat up. When the pressure in the load chamber reached 756 Torr, the catalyst substrate in the load chamber was loaded into the growth chamber and placed in the center of the heating zone, as shown in Figure 3.1 (b). The growth chamber was vacuumed again to 0.3 Torr and then refilled with argon gas at a flow rate of 4.0 L/m to a pressure of 756 Torr (atmospheric pressure). After that, the growth chamber was heated to 710°C within 10 min at its maximum heating rate with flowing of a mixture of hydrogen at 0.3 L/m and argon at 1.3 L/m. When the temperature reached 710°C, the gas mixture changed to hydrogen at a flowing rate of 0.1 L/m and argon at a flowing rate of 1.6 L/m, while continue heating the chamber. When the temperature of the growth chamber reached 740°C, ethylene was inflated

(a)

(b)

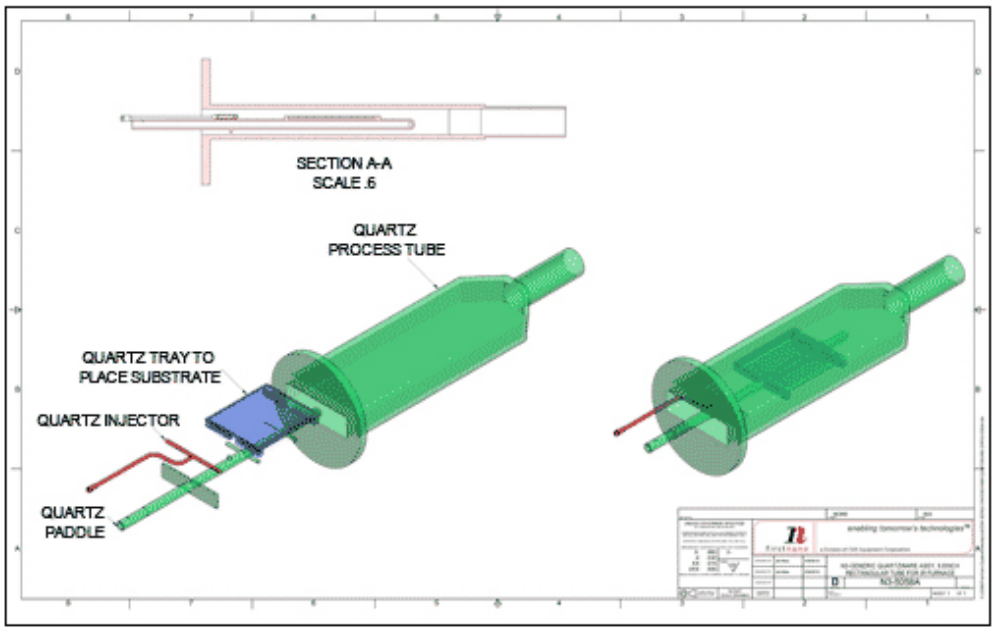

Figure 3.1 (a) Image of *EasyTube® 3000* CVD growth furnace made by *FirstNano®* cooperation; (b) Schematic of the CVD growth chamber and the insertion of the catalyst substrate.

into the chamber at a flow rate of 0.3 L/m, and CNTs started to grow. The growth gas mixture of ethylene, hydrogen, and argon remained at atmospheric pressure during the growth process. The array was grown for 10-20 min, and then the chamber was cooled down and vacuumed again to stop the growth procedure. In order to get the as-grown CNT array out of the growth chamber, argon gas was used to flush the chamber at a rate of 3.0 L/m to increase the pressure of the growth chamber to 756 Torr. Then, the array would be unloaded to the load chamber of the furnace. When the temperature was cooled to approximately 490°C, the load chamber could be opened and the array was taken out. The CNTs grown in this way mainly have 2-5 walls with diameters of 4-8 nm.

3.2 Fabrication of Carbon Nanotube Dry Films and Composite Films

Aligned dry CNT films were fabricated using drawable CNT arrays by a winding technique used widely in previous studies [104,105,107]. In order to study the length effects on the film properties, CNTs with different lengths were produced. The arrays were grown for different time to obtain CNTs with different lengths: 230 μm, 300 μm, and 360 μm. The dry film was formed by drawing a layer of CNT sheet from the CNT array and then wound on a rotating mandrel with a diameter of 3 cm at a rotational speed of 20 RPM. A small needle with a diameter of 0.65 mm and was bent into 90° was placed at 1 o'clock position on the rotating mandrel, with no pressure applied to the CNT sheets. A solution of equal volume of deionized water and ethanol was used to condense the as-wound CNT sheets, and was applied on the needle by a dropper. Two hundred revolutions produced a film with a thickness of 3-5 μm. Then, the film was peeled off from the mandrel and hot-pressed under a

pressure of about 10 MPa at 80°C for 2 hrs to dry the film and further compress it to reduce the thickness and improve the nanotube packing. After hot-pressing, the film thickness was about 2-4 μm.

Dry CNT films and CNT/poly(vinyl alcohol) (PVA) composite films with reduced CNT waviness and improved alignment were fabricated by a newly developed method named "microcombing". In this approach, surgical blades with a teeth width of ~2 μm, and teeth depth of ~0.5 μm were used as micro-combs to disentangle and straighten the wavy CNTs in the dry-drawn CNT sheet. A layer of CNT sheet was drawn out from the as-grown SACNT array, and then passed a pair of parallel surgical blades which were positioned oppositely to comb both the top and the bottom of the sheet. The contact angle between the CNT sheet and the blade was controlled at 80°-85° for an effective microcombing but not causing damage to the CNTs. The degree of microcombing increases with decreasing the contact angles. The CNT sheet with reduced waviness was then taken up to a rotating mandrel with a diameter of 3 cm at a speed of 20 r/min. A metal needle with a diameter of 0.65 mm bent into 90° was placed on the mandrel at 1 o'clock position. When dry CNT films were to make, a condensing solution of equal volume of deionized water and ethanol was dropped on that metal needle to condense the CNT sheet layer by layer during the winding process. The metal needle helped a uniform dispersion of the solution on the CNT sheet. When CNT/PVA composite films were to be fabricated, a PVA solution was used. PVA powder with a molecular weight of 75,000-80,000 and is ≥99.0% hydrolyzed was purchased from Sinopharm Chemical Reagent Co., Ltd.. And the PVA solution was prepared by dissolving 0.1 wt.% of PVA powder into equal volume of deionized water and ethanol.

3.3 Microstructural Analysis

Scanning electron microscopy (SEM) images were taken by HITACHI S-4800 and Verios 460L. The thickness of the as-produced samples and the lengths of the CNTs were measured; the surface morphologies of the microcombing surgical blades, as well as the sample surface and cross-sectional surface morphologies were analyzed. The film samples were mounted on the stage using conductive carbon tapes as the CNTs are conductive.

Transmission electron microscopy (TEM) images were acquired by Tecnai G2 F20 S-TWIN and JEOL-2010F at 200 kV. These images were used to examine the diameter and number of walls of the as-grown CNTs and the surface morphologies of the uncombed and combed CNT sheets. The drawable CNT sheet was pulled out from the array and directly placed on the Cu TEM grid with holey carbon. Then, a droplet of acetone flew through the grid so that the CNT sheet could firmly attach the grid.

3.4 Raman Analysis

The quality of the as-produced CNT arrays were assessed using the Raman spectra collected by a Horiba Labram HR800 system with a 442 nm laser as the excitation source. Samples of CNT arrays were scanned in the Raman shift range of 1200-1800cm^{-1} which covers both D-band and G-band of CNTs. Background noise were reduced before acquiring the intensities, and three different locations were tested for each sample to ensure the consistency of the results.

The degree of CNT alignment in the as-produced dry films was statistically characterized by polarized Raman spectroscopy (BaySpec, 3 in 1 Nomadic^{TM}) using a 532 nm laser beam.

Vertically polarized incident light passed through a notch filter and then scattered within the sample whose alignment axis is rotated to an angle θ with respect to the incident polarization direction. At θ=0°, or when the polarization of the excitation laser's oscillating electromagnetic field is parallel to the nanotube longitudinal axis, the Raman intensity is maximized. While at θ=90°, the Raman scattering from the SWNTs should display a minimum. The ratio of the intensity of the G-band in the parallel configuration to the perpendicular configuration ($I_{G//}/I_{G\perp}$) is particularly sensitive to CNT alignment degree: higher intensity ratio indicates higher degree of CNT alignment.

3.5 X-ray Diffraction Analysis

X-ray diffraction (XRD) analysis was also used to examine the degree of CNT alignment in the film samples. Azimuthal scans of the XRD measurements were performed using Rigaku SmartLab with Eulerian cradle equipped with Cu rotating anode (Kα wavelength of 1.5418 Å). Each pattern was measured using a step size of 1° and a scan rate of 1°/s at 2θ = 23.5°. The CNT alignment can be characterized by the anisotropic angular distribution intensity of the (002) reflection, which is related to the inter-wall distance of nanotubes. A non-uniform (002) intensity indicates the CNTs are aligned. And a smaller full width at half-maximum (FWHM) indicates a higher degree of CNT alignment in the CNT films.

3.6 Mechanical Property Characterization

Mechanical properties of the as-produced CNT films were performed using an Instron 3365 tensile test machine with a load cell of 10 N and a strain rate of 0.5 mm/min. Testing

specimens were made by cutting the films into narrow strips, which were typically 1 mm wide and 15-20 mm long. The samples were then mounted to templates cut from a piece of 1000 grit sandpaper in order to avoid slippage between the samples and grips during testing. The grips were custom built with screw driven clamps. Gauge length of the test was fixed at 10 mm. The width of the specimen was measured using a calibrated scale bar in an optical microscope. The thickness was measured by a micrometer and further confirmed by SEM. At least 10 specimen were tested for each type of CNT film. Failure strain was measured from the grip distance until the sample was fractured. Young's modulus was calculated from the slope of the initial straight-line loading region.

3.7 Electrical Property Characterization

Electrical resistances of the samples were measured using a 4-probe Agilent 34410A 6.5 digit multimeter along the CNT alignment direction. The testing samples were strips of the CNT films which have a width of 1-2 mm and length of 10-30 mm. In order to ensure good electrical contact, silver was coated as electrodes on the samples by magnetron sputtering. The the electrical conductivities of the films were then calculated from the measured resistance values.

Chapter 4

Effects of CNT Growth Length on the Structure and Properties of Aligned Dry CNT Films

Liwen Zhang[a], Xiaolong Ma[a], Da Li[b], Haotian Deng[a], Qingwen Li[b], Philip D. Bradford[c], Yuntian Zhu[a,*]

[a] Department of Materials Science and Engineering, North Carolina State University, Raleigh, NC 27695, USA

[b] Key Laboratory of Nano-Devices and Applications, Suzhou Institute of Nano-Science and Nano-Biotics, Chinese Academy of Sciences, Suzhou 215123, China

[c] Department of Textile Engineering Chemistry and Science, North Carolina State University,Raleigh, NC 27695, USA

Abstract

In this paper we try to discuss the effects of carbon nanotube (CNT) growth length on the structure and properties of the aligned pure CNT films. Few-walled CNTs with the same diameter but different lengths were used to fabricate dry films. The lengths of the CNTs were 230 μm, 300 μm, and 360 μm, respectively. It was found that with increasing CNT length, both the mechanical and electrical properties of the as-produced films decreased. Scanning electron microscopy (SEM) images and polarized Raman spectroscopy revealed that when

CNTs were shorter, they tended to form more tightly packed film structures; the bundles of the CNTs were larger and exhibited a higher degree of alignment. Although shorter CNTs would form more broken ends in the films, the better CNT alignment and tighter nanotube packing played a bigger role in defining the overall properties of the films.

(Submitted to *Nanotechnology*)

4.1 Introduction

Carbon nanotube (CNT) has been a hot research target for the last two decades due to its diverse features, especially the unique and superior mechanical and electrical properties [34,37,42,127]. CNTs' high tensile strength and stiffness along with the low mass density make them attractive fillers for making high performance but lightweight structural composites [20,128]. Their good electrical properties help them find many uses as sensors [129], actuators [130,131], electrodes [132–134], and energy storage devices [19,122,135]. However, it remains a problem that taking full advantage of CNTs' excellent properties when converting them into large-scale structures, limiting their practical applications [136].

Extensive studies have been done in finding ways of exploiting the potential of CNTs. One way is to use long length CNT to fabricate macroscopic CNT products. The highest reported length for the CNTs to date is over half-meter [65], however, CNT lengths usually vary from several micrometers [137] to a few millimeters [85]. The discovery of spinnable super-aligned CNT arrays, where the vertically aligned CNTs could be drawn out to form a continuous CNT sheet with the nanotubes aligned horizontally in the drawing direction [73,84], has provided the most simple and elegant way to utilize the unique one-dimensional properties of CNTs. The CNT sheets are often formed into continuous CNT structures [81], such as CNT yarns [74,81,83,99] and/or films [66,102,103,108,122]. Attempts have been made to improve the mechanical properties of both CNT yarns and films, obtaining strengths ranging from several hundred megapascals to a few gigapascals [83,99,102,103].

The strongest dry CNT yarn (without matrix) exhibited a strength higher than 3 GPa and had a Young's modulus of 205 GPa [99]. In that study, it was found that the CNT yarns made

by longer CNTs tended to have higher strengths. They ascribed this phenomenon to two factors: first, longer CNTs are better load carriers; and second, longer CNTs have less broken ends, which are the flaws that weaken the yarn properties. Fundamental yarn strength equations show that the ratio of the tensile strength of a yarn (σ_y) to that of the component fibers (CNTs) (σ_f) can be approximated by:

$$\frac{\sigma_y}{\sigma_f} \approx \cos^2\alpha[1-(k\csc\alpha)] \quad (1)$$

where $k=(dQ/\mu)^{1/2}/3L$, α is the helix angle that CNTs make with the yarn axis, d is the CNT diameter, μ is the friction coefficient between CNTs, L is the CNT length, and Q is the CNT migration length [138]. From this equation, we can predict that longer CNT length, L, produces higher yarn strength, σ_y.

Ideally, it should also apply to the films that made of CNTs. However, studies show different situations when the aligned CNTs are assembled into films with no twisting. Wang et al. produced CNT/bismaleimide (BMI) composite films with CNT lengths ranging from 0.65 mm to 1.3 mm, with the longer CNTs possessing larger diameters [66]. No apparent relationship was found between the CNT length and the composite mechanical properties. However, the thermal and electrical properties of the composite films increased with the increasing CNT diameter and length, which the authors attributed to more effective phonon and electron conduction path provided by thicker CNTs. Contrary results were reported by Liu et al. [102], in which dry CNT films were made using the CNTs with different lengths and number of walls. It was reported that the films made with shorter CNTs with less number of walls exhibited the highest tensile strength and Young's modulus, but the electrical

property showed no length dependency, which was quite different from Wang's results. Liu et al. attributed the decreasing of the mechanical properties of longer and thicker CNTs to their reduced load carrying capacities. Since the outermost layer of a CNT carries most of the load before fracture, the CNTs with the most number of walls have the lowest ratio of the effective cross sectional area of the outermost layer to the total cross sectional area, i.e. they have the lowest load carrying capacities.

Studies on how the film properties change with CNT lengths have been very limited, and the mechanisms are not clear. Therefore, in this work, we studied in detail the length-based effects of the CNTs and eliminated the effect of the CNT diameter, which was an issue in the above-mentioned studies. It was found that dry aligned films made by shorter CNTs exhibited better mechanical and electrical properties, which arose from greater level of alignment and tighter nanotube packing of the shorter CNTs. Therefore, we conclude that rather than the broken ends which weaken the film properties, the CNT alignment and tight packing are the dominant factors in determining the film's final properties.

4.2 Experimental

4.2.1 Growth of CNT Arrays

The spinnable super-aligned CNT arrays used in the experiment were grown on silicon substrates using a chemical vapor deposition (CVD) method. The catalyst used in the study were Al_2O_3 (20 nm)/Fe (1 nm), which were deposited on a silicon wafer (with a 30 nm SiO_2 layer) using an electron beam evaporation technique. Then, the substrate was put in a 5-inch quartz tube furnace to grow the CNT array at 740°C by introducing a mixture of ethylene,

argon, and hydrogen into the reaction system at atmospheric pressure. Ethylene was the carbon source, and argon and hydrogen acted as the forming gas. The flow rates of argon, hydrogen and ethylene were 1.6 L/min, 0.1 L/min, and 0.3 L/min, respectively. By varying the growth time, arrays with different CNT lengths were obtained. Three different CNT lengths of 230 μm, 300 μm, and 360 μm were produced, with respective growth times of 12 min, 15 min, and 20 min. Attempts have also been made to grow shorter and longer CNTs. But due to the limitation of our technique, those arrays did not have a good spinnability, which would introduce a big human error when used for fabricating films.

4.2.2 Preparation of the Dry CNT Films

The aligned dry CNT films were fabricated by a winding technique used widely in previous studies [104,105,107]. Figure 4.1 is the schematic of the process. A layer of CNT sheet was drawn out from the spinnable CNT array and then wound on a rotating mandrel with a diameter of 3 cm at a rotational speed of 20 RPM. A small needle with a diameter of 0.65 mm and was bent into 90° was placed at 1 o'clock position on the rotating mandrel, with no pressure applied to the CNT sheets. A solution of equal volume of deionized water and ethanol was used to condense the CNT sheets, and was applied on the needle by a dropper, as shown in Figure 4.1. The needle helped to uniformly spread the solution on the CNT sheets, bringing an even condensation of the CNTs.

Two hundred revolutions produced a film with a thickness of 3-5 μm. Then, the film was peeled off from the mandrel and hot-pressed under a pressure of about 10 MPa at 80°C for 2

hrs to dry the film and further compress it to reduce the thickness and improve the nanotube packing. After hot-pressing, the film thickness was about 2-4 μm.

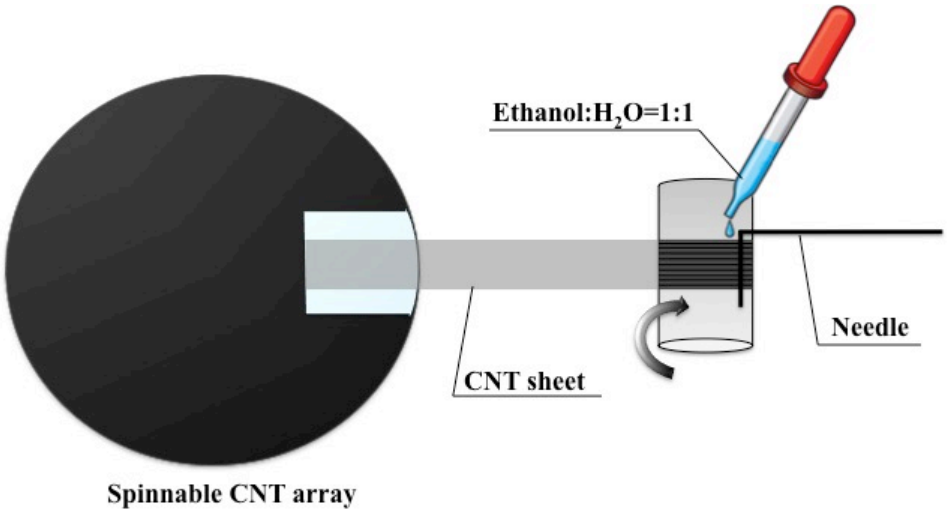

Figure 4.1 Schematic of the preparation of the dry CNT films.

4.2.3 Characterization Methods

Transmission electron microscopy (TEM) images of the individual CNTs were obtained using a JEOL-2010F microscope operated at 200 kV to characterize the diameter and number of walls of individual CNTs. For each CNT length, about 120-150 images were taken, and then were analyzed by ImageJ software. Quality of the CNT arrays were assessed using the Raman spectra collected by a Horiba Labram HR800 system with a 442 nm laser as the excitation source. 6 measurements were made for each array. Scanning electron microscopy (SEM, Verios 460L) was used to measure the lengths of the CNTs and the structures of both the CNT arrays and the as-produced dry CNT films.

Mechanical tests were performed using an Instron 3365 tensile test machine with a load cell of 10 N and a strain rate of 0.5 mm/min. The testing specimens were narrow strips, which were typically 1 mm wide and had a gauge length of 10 mm. More than 10 specimens were tested for each type of samples. The width of the specimen was measured using a calibrated scale bar in an optical microscope. The thickness was measured by a micrometer and further confirmed by SEM. A 4-probe Agilent 34410A 6.5 digit multimeter was used to measure the electrical conductivity of the films along the CNT alignment direction. Silver electrodes were applied to the samples using magnetron sputtering. To calculate the film density, the weight of each specimen was determined using a MX5 microbalance by Mettler-Toledo, Inc., which had an accuracy of 1 microgram. The CNT alignment degrees in the as-produced dry films were statistically characterized by polarized Raman spectroscopy (BaySpec, 3 in 1 Nomadic^{TM}) using a 532 nm laser beam. 3 to 7 measurements were taken for each sample.

4.3 Results and Discussion

4.3.1 Morphologies of Individual CNTs

The CNTs were grown vertically on the array substrates using the CVD method, therefore the lengths of the CNTs could be determined by the array heights, as shown in SEM images in Figure 4.2. The distributions of the number of walls and diameters are displayed in the histograms in Figure 4.2, which were obtained from statistical analysis of the TEM images of the nanotubes. The TEM samples of the CNTs were prepared in the same way as described in ref. [66], in which way the observed morphologies of the CNTs were

mostly preserved as they were in the dry films. It was found that for all different CNT lengths, the CNTs mainly had 2-3 walls and a diameter range of 4-10 nm. The average diameters for the CNTs with three different lengths were about 5 nm, with no significant statistical differences between them, as shown in Figure 4.2 (d) and Table 4.1.

In order to characterize the array qualities, Raman spectra were recorded. The results are summarized in Table 4.1 and the representative spectra are shown in Figure 4.3. For 230 μm CNT array, the ratio of the intensity of the G-band to that of the D-band (I_G/I_D) has an average value of about 3.64, while for 300 μm and 360 μm CNT arrays, they are 2.96 and 2.42, respectively. The larger I_G/I_D ratio for shorter CNTs indicates a more graphitic structure with less disorder such as structural defects and amorphous carbons [139]. Amorphous carbons are likely the major issue for our CNT arrays, since it takes longer time to grow longer CNTs, more amorphous carbons can deposit on the surfaces of already grown CNTs [74].

Table 4.1 CNT morphological changes as a function of growth time.

CNT length (μm)	Growth time (min)	Diameter (nm)	Aspect ratio	Raman I_G/I_D
230	12	5.37 ± 1.14	43,000	3.64 ± 0.30
300	15	5.50 ± 0.83	55,000	2.96 ± 0.26
360	20	5.71 ± 0.76	63,000	2.42 ± 0.20

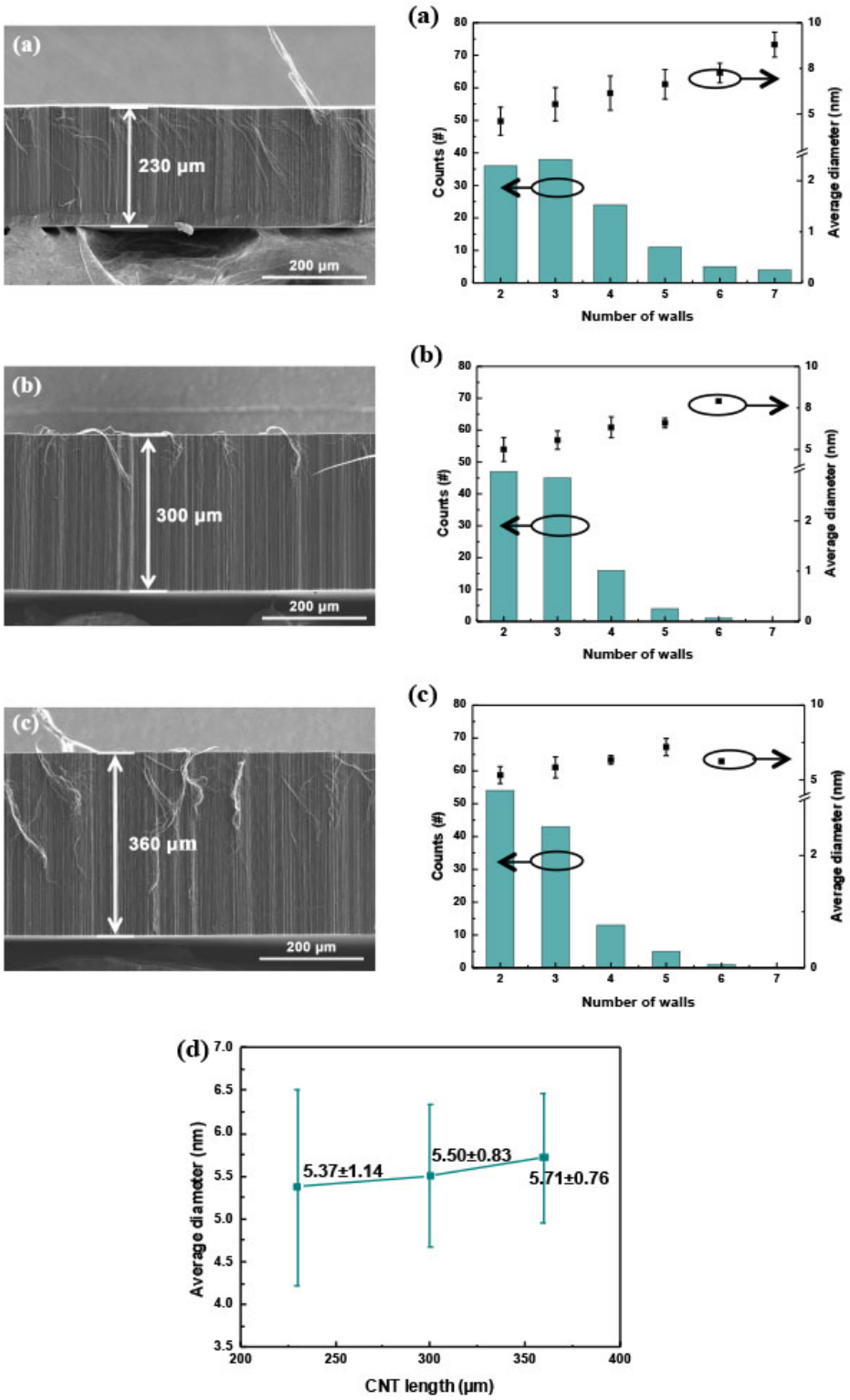

Figure 4.2 Figures showing the lengths of the CNTs, and the distribution of the diameters and number of walls of the CNTs with different lengths.

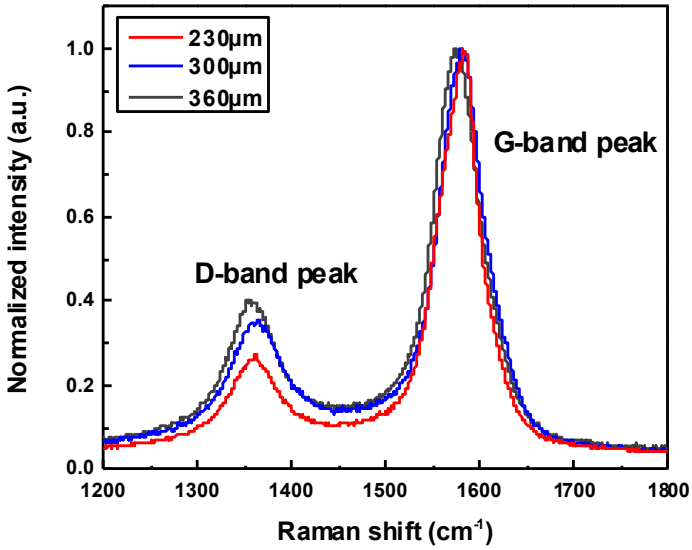

Figure 4.3 Representative Raman spectra of the CNT arrays with different CNT lengths.

4.3.2 Film Mechanical and Electrical Properties

We used a winding process to fabricate our aligned CNT films with ethanol solution condensing the film during the process. While CNTs were drawn and wound, the interactions between the CNTs and the CNT and ethanol solution were all determined by the original properties of the CNTs. As discussed earlier, the only differences for the three types of CNTs used in our study are the amorphous carbons and structural defects, which were caused by different growth times that directly resulted in different CNT lengths. In this case, we can say that the CNTs grown into different lengths exhibit different properties, and these properties determine how the CNTs assemble in the as-produced dry films. Therefore, we use the CNT length as the feature, and the three different types of aligned dry CNT films fabricated using different CNT lengths are named CNTF 230, CNTF 300, and CNTF 360, respectively.

The mechanical and electrical properties of the as-produced dry CNT films are summarized in Figure 4.4 and Table 4.2. Whereas CNT yarns showed increasing mechanical properties for longer CNTs [99], our results revealed that both the mechanical and electrical properties of the films decreased with increasing nanotube length, and the trend was not linear. The dry films made of the 230 μm long CNTs had an average Young's modulus of about 151 GPa, which was dramatically higher than that of the CNTF 300 and CNTF 360 samples, which were about 35 GPa and 31 GPa, respectively. The difference between the CNTF 300 and CNTF 360 samples was not statistically significant. The tensile strengths and electrical conductivities of the 3 films followed the same trend as the Young's modulus, as shown in Figure 4.4 (c).

Table 4.2 Summary of mechanical and electrical properties of CNTF 230, CNTF 300, and CNTF 360.

Type of films	Density (g/cm^3)	Modulus (GPa)	Tensile strength (MPa)	Strain (%)	Electrical conductivity (S/cm)
CNTF 230	0.8413±0.0024	151±18	1561±188	2.95±0.32	985±12
CNTF 300	0.8409±0.0117	35±2	956±67	3.51±0.32	560±1
CNTF 360	0.7404±0.0407	31±4	817±119	3.52±0.56	443±41

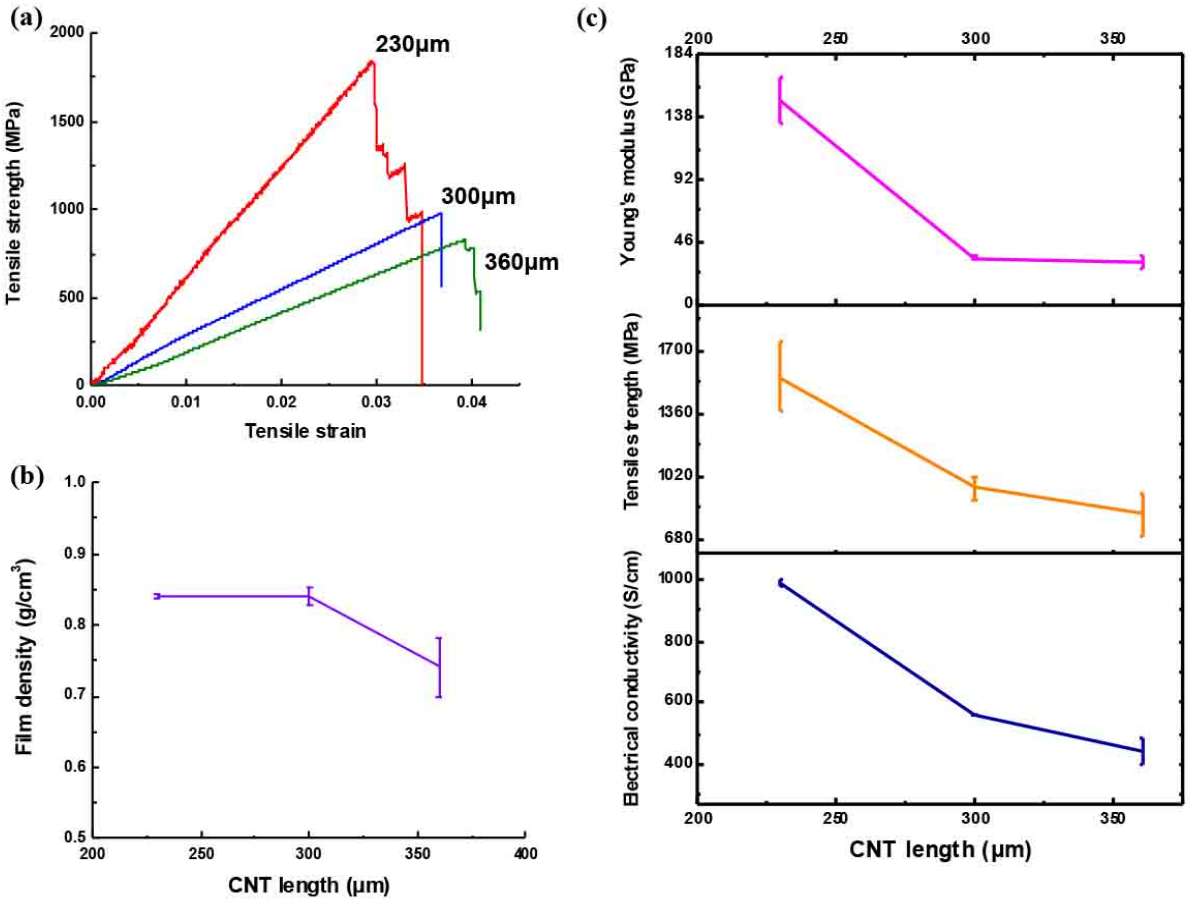

Figure 4.4 Mechanical and electrical properties of the as-produced dry CNT films made with different CNT lengths: (a) Typical stress-strain curves; (b) Film densities; (c) Comparison of the Young's modulus, tensile strength, and electrical conductivity of the dry films.

The densities of the as-produced dry films were measured, and the result was presented in Figure 4.4 (b). It was found that all three films had a very low density (< 1.0 g/cm^3), in the meantime films made by shorter CNTs showed a little bit higher value, indicating denser structural packing. This could also be seen in the low magnification SEM images in Figure 4.5, which showed the overall morphologies of the film CNTF 230, CNTF 300, and CNTF 360. It was obvious that film CNTF 230 exhibited more dense regions than film CNTF 300 and film CNTF 360. Large part of the CNTs in film CNTF 230 were tightly bound together

forming a very smooth film surface. The region of loose CNT bundles was small. When the CNTs became longer to 300 μm, the dry film contained more regions of loose CNT bundles and the tight-packing region became smaller. The structure was even looser for film CNTF 360. These were in accordance with the Raman results of the CNT arrays, that the growth of longer CNTs accumulated more amorphous carbons deposited on their surface, the presence of more amorphous carbons would increase the roughness of the CNTs, and thus, hinder the tight packing between the CNT bundles, decreasing the load transfer. The well graphitized CNTs usually favor increased van der Waals interactions and electron transfer along the CNTs, which in turn would benefit the overall mechanical and electrical properties for the dry CNT films [66].

Although shorter CNTs tend to have more broken ends, which would be the weak points for the films during deformation [99], the higher Young's modulus and tensile strength for the films made by shorter CNTs reveal that tight structural packing of the CNTs, rather than the number of ends, is the dominant factor in determining the mechanical properties of the films. Further more, higher graphitic structures in the shorter CNTs support electron transfer along the nanotubes [66], and more inter-tube contact areas resulted from tighter nanotube packing facilitates the electron transfer between the CNTs [107]. These factors all together resulted in better electrical conductivity for the dry CNT films made by shorter CNTs.

The alignment degree of the CNTs in the film is another essential factor that significantly affects the film's mechanical and electrical properties. Although the CNTs in the spinnable arrays were super-aligned and quite straight (Figure 4.6), they exhibited an entangled and wavy morphology when they transformed from vertically aligned state in the arrays to

horizontally aligned state in the dry films, and three different CNT lengths might result in different CNT alignment degrees, as indicated by the high magnification SEM images as shown in Figure 4.7. When forming the dry films, CNTs bound together to form large bundles, and those bundles had a preferred orientation in the film winding direction. From the SEM images in Figure 4.7, it was obvious that the film CNTF 230 contained much larger bundles than the other two films made by longer CNTs, and those large bundles had a much higher degree of alignment. For film CNTF 300 and film CNFT 360, the alignments of the CNT bundles were worse and there were much smaller and wavier bundles.

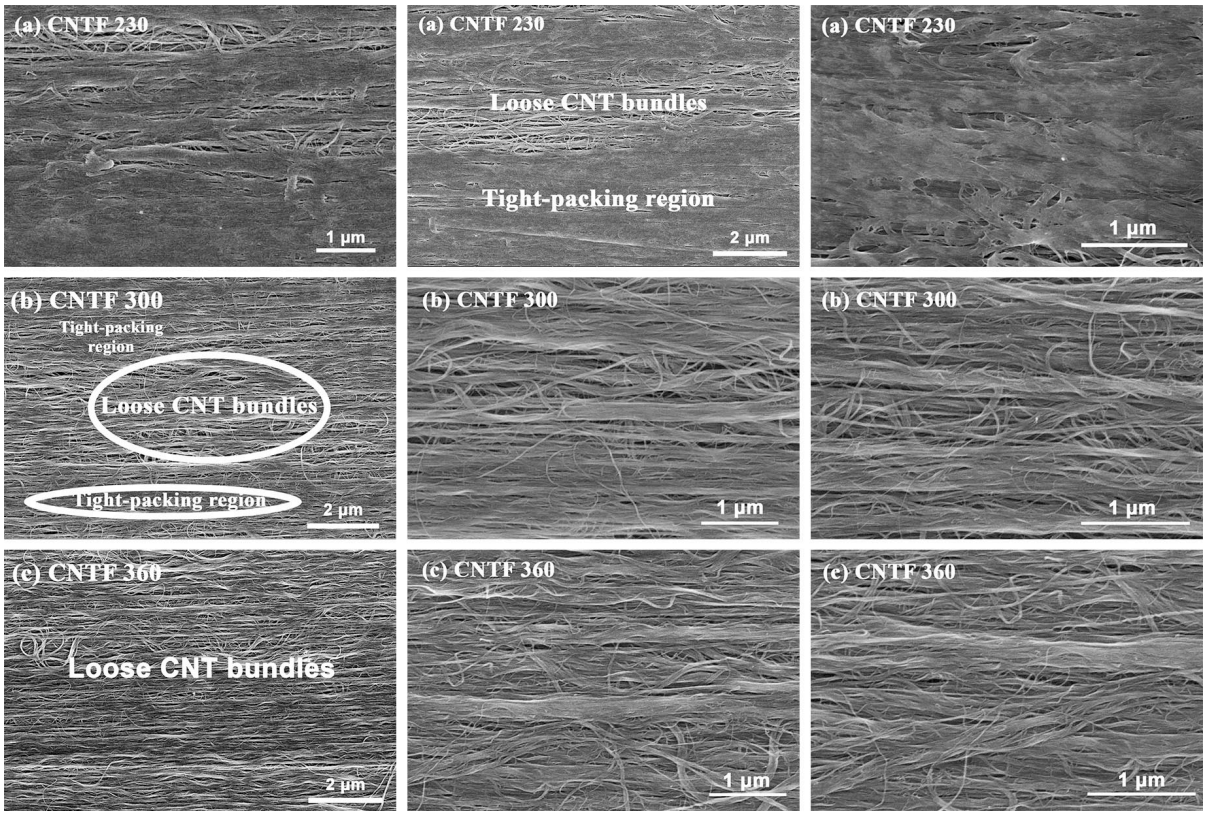

Figure 4.5 Low magnification SEM images showing the overall morphologies of the film CNTF 230 (a), CNTF 300 (b), and CNTF 360 (c).

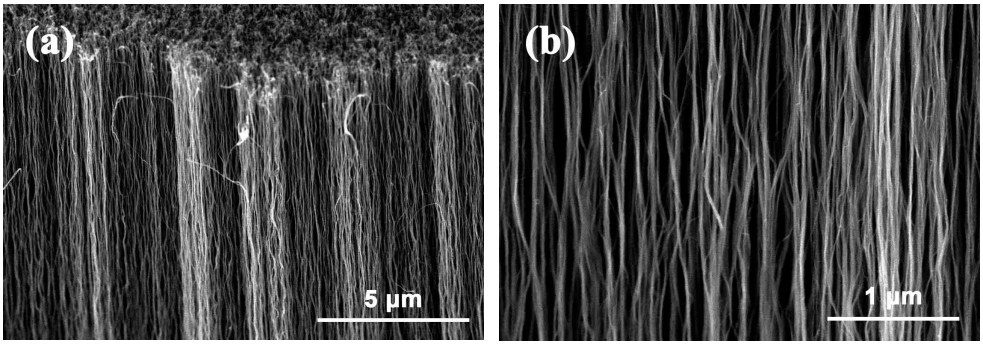

Figure 4.6 SEM images of the super-aligned CNTs in the array.

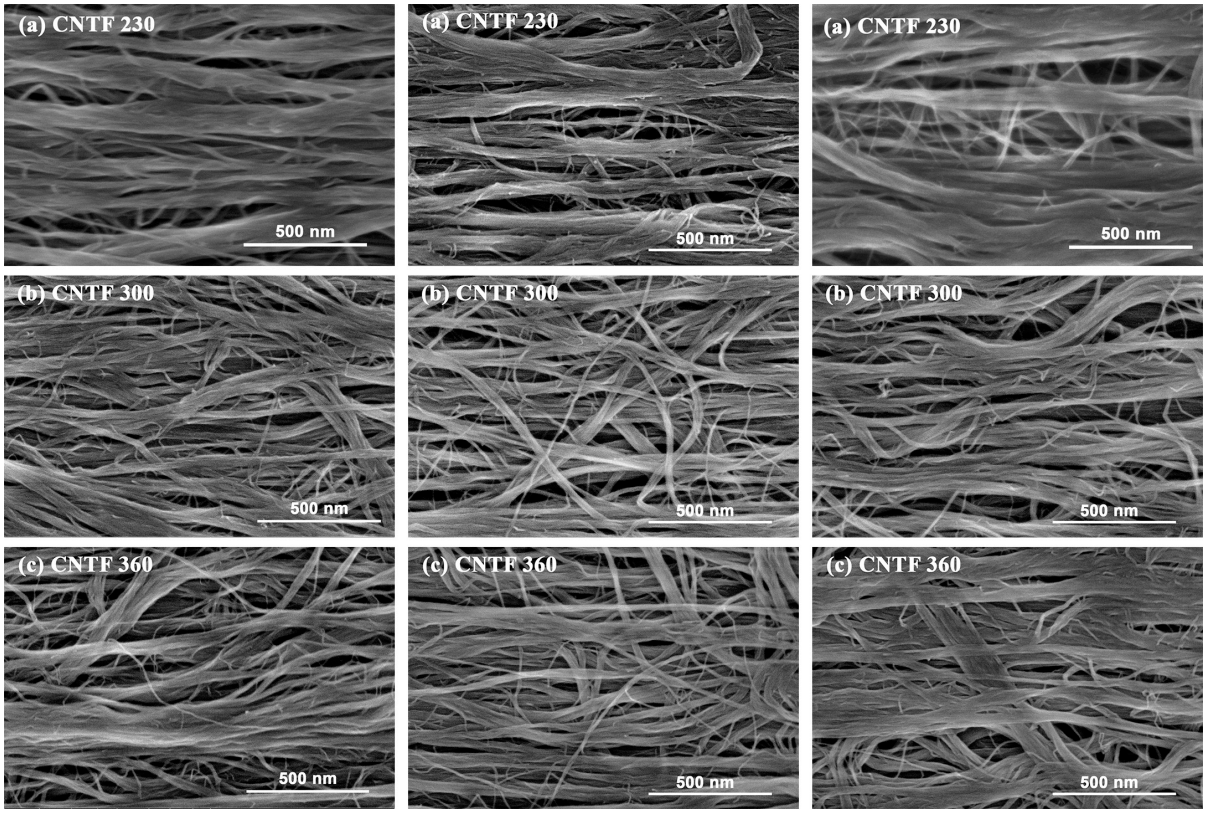

Figure 4.7 High magnification SEM images showing the degree of alignment and wavy morphologies of the CNT bundles in the film CNTF 230 (a), CNTF 300 (b), and CNTF 360 (c).

To better characterize this feature, polarized Raman spectroscopy was conducted and the results were shown in Figure 4.8. Theoretically, the CNT alignment degree can be described by the ratio of the intensity of $G_{//}$ to the intensity of $G_{\perp}$, where parallel configuration represents that the polarization direction of the excitation laser beam is parallel to the nanotube alignment direction, i.e. $\theta=0°$; and the perpendicular configuration is when $\theta=90°$ [140–142]. Higher CNT alignment degree should result in a higher intensity ratio. As shown in Figure 4.8, a typical G-band intensity ratio for film CNTF 230 is about 2.54; while for film CNTF 300 and CNTF 360, the ratios show a great decrease to 1.15 and 1.10, respectively. This quantitative analysis suggested a much higher CNT alignment degree in the film CNTF 230 than that for film CNTF 300 and CNTF 360. On the other hand, the decrease of the $G_{//}$ to $G_{\perp}$ ratios followed a similar trend as the decrease of the film's mechanical and electrical properties (Figure 4.4c). This explains what has not been clarified previously by the film packing density: film CNTF 230 and film CNTF 300 exhibited a similar density, but their mechanical and electrical properties showed a great difference. In comparison, although the density for film CNTF 300 was higher than that for film CNTF 360, their CNT alignment degrees were similar, resulting in similar mechanical and electrical properties. Therefore, in this case we conclude that the CNT alignment played a more significant role than the film packing density in determining the overall performance of the CNT films. Interestingly, the failure strains of film CNTF 300 and film CNTF 360 were larger than that of film CNTF 230 (Figure 4.4a), because during tensile deformation, the wavy bundles would be straightened first, and then aligned in the tensile direction to carry load.

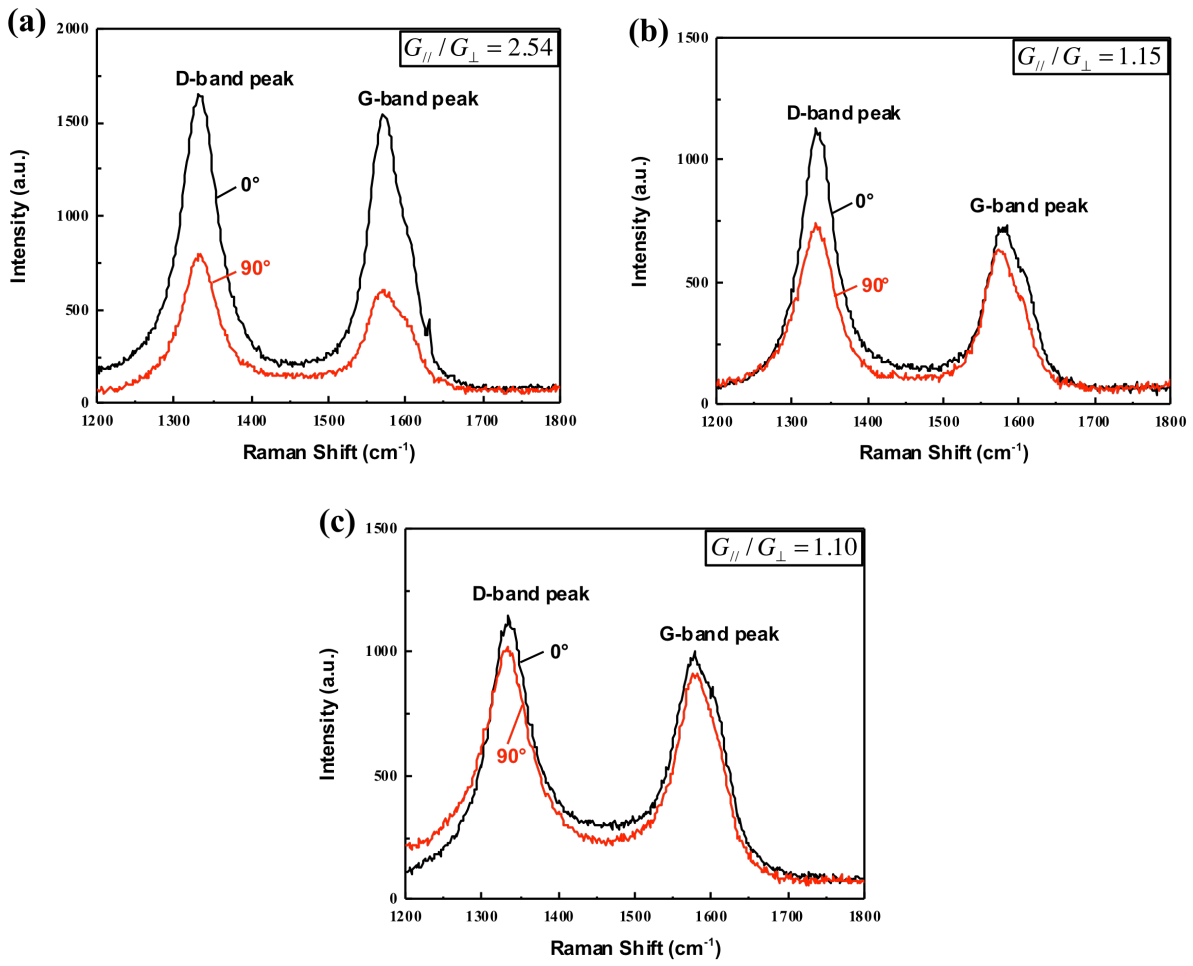

Figure 4.8 Polarized Raman spectra of the D and G bands from film CNTF 230 (a), CNTF 300 (b), and CNTF 360 (c). 0° corresponds to a configuration where the polarization direction of the laser beam is parallel to the CNT alignment direction, while 90° corresponds to a configuration where the polarization direction of the laser beam is perpendicular to the CNT alignment direction.

4.4 Conclusions

In this study, dry CNT films made by 230 μm-, 300 μm- and 360 μm-long CNTs were fabricated by a winding process, and were used to examine the length effects on the film's structure and mechanical and electrical properties. It was found the films made of 230 μm CNTs exhibited the highest Young's modulus, tensile strength, and electrical conductivity.

The mechanical and electrical properties decreased sharply for the films made of 300 μm and 360 μm CNTs. Although shorter CNTs have more broken ends, our study reveals the degree of CNT alignment and tight structural packing are more important in determining the film overall properties. When CNTs are longer, they are wavier and have more amorphous carbons and structural defects, all of which decrease the van der Waals interactions between the CNT bundles, leading to looser packing of the as-produced dry films, thus, lower mechanical and electrical performance. If we can grow higher CNT arrays with the same quality as the lower ones, then, the dry films made by longer CNTs are expected to have the same CNT alignment degree and structural packing density as those made by shorter CNTs. In this case, the longer CNTs would result in better overall performance of the dry films, which is a different case from our study.

Acknowledgements

This work was funded by the US Air Force Office of Scientific Research (Grant No. FA9550-12-1-0088). The authors thank Jiali Yu, a student in University of Delaware, in measuring the weights of the dry films. The authors acknowledge the use of the Analytical Instrumentation Facility (AIF) at North Carolina State University, which is supported by the State of North Carolina and the National Science Foundation.

Chapter 5

Strong and Conductive Dry CNT Films by Microcombing

Liwen Zhang[a], Xin Wang[a], Weizong Xu[a], Yongyi Zhang[b], Qingwen Li[b], Philip D. Bradford[c], Yuntian Zhu[a,*]

[a] Department of Materials Science and Engineering, North Carolina State University, Raleigh, NC 27695, USA

[b] Suzhou Institute of Nano-Science and Nano-Biotics, Chinese Academy of Sciences, Suzhou, Jiangsu 215123, China

[c] Department of Textile Engineering Chemistry and Science, North Carolina State University, Raleigh, NC 27695, USA

Abstract

In order to maximize the carbon nanotube (CNT) buckypaper properties, it is critical to improve their alignment and reduce their waviness. In this paper, a novel approach, microcombing, is reported to fabricate aligned CNT films with a uniform structure. High level of nanotube alignment and straightness was achieved using sharp surgical blades with microsized features at the blade edges to comb single layer of CNT sheet. These microcombs also reduced structural defects within the film and enhanced the nanotube packing density. Following the microcombing approach, the as-produced CNT films demonstrated a tensile

strength of up to 3.2 GPa, Young's modulus of up to 172 GPa, and electrical conductivity of up to 1.8×10^5 S/m, which are much superior to previously reported CNT films or buckypapers. More importantly, this novel technique requires less rigorous process control and can construct CNT films with reproducible properties.

(Published in *Small*, 2015, 11(31): 3830-3839)

5.1 Introduction

Carbon nanotubes (CNTs), with superior mechanical properties, high thermal and electrical conductivities, have been the focus of extensive research for structural composites [99,105], thermal interface materials [127,143,144], and electrical conductors [145–147]. Researchers have devoted great effort to exploring high strength and lightweight CNT reinforcements for composites, by designing novel structures of CNT assemblies at the micro- and nano- scales [21,73,122,128,148,149]. CNTs, as reinforcements for composites, have been developed in the forms of fibers and films (also named buckypapers, sheets, where buckypaper often specifically refers to randomly oriented CNT paper). Among these, CNT films and buckypapers have drawn increasing interest due to their outstanding 2D or 3D properties, easy fabrication, and amenability for scaled-up production.

In solution-based or melt-processing fabrication of CNT films and buckypapers, the large surface area and high aspect ratio of CNTs make them extremely difficult to disperse in solution or melt, and thus gives rise to non-uniform structures [122]. Short CNTs (< 10 μm), although easier to disperse, usually render inefficient load transfer across the weakly bonded interfaces in resultant composites [128], as the short nanotubes are only held by weak van der Waals forces. Consequently, the mechanical properties of CNT buckypapers produced by short-CNT dispersion have very low strengths of only about 10 MPa and low Young's moduli of less than 1 GPa [118,119,130,150–152]. These are far below the properties of individual CNTs and would limit their potential for envisioned applications. Many attempts have been made to improve the mechanical and electrical properties of buckypapers through promoting nanotube dispersion [150,151,153,154] or increasing inter-tube bonding to

construct a 2D or 3D CNT network within the buckypaper [118,155]. However, no significant progress has been made in achieving the predicted properties.

Recently, it has been found that the CNT alignment has a profound impact on the mechanical and electrical properties of CNT films and buckypapers [112,115,152,156,157]. "Domino pushing" and "shear pressing" approaches have been developed to fabricate aligned CNT buckypapers directly from vertically aligned CNT arrays [112,115]. The long and aligned CNTs have effective contacts against each other along their alignment direction, and thus contributing to efficient load and electron transfer. However, the size of the as-produced buckpaper is usually limited by the size of the array substrate because of the nature of "domino pushing" and "shear pressing" approaches. In another work, CNT buckypapers produced by the floating catalyst chemical vapor deposition (FCCVD) method were processed by a stretching-pressing approach and resulted in a high degree of CNT alignment and thus increased the tensile strength by 200% [157] compared with the nonstretched ones [158,159]. In 2002, Fan and coworkers developed drawable CNTs, which allow a vertically super-aligned CNT array to convert into a horizontally aligned 2D CNT sheet [73]. Rather than the 3D CNT array, this 2D CNT sheet has a high degree of CNT alignment in the horizontal direction, which maximizes the potentials of the CNTs while constructing them into multiple forms, such as CNT yarns and layered CNT films. Inoue et al. took advantage of this drawable feature of the super-aligned CNTs, used a winding method to fabricate anisotropic CNT films from multi-walled CNT arrays, and achieved a tensile strength of 75.6 MPa and an electrical conductivity of 4×10^4 S/m [136]. In 2012, Di et al. used few-walled CNT arrays to produce aligned CNT films by a similar winding method coupled with

ethanol-densification, and achieved a tensile strength up to 2 GPa and Young's modulus up to 90 GPa [120]. More recently, they renewed their record to 2.96 GPa and 124 GPa for the tensile strength and Young's modulus by densification using ethanol and acetone, respectively [121].

Apart from CNT alignment, another critical issue that limits the CNT film property is CNT waviness, as pointed out in our previous work [104,107]. In approaches of fabricating CNT/Polymer composite films, stretching was proved effective in reducing CNT waviness and improving composite properties. However, stretching of a single layer of aligned CNT sheet is extremely difficult. It requires exceptionally careful control of stretching rate and very high quality of drawable CNT arrays.

In this work, we present a simple and effective approach, called "microcombing", to reduce CNT waviness directly at their single-layer level before the potential formation of large CNT bundles. Principally based on the previously reported winding technique, this method, for the first time, utilizes a micro-scale rough surface to locally mitigate entangled bundles and straighten the wavy CNTs. The as-combed single layer of CNT sheet exhibits high level of nanotube alignment and straightness, which leads to a uniform structure of CNT film with a tensile strength of up to 3.2 GPa, Young's modulus of up to 172 GPa, and electrical conductivity of up to 1.8×10^5 S/m. More importantly, the microcombing approach is not restricted to high quality of drawable arrays, requires less rigorous process control, and can construct CNT films with reproducible properties.

5.2 Experimental

5.2.1 Materials

The drawable CNT arrays used in the experiment were synthesized using a chemical vapor deposition method [120]. The CNT arrays were approximately 200 μm in height, with individual nanotubes having 2-5 walls and 5-7 nm in diameters.

5.2.2 Microcombing Process

The key component of the process, microcombing of individual layer of CNT sheets, is accomplished by using two oppositely positioned surgical blades. Scanning electron microscopy (SEM) images (Figure 5.1) of the blade edge show micro-features (teeth width: ~2μm, teeth depth: ~0.5μm), which can act as micro-combs to disentangle and straighten the wavy CNTs.

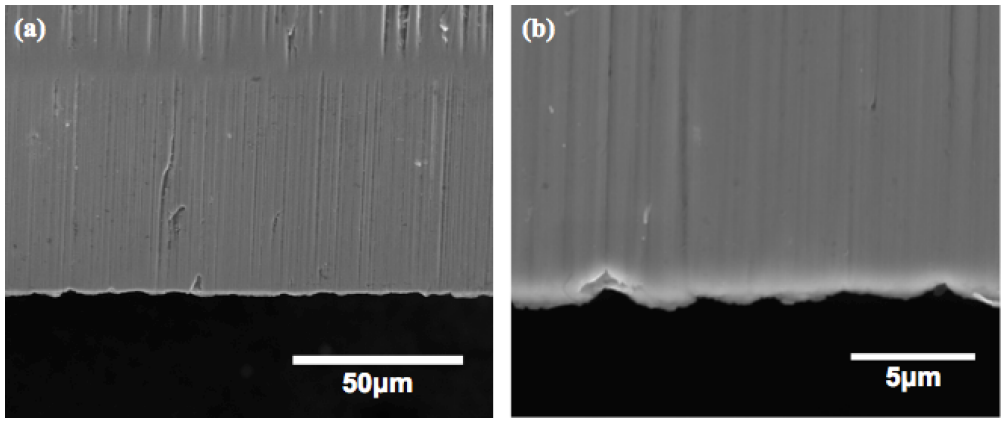

Figure 5.1 Micro-features of the edge of the microcombing blade.

The experimental setup is shown by the schematics in Figure 5.2, when a layer of CNT sheet was drawn out from the CNT array, it passed two surgical blades, then wound to a rotating mandrel with a diameter of 3 cm at a speed of 20 r/min. The contact angle between the CNT sheet and the blade was controlled at 80°-85°. A metal needle with a diameter of 0.65 mm bent into 90° was placed on the mandrel at 1 o'clock position, coating the densifying solution on the CNT sheet layer by layer during the winding process, as shown in Figure 5.2 (b). The densifying solution consists of deionized water and ethanol with a mixing ratio of 1:1 by volume.

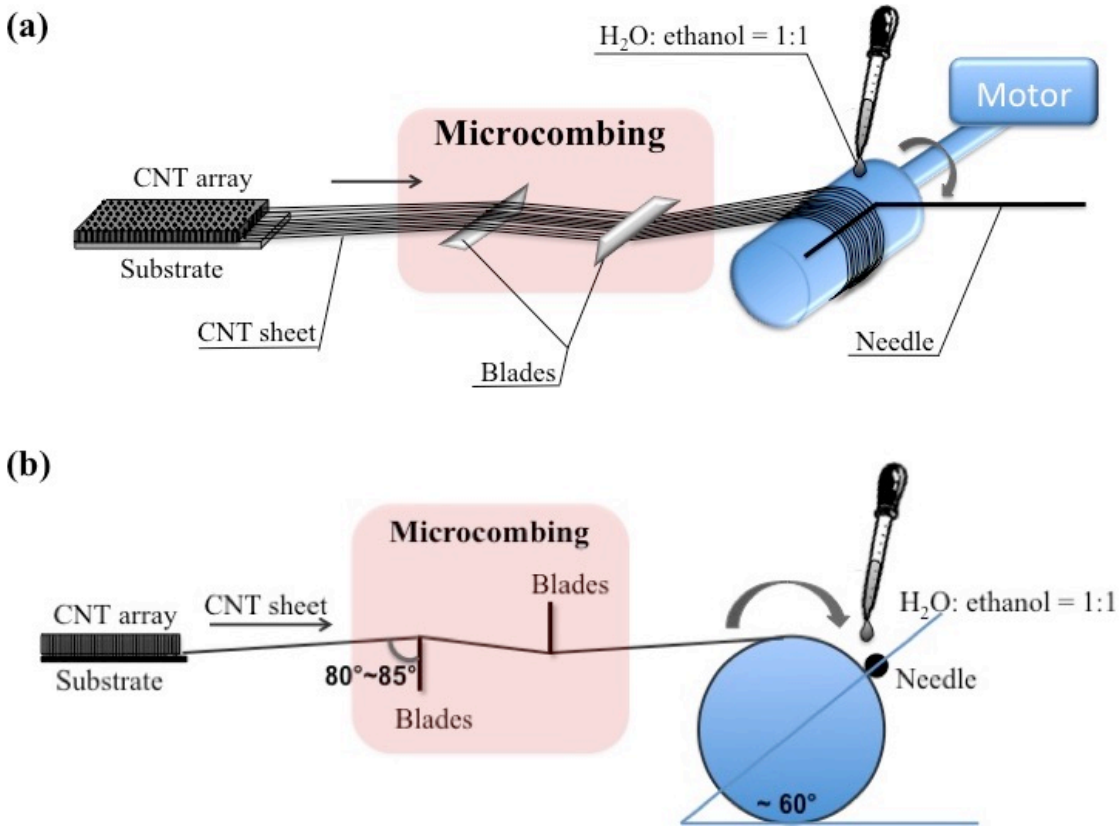

Figure 5.2 Microcombing process: (a) Schematic overview; (b) Schematic side view.

200 revolutions produced a film with a thickness of about 3 μm. The CNT film was then peeled off from the mandrel and hot-pressed at 80°C for 2 hrs under a pressure of 10 MPa. Under high pressure, the film was condensed to about 2 μm. Since the coating solution was H_2O and ethanol, they evaporated during the process, leaving a pure dry CNT film with aligned long CNTs.

5.2.3 Characterization Methods

Tensile test specimens were cut from both the uncombed and combed dry CNT films. The test coupons are typically 1-mm wide and a gauge length of 10 mm. The width was measured using a calibrated scale bar in an optical micrometer. The sample thickness was measured by a micrometer and further confirmed by SEM (HITACHI S-4800). Tensile tests were conducted using an Instron 3365 tensile testing machine with a load cell of 10 N and a strain rate of 0.5 mm/min. The weight of each specimen was measured at University of Delaware using a MX5 microbalance by Mettler-Toledo, Inc., which had an accuracy of 1 mg. Specimen density was calculated based on the measured dimension and weight. Surface morphology of both the combing blades and the as-produced dry films were analyzed by SEM (Verios 460L) and transmission electron microscope (TEM, Tecnai G2 F20 S-TWIN). A 4-probe Agilent 34410A 6.5 digit multimeter was used to test the electrical conductivity of the films along the CNT direction. Silver electrodes were produced by magnetron sputtering.

5.3 Results and Discussion

5.3.1 Mechanical Properties

Table 5.1 and Figure 5.3 compare the mechanical properties of the dry CNT films produced by microcombing with previously reported data. The CNT buckypapers made of short CNTs are named as short-CNT buckypapers; the buckypapers produced by FCCVD method are called floating-CNT buckypapers; and the CNT films made by winding 2D CNT sheet from the drawable arrays are called aligned CNT films. The tensile strength of the as-produced uncombed dry CNT films of (1.56 ± 0.19) GPa agrees well with the previously reported data for aligned CNT films (1.0-2.0 GPa). By microcombing, the tensile strength of the CNT film was improved by 105% from (1.56 ± 0.19) GPa to (3.21 ± 0.21) GPa, which surpasses the mechanical properties of CNT films or buckypapers reported earlier. Also, the Young's modulus has a ~14% increase to (172 ± 13) GPa compared with the uncombed films. The density of the uncombed dry films is 0.84 g/cm^3, whereas the density of the combed dry films is 1.04 g/cm^3. Thus, the specific tensile strength of the combed dry CNT films is calculated to be 3.08 GPa g/cm^3. The higher density of the combed dry CNT films indicates enhanced nanotube packing resulted from microcombing. In comparison, the reported density of the aligned CNT films is typically 0.9 g/cm^3 [120], which is lower than our combed films. With a higher packing density, the aligned CNTs have a stronger inter-tube interaction, which in turn results in a more effective load transfer in the structure.

Table 5.1 Mechanical property comparison for buckypapers and dry CNT films.

Type	Material	Treatment	Young's modulus (GPa)	Tensile strength (MPa)	Ref.
Short-CNT buckypapers	SWCNT		1.2	10	[130]
	SWCNT	HNO_3	0.8 5	10 74	[150]
	SWCNT	$SOCl_2$	0.66 0.95	11 37	[151]
	SWCNT	Irradiation	1.5 3.5	6 ~ 15 80	[118]
	MWCNT		0.4 ~ 0.8	4.3 ~ 7.5	[119]
	SWCNT		0.9	14.2	[152]
	SWCNT	Oleum + heat	8	30	[153]
	MWCNT	Chemicals	0.08 ~ 1.16	0.42 ~ 3.88	[154]
Floating-CNT buckypapers	MWCNT	30% stretch 35% stretch 40% stretch	1.10 11.93 18.21 25.45	205 390 508 668	[156]
	Few-walled CNT	Stretch Stretch+press once Stretch+press twice	3.2 ± 0.5 11.9 ± 0.6 13.4 ± 0.5 15.4 ± 1.0	186 ± 19 307 ± 28 416 ± 25 598 ± 36	[157]
	SWCNT	Purification	188 139	144 107	[158]
	SWCNT		5	360	[159]
Aligned CNT films	Few-walled CNT		33.4 ~ 92.5	950 ~ 1973	[120]

Table 5.1 Continued.

Few-walled CNT		40 ± 5	1.04 ± 0.07 (GPa)	[121]
	Ethanol-densified	124 ± 14	2.34 ± 0.31 (GPa)	
	Acetone-densified	99 ± 11	2.96 ± 0.29 (GPa)	
Few-walled CNT	**Uncombed**	**151 ± 18**	**1561 ± 188**	**This work**
	Combed	**172 ± 13**	**3206 ± 212**	

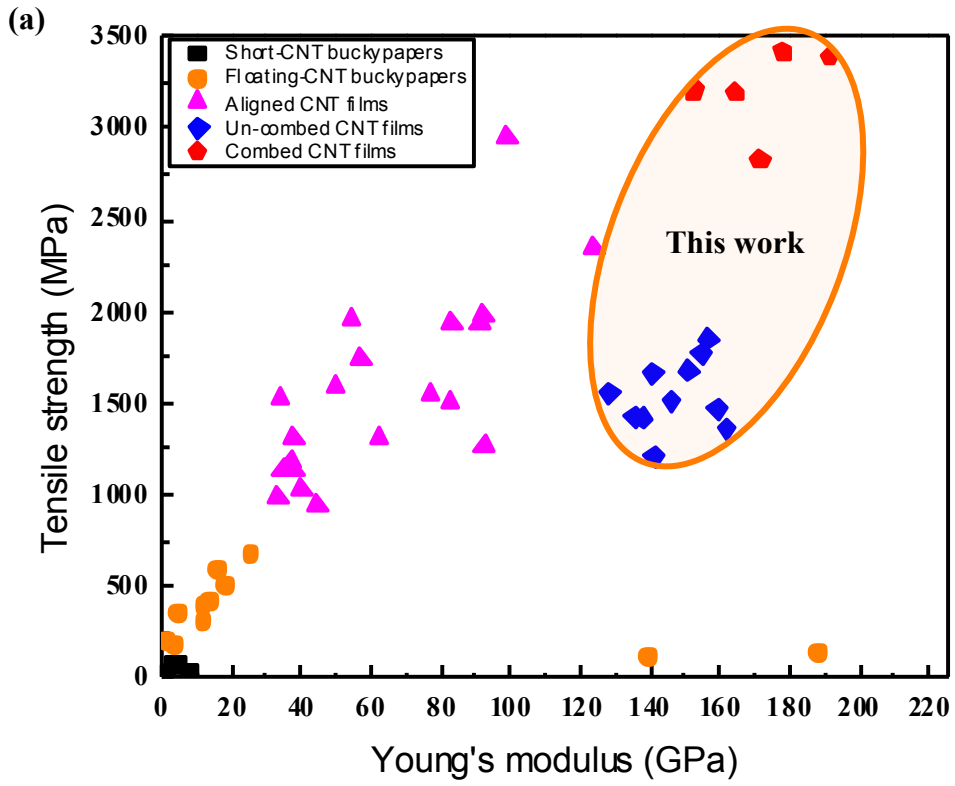

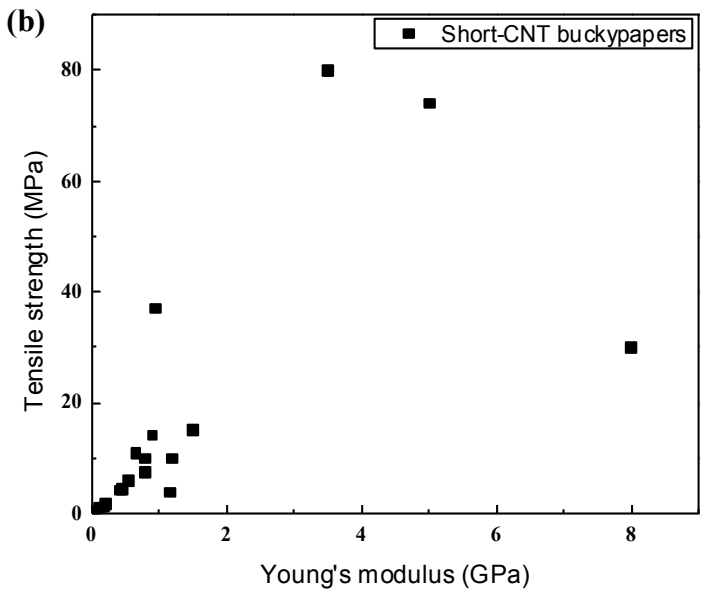

Figure 5.3 Mechanical properties of CNT films: (a) Comparison of combed CNT films with previously reported buckypapers and other aligned CNT films; (b) Enlargement of the data area for buckypapers produced by short CNT dispersion.

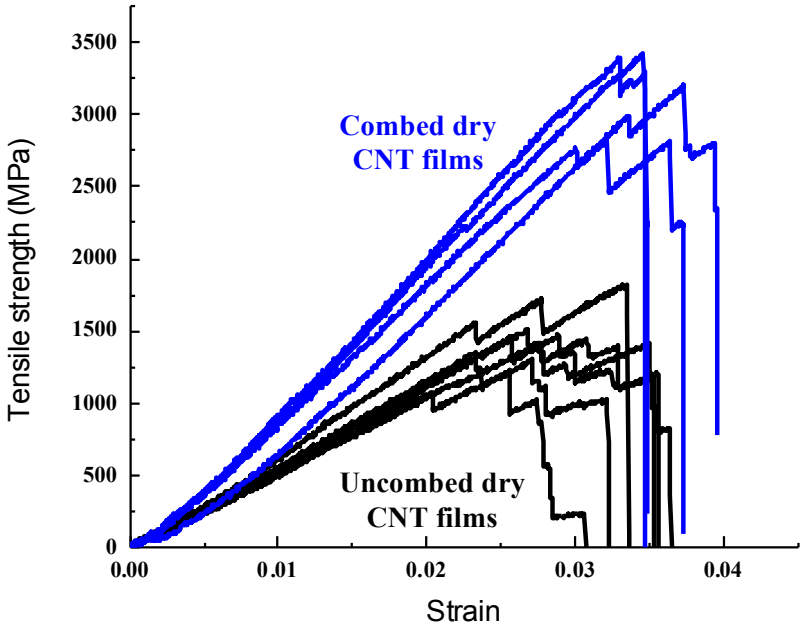

Figure 5.4 Typical tensile stress-strain curves of the uncombed and combed dry CNT films.

Figure 5.4 displays typical tensile stress-strain curves for the uncombed and combed dry CNT films. The slopes of the combed films show an apparent change compared with the uncombed ones. The Young's modulus is significantly improved by the microcombing. This is a direct evidence of the reduction of the CNT waviness and the improvement in the CNT alignment. In addition, the combed CNT films exhibit a higher tensile strain than that of the uncombed films, suggesting a reduction of structural defects induced by microcombing. The microcombing is simple, effective, and does not require a narrow window of controlled parameters, which greatly promotes the reproducibility and repeatability of the film properties.

5.3.2 Electrical Properties

Table 5.2 compares the electrical conductivity of the combed CNT films and other CNT buckypaprs and films. In our work, the uncombed CNT films exhibit a high electrical conductivity of 1.0×10^5 S/m, which is among the highest reported values. After microcombing, the electrical conductivity is further improved by 80% to 1.8×10^5 S/m. This substantial increase in electrical conductivity is also a direct result from better inter-tube contact to facilitate electron transfer due to the improved CNT straightness, enhanced CNT alignment, and higher nanotube packing density.

Table 5.2 Electrical conductivity values of the CNT films produced in our work and the data from the literatures.

Type	Material	Treatment	Electrical conductivity (S/m)	Ref.
Short-CNT buckypapers	SWCNT		3×10^4	[150]
		HNO_3	1.2×10^4	
	SWCNT		7×10^4	[151]
		$SOCl_2$	3.5×10^5	
	MWCNT		$0.83 \times 10^4 \sim 1.0 \times 10^4$	[119]
	SWCNT	Oleum	1.3×10^5	[153]
		Oleum + heat	9×10^4	
	MWCNT	Chemicals	$6.53 \times 10^2 \sim 18.18 \times 10^2$	[154]
	MWCNT		1.5×10^4	[115]
		Oriented	2×10^4	
Floating-CNT buckypapers	MWCNT		4.2×10^4	[156]
		40% stretch	6.0×10^4	
	SWCNT		2×10^5	[159]
Aligned CNT films	MWCNT		4×10^4	[136]
	Few-walled CNT		3.5×10^4	[120]
	Few-walled CNT		1.16×10^4	[121]
		Ethanol-densified	3.18×10^4	
		Acetone-densified	3.49×10^4	
	Few-walled CNT	**Uncombed**	**$1.0 \times 10^5 \pm 1156$**	**This work**
		Combed	**$1.8 \times 10^5 \pm 21173$**	

5.3.3 Effect of Microcombing on the CNT Structure

Combing, which has been used for centuries in the textile industry, is a process to disentangle and straighten staple fibers in order to achieve higher level of fiber alignment in the fiber web [160]. In this work, sharp surgical blades with micro-scale features at the blade edges were used to disentangle and straighten the wavy CNTs in the as-drawn CNT sheet. One pair of the blades was used to comb both the top-side and bottom-side of the CNT sheet, giving a uniform microcombing (Figure 5.2). Combing with more blades was found to break CNT sheets or to group CNTs into non-uniform bundles, which is not desired. Additionally, the rotating speed and the contact angle between the CNT sheet and the combing blades are important. It was found fast drawing/rotating speed of the CNT sheet could benefit the CNT alignment. But when the speed was too fast, weak van der Waals forces could not hold the CNTs together any more, leading to the breakage of the CNT sheet. 20 r/min was the fastest speed that we found to operate successfully. In our experiment, the contact angle between the CNT sheet and the combing blades was controlled at 80°-85° (Figure 5.2b), which was the optimum angle that we found to allow CNT sheet to be fully combed without breakage. When using smaller contact angles (less than 80°-85°), the contact surface between the CNT sheet and the blade became larger. The increased friction made the nanotubes accumulate onto the edge of the blade, and break the CNT sheet at the blade. When using larger contact angles, the effect of microcombing was less effective in improving the packing and alignment of CNTs.

Figure 5.5 shows both the optical photos and SEM images of the dry CNT sheets before and after microcombing, and before and after solution treatment, respectively. After the

microcombing process, it is evident that the CNT sheets become shiny due to their smoothened surfaces (Figure 5.5a, b). As shown in the SEM images (Figure 5.5b, c, e, f), the microcombing process reduced the waviness of CNTs and enhanced the structural uniformity. This is also demonstrated by the TEM images of a single layer of CNT sheet before and after microcombing, as shown in Figure 5.6. After solution treatment (Figure 5.5e, f), the nanotubes formed larger bundles and the sheets became denser. This was caused by the shrinking and densification effect of the ethanol in the coating solution.

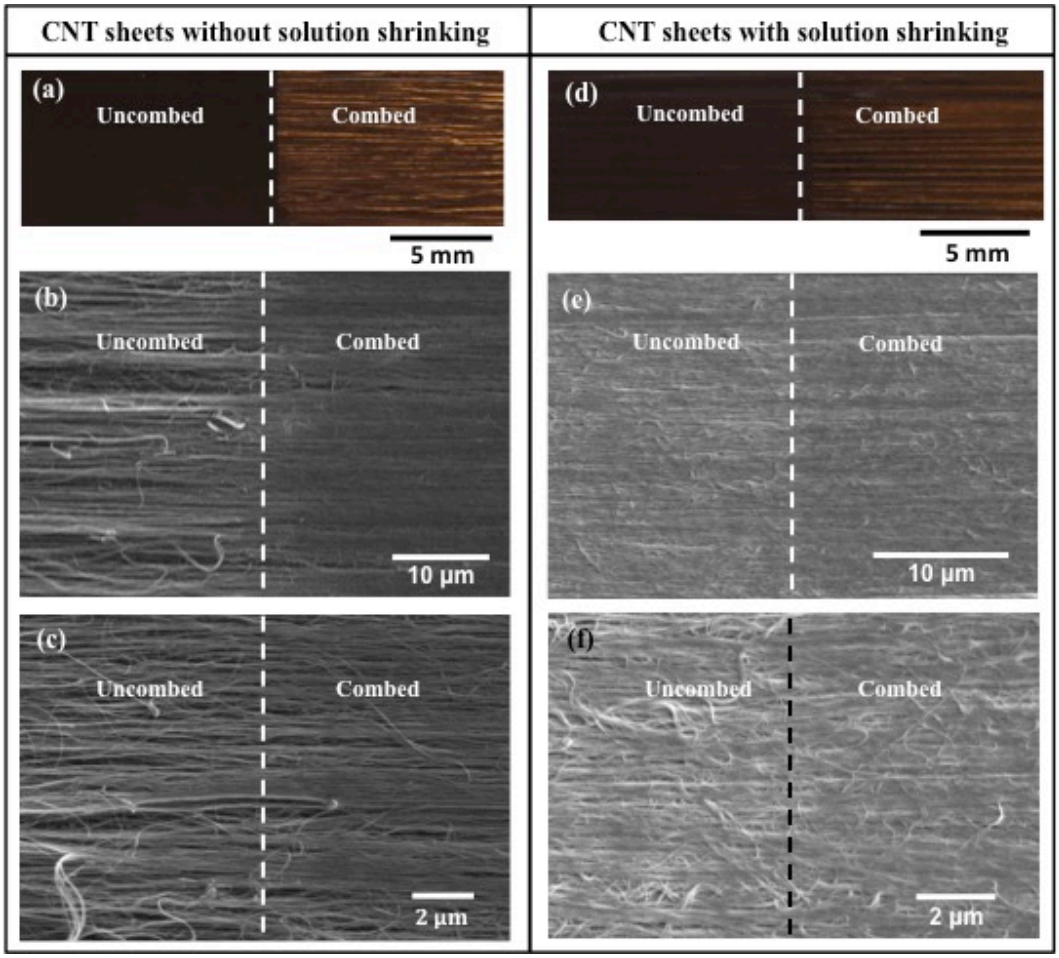

Figure 5.5 Optical photos (a, d) and SEM images (b, c, e, f) showing the differences between the uncombed and combed dry CNT sheets.

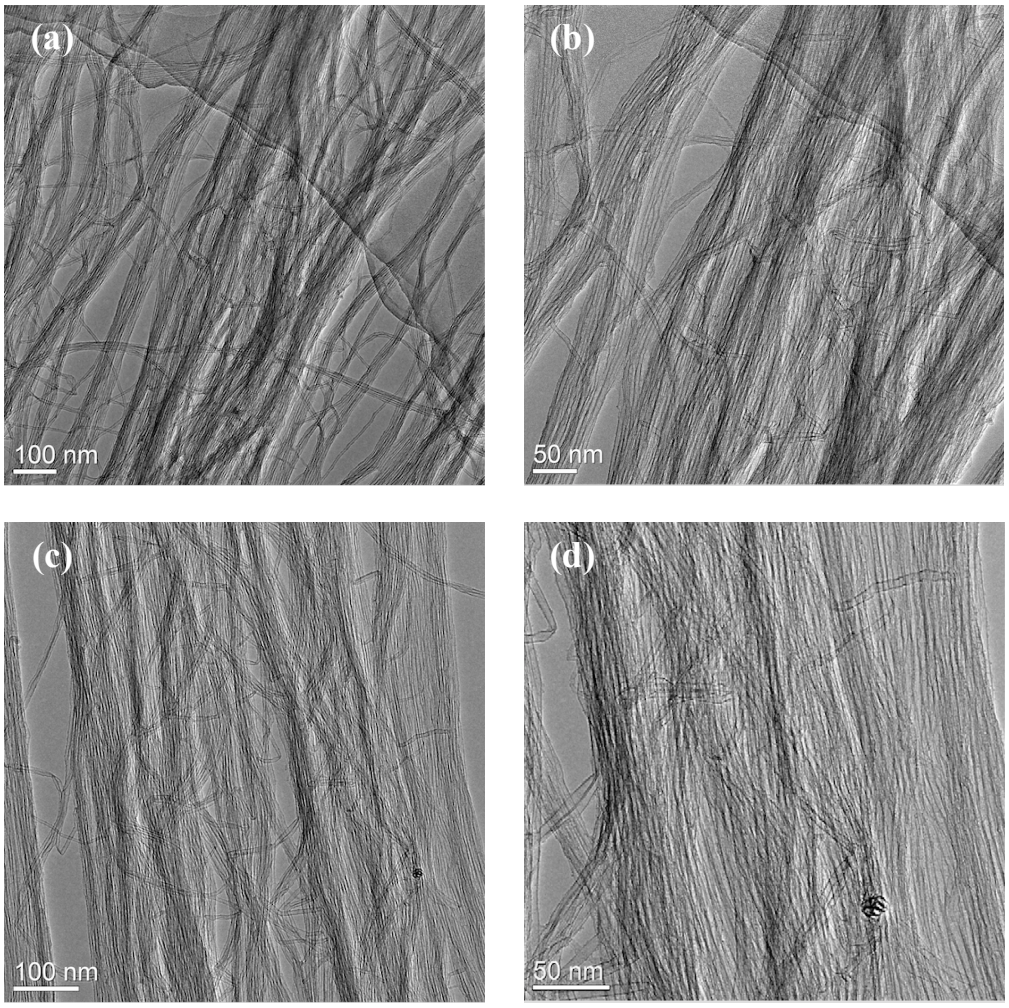

Figure 5.6 TEM images of one single layer of CNT sheet before (a, b) and after microcombing (c, d).

5.4 Conclusions

A novel "microcombing" approach is developed in this study to fabricate dry CNT films with ultrahigh mechanical properties and exceptional electrical performances. The approach has been shown to be effective in mitigating CNT waviness, reducing film defects, and improving CNT alignment and packing. The dry CNT films produced by microcombing

exhibited very high Young's modulus of 172 GPa, excellent tensile strength of 3.2 GPa, and unprecedented electrical conductivity of 1.8×10^5 S/m. This approach is simple and effective, and can greatly improve the reproducibility and repeatability of the CNT film properties.

Acknowledgements

Our authors are grateful to Suzhou Institute of Nano-Science and Nano-Biotics for providing the CNT arrays. The authors also thank Jiali Yu, a student in the University of Delaware, for her help with the sample weight measurement. This work was funded by the US Air Force of Scientific Research (Grant No. FA9550-12-1-0088).

Chapter 6

Microcombing enables High-Performance Carbon Nanotube Composites

Liwen Zhang[a], Xin Wang[a], Ru Li[b], Qingwen Li[b], Philip D. Bradford[c], Yuntian Zhu[a,*]

[a] Department of Materials Science and Engineering, North Carolina State University, Raleigh, NC 27695, USA

[b] Suzhou Institute of Nano-Science and Nano-Biotics, Chinese Academy of Sciences, Suzhou, Jiangsu 215123, China

[c] Department of Textile Engineering Chemistry and Science, North Carolina State University, Raleigh, NC 27695, USA

Abstract

A processing approach, microcombing, has been reported recently to produce dry carbon nanotube (CNT) films with superior mechanical and electrical properties by taking advantage of its efficiency in straightening the wavy CNTs and aligning the strands. Here, we report the fabrication of CNT composite films with aligned CNTs and CNT strands, reduced waviness, high CNT weight fraction, and relatively uniform CNT distribution, using poly(vinyl alcohol) (PVA) as a model matrix. These structural features give the micro-combed CNT/PVA composite films electrical conductivity of 1.84×10^5 S/m, Young's modulus of 119

GPa, tensile strength of 2.9 GPa, and toughness of 52.4 J/cm^3, which improve over those of uncombed samples by 300%, 100%, 120%, and 200%, respectively, and are also much higher than those obtained by other processing approaches. Moreover, this method is expected to be applicable to various polymer matrices as long as they can be dissolved in the solution.

(Published in *Compo. Sci. & Techno.*, 2016, 123: 92-98)

6.1 Introduction

Carbon nanotubes (CNTs) possess remarkable mechanical [35,37] and electrical properties [42]. In combination with their low density and high aspect ratio, CNTs are ideal candidates as advanced reinforcements for nanocomposites, which offer tremendous opportunities for developing multifunctional materials, such as structural composites, transparent electrodes, energy storage devices, field and thermionic emission electron sources [19,20,122,161]. For decades, CNT/polymer composites have been the focus of scientific research. Various techniques have been explored to achieve organized CNT structures with superior performance, from short-CNT-reinforced polymer fibers [162–164] to long and aligned CNT/polymer composite films [112,125], from solution-based methods [165–169] to dry-processable approaches [66,101,104–107,120].

CNTs have one-dimensional tube structures with unidirectional mechanical, electrical, and thermal properties. Therefore, it is of great importance to control their orientation and configurations when assembling them into macroscopic composites [84,161]. Studies have shown that the excellent intrinsic properties of CNTs can be better utilized when unidirectionally-aligned long nanotubes are assembled in a composite structure with a high CNT fraction [101,105,122,168], and nanotube waviness is a critical factor that limits the overall performance of CNT composites [89,104,107].

Recently, our group reported a novel approach known as "microcombing" to fabricate dry, pure CNT films (without any matrix) by utilizing unidirectionally aligned long nanotubes [103]. By passing a single layer of CNT sheet through micro-scale rough edges of surgical blades, the microcombing process straightened wavy CNTs, reduced the impurities

in the film structure, and increased the film packing density and uniformity, which in turn greatly improved the properties of the assembled CNT films. The method is simple and reliable to fabricate CNT films with reproducible properties. However, the greatly improved CNT straightness and packing density may cause another issue – strand agglomeration – in the films, which causes problems when this kind of CNTs are used to produce CNT/polymer composites. It is believed that the high performance CNT/polymer composites require the CNTs to be well dispersed in order to achieve a good interfacial load transfer with the polymer matrix [165,166]. This casts doubt on if the microcombing method can be used to fabricate high performance CNT/polymer composites. This is an issue that we need to address, otherwise our method will only have limited applications.

In this study, we incorporated our microcombing method into a one-step winding approach [104] to fabricate CNT/polymer composites. A layered composite structure was designed as it maintains the aligned structure of nanotubes, realizes high CNT loading, and ensures intimate interaction between the matrix and nanotubes, all of which promote load transfer [170,171]. PVA was used as a model matrix in our study to represent other soluble polymer matrices, because it has great processability and excellent adhesive property, and has been widely used to enhance the strength of CNT yarns and films [101,105,106,149,168,169]. Moreover, PVA is biocompatible and nontoxic. The CNT/PVA yarns and films can be made into fabrics which show potential applications in spacesuits, bullet-proof vests, and radiation protection suits. In addition, they are promising materials for bioapplications [101,172].

It is found that the as-produced micro-combed CNT/PVA composite films are strong (2.9 GPa) and stiff (119 GPa), which are much higher than other reported values for CNT/PVA composite yarns and sheets. They also exhibit a high toughness of 52.4 J/cm^3 and a high electrical conductivity of 1.84×10^5 S/m at a high CNT weight fraction of ~75%. Moreover, this method is simple, reliable, and reproducible, which provides for a new way to produce high performance CNT/polymer composites at large scale and low cost, while a wide range of soluble polymer matrices can be utilized.

6.2 Experimental

6.2.1 Growth of CNT Arrays

The drawable CNT arrays used in this study were synthesized using a chemical vapor deposition method, as described in our previous work [120]. Briefly, electron beam evaporation technique was used first to prepare the catalyst by depositing an alumina layer (20 nm) and an iron layer (1 nm) on a silicon substrate with thermal oxide (30 nm). Then, this substrate was put in a 5-inch quartz tube to grow CNT array at 740°C. A gas mixture of argon with 6% hydrogen and pure ethylene were used for CNT growth. The total flow rate of gases was set at 1.5 L/min. After growing for 15 min, the array was approximately 200 μm in height. Most nanotubes have 2-5 walls and are 4-8 nm in diameters (Figure 6.1).

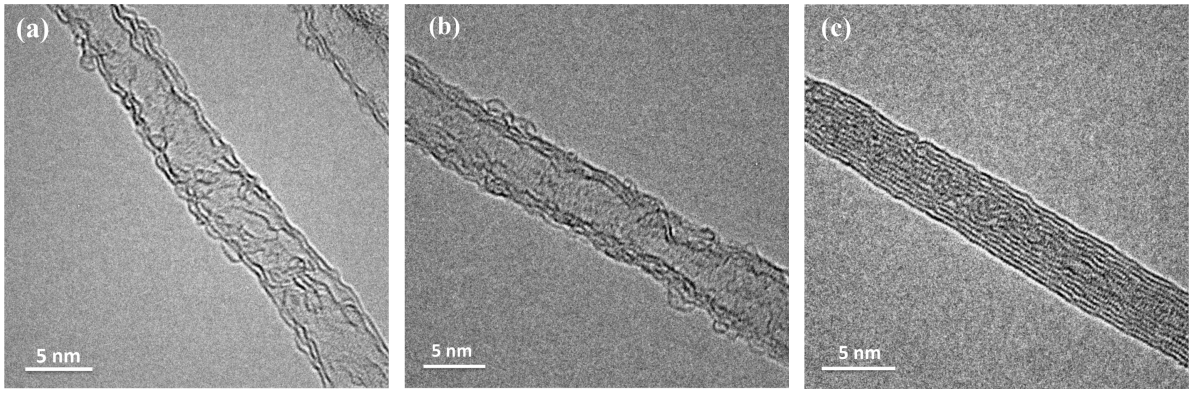

Figure 6.1 TEM images showing the diameter and number of walls of individual CNT.

6.2.2 Preparation of the Polymer Solution

PVA (MW=75,000-80,000, ≥99.0% hydrolyzed) was purchased from Sinopharm Chemical Reagent Co., Ltd. The PVA solution used in the experiment had a concentration of 0.1 wt.%, which was found to be optimal in our previous study [105]. The solution was prepared by dissolving PVA into equal volume of deionized water and ethanol.

6.2.3 Fabrication of the Micro-Combed CNT/PVA Composite Films

The experimental setup of microcombing for making the CNT/PVA composite films is shown in Figure 6.2. The microcombing zone consisted of a pair of sharp surgical blades, which were positioned oppositely. A layer of CNT sheet was drawn from a drawable CNT array, and then went through the microcombing zone. The contact angle between the CNT sheet and the blade was controlled at 80°-85°, and the inter-blade distance was set at about 6 cm (Figure 6.2b). In the microcombing zone, micro-scale rough edges of the surgical blades acted as combs that straightens the wavy CNTs and provides better CNT alignment. A

rotating mandrel with a diameter of 3 cm was used to wind the CNT sheet into macroscopic film at a rotational speed of 20 r/min. The PVA matrix was applied on the CNT sheet layer-by-layer using a needle. And another needle was bent into 90° and placed at 1 o'clock position of the rotating mandrel. The needles had a diameter of 0.65 mm. The bent-needle contacted the surface of the mandrel so that a little pressure from the needle's weight was applied to the CNT sheet. The PVA solution was applied in between the mandrel and the bent-needle at a rate of about 0.3 g/min. In this way, the bent-needle surface helped to spread the matrix more uniformly compared with only the drop-process [104].

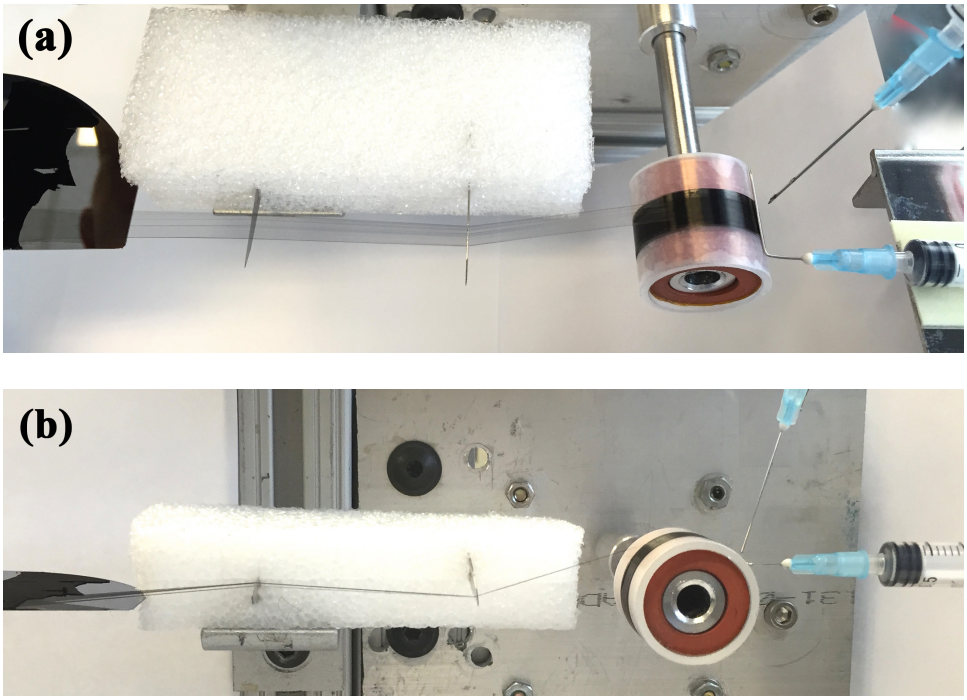

Figure 6.2 Experimental setup of the one-step approach of making CNT/polymer composite films.

Two hundred revolutions produced a film with a thickness of about 4 μm. The CNT film was then peeled off from the mandrel and hot-pressed under a pressure of 10 MPa at 80°C

for 2 hrs followed by 160°C for another 2 hrs in order to remove air bubbles and improve CNT-polymer integration. The hot-pressing reduced film thickness to about 3 μm.

For comparison, CNT/PVA composite films without microcombing were produced using the same parameters.

6.2.4 Characterization methods

Transmission electron microscopy (TEM, JEOL-2010F) analysis was conducted at 200 kV to reveal the diameter and number of walls of individual nanotubes. The CNT alignment was studied by both SEM and X-ray diffraction (XRD). Azimuthal scans of the XRD measurements were performed using Rigaku SmartLab with Eulerian cradle equipped with Cu rotating anode (Kα wavelength of 1.5418 Å). Each pattern was measured using a step size of 1° and a scan rate of 1°/s at 2θ = 23.5°. The fracture surface morphology of the as-produced films was also analyzed by SEM. Weight fractions of the CNT composites were determined by thermogravimetric analysis (TGA, Perkin Elmer Pyris 1) in nitrogen (99.999%) at a heating rate of 10°C/min.

A 4-probe Agilent 34410A 6.5 digit multimeter was used to test the electrical conductivity of the films along the CNT alignment direction. Electrodes were made of silver by magnetron sputtering. Tensile test specimens were prepared by cutting the as-produced films into narrow strips, which were typically 1 mm wide and 10 mm in gauge length. The width of the specimen was measured using a calibrated scale bar in an optical micrometer. The thickness was measured by a micrometer and further confirmed by scanning electron microscopy (SEM, Verio 460L). The specimens were tested in tension by an Instron 3365

tensile testing machine using a load cell of 10 N and a displacement rate of 0.5 mm/min. In order to calculate the film density, the weight of each specimen was measured using a MX5 microbalance (Mettler-Toledo, Inc.), which had an accuracy of 1 microgram.

6.3 Results and Discussion

6.3.1 Morphologies of the Uncombed and Combed CNT/PVA Composite Films

Figure 6.3 presents SEM images showing both the surface morphologies and the fracture surfaces of uncombed and combed CNT/PVA composite films. As shown, microcombing produced CNT/PVA composite films with straighter CNTs, improved alignment, enhanced nanotube packing, and increased film uniformity, which was consistent with the results from our previous study on dry CNT films [103]. The CNT alignment can also be characterized by the anisotropic angular distribution intensity of the (002) reflection, which is related to the inter-wall distance of nanotubes [96,173,174]. A non-uniform (002) intensity indicates the CNTs are aligned. Figure 6.4 shows the integrated X-ray intensity of the (002) reflection along the 2θ axis versus the azimuth (ϕ). Two peaks are centered at $\phi \approx -1°$ and 178°, respectively, indicating a preferred orientation of nanotubes. The full width at half-maximum (FWHM) of the uncombed films is approximately 25°, while that of the combed films is about 23°, demonstrating an improved alignment of the CNTs by microcombing [173].

The CNT-polymer interaction is an essential factor that affects the efficiency of load transfer across the CNT-polymer interface [149]. Traditional infiltration method usually involves a densely-packed CNT film infiltrated with polymer matrix, where the nanotubes are not uniformly distributed in the matrix [112]. The “spray-winding” approach enables the

polymer to be infiltrated into each layer of the CNT sheet with a more uniform CNT distribution [105–107]. However, the airflow generated by the sprayer usually disturbs the CNT alignment in the as-wound CNT sheet. The matrix-applying method used in the microcombing approach avoided this issue by applying polymer matrix using the smooth surface of a needle (Figure 6.2). This method allowed CNTs to interact with the PVA matrix at molecular level with higher CNT-matrix contact area than that produced by the "spray-winding" approach, leading to more effective load transfer. As shown in Figure 6.3 (c) & (d), the as-produced composite films exhibited a layered structure with PVA matrix homogeneously wrapping the CNT strands. The combed films showed a more severe strand agglomeration than the uncombed ones, since the CNTs were straighter and packed denser. In addition, the combed composites exhibited reduced defects along the axial direction of the composites, thus they were more likely to be torn apart instead of fracturing during tensile deformation (Figure 6.5). The delamination was more severe for the combed films than the uncombed ones, suggesting the formation of strong CNT strands by microcombing. Therefore, it has been a challenge to take SEM images of the fracture surfaces of the combed CNT/PVA composite films. The as-produced CNT/PVA composite films had a high CNT weight fraction of ~75%, as calculated from the TGA results (Figure 6.6), which helped to enhance the mechanical properties of the composites.

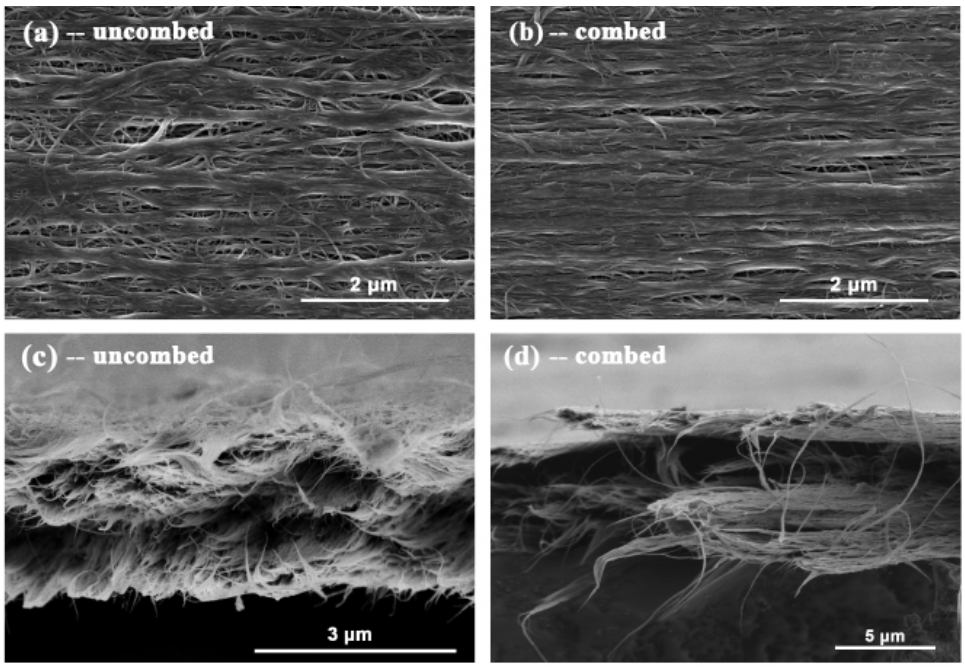

Figure 6.3 SEM images showing the differences of surface morphologies and the fracture surfaces between the uncombed and combed CNT/PVA films.

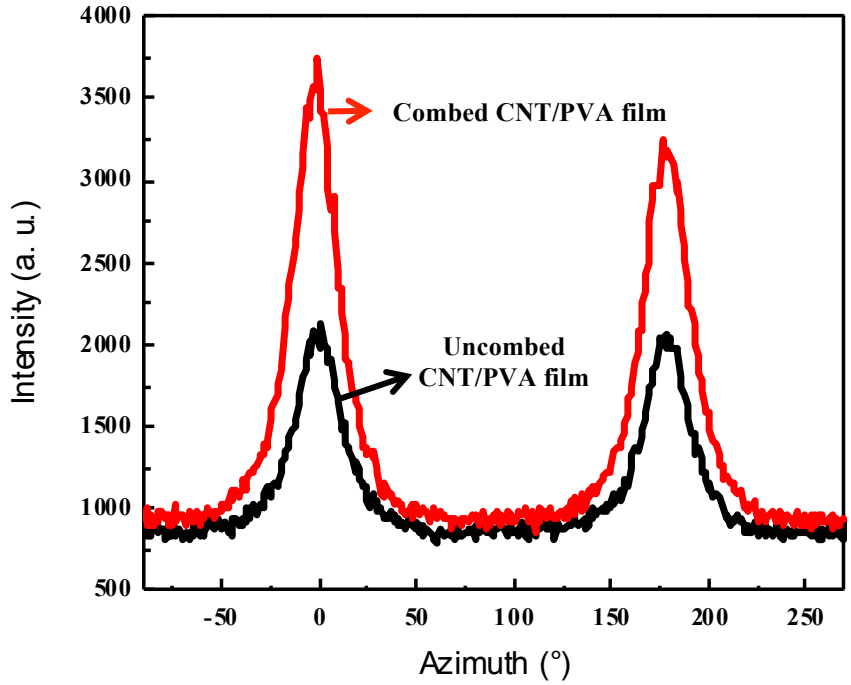

Figure 6.4 The integrated X-ray intensity of the (002) reflection along the 2θ axis versus the azimuth (ϕ) before and after microcombing.

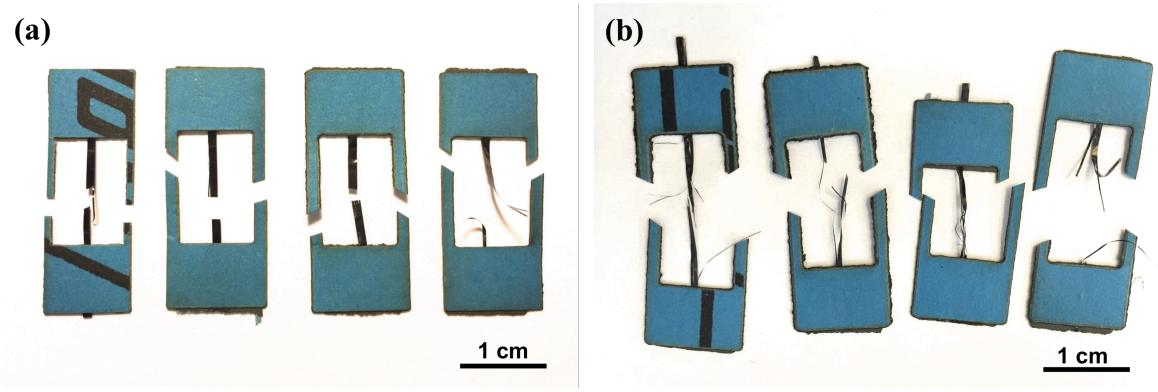

Figure 6.5 Photos showing the fracture of the uncombed (a) and combed (b) CNT/PVA films.

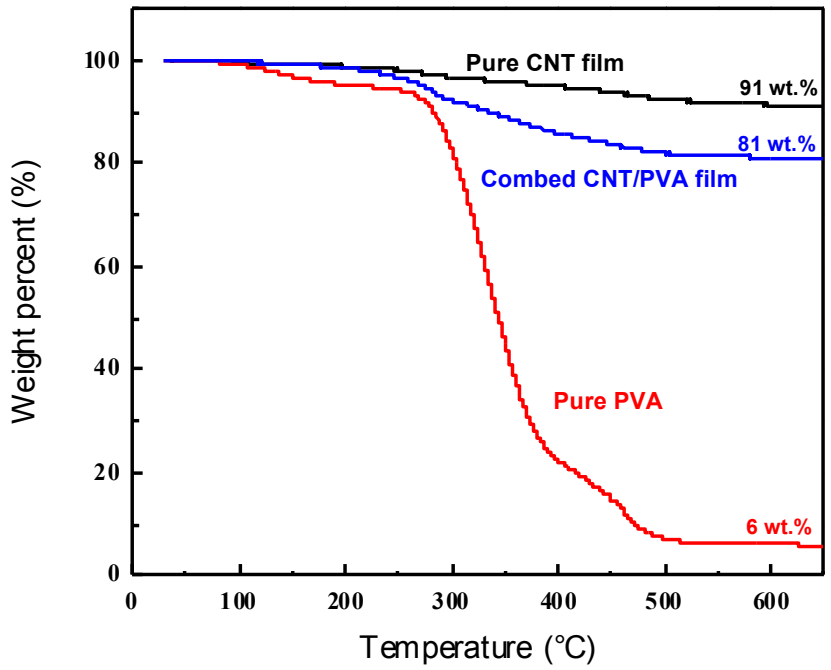

Figure 6.6 TGA curves of pure CNT film, a combed CNT/PVA composite film, and pure PVA.

6.3.2 Electrical Properties

The electrical conductivities of the uncombed and combed CNT/PVA composite films are shown in Figure 6.7, and they are compared with the values reported for the uncombed and combed dry CNT films [103]. Microcombing increased the electrical conductivity of the CNT/PVA films by 300% from 0.45×10^5 S/m to 1.84×10^5 S/m, which was to our knowledge higher than any other reported values for CNT/PVA composite yarns and films [101,105,106]. This improvement could be accredited to the enhanced nanotube alignment, straightness, and packing by microcombing (Figure 6.3), which resulted in increased inter-tube contact area for more efficient electron transfer [140,175]. The enhanced packing could be inferred from the increased film density: 0.86 g/cm^3 for uncombed CNT/PVA composite films, and 0.96 g/cm^3 for combed ones (Table 6.1).

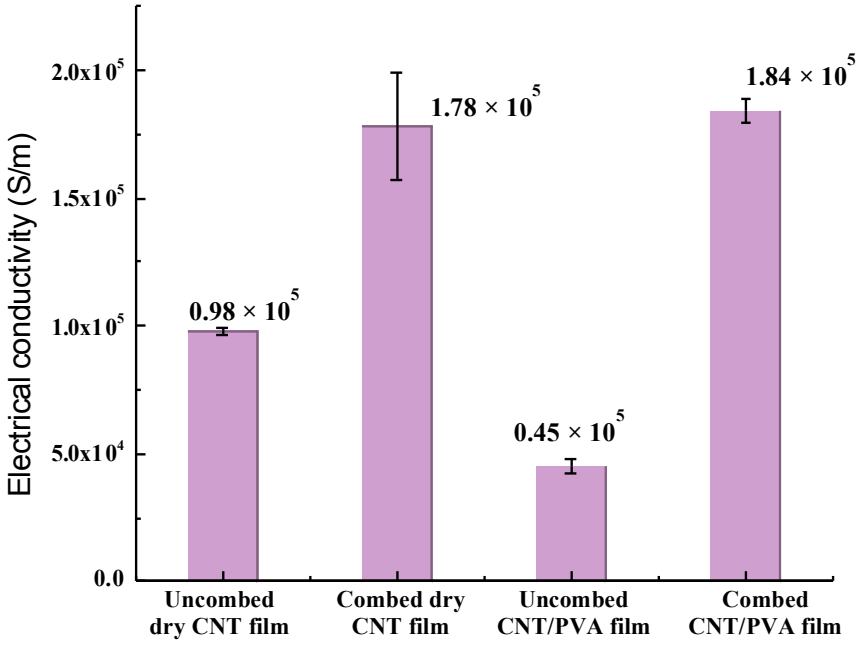

Figure 6.7 Electrical conductivity of the CNT/PVA composite films in comparison with that of the dry CNT films.

Table 6.1 Summary of mechanical properties of the as-produced uncombed and combed CNT/PVA composite films.

Film type	Density (g/cm^3)	Young's modulus (GPa)	Tensile strength (GPa)	Strain (%)	Toughness (J/cm^3)
Uncombed CNT/PVA films	0.86	60±4	1.3±0.04	2.7±0.2	17.4±1.8
Combed CNT/PVA films	0.96	119±6	2.9±0.2	3.1±0.2	52.4±5.2
Improvement	12%	100%	120%	15%	200%

Interestingly, the incorporation of the insulating PVA matrix decreased the average electrical conductivity of the uncombed films, but did not decrease the conductivity of the combed films. In particular, the combed CNT/PVA composite films showed 3.4% (6×10^3 S/m) higher average electrical conductivity than the combed dry CNT films. This phenomenon was also found in the reported work of CNT/PVA yarns and films [101,105]. Since electron transfer was largely controlled by the contact area between the nanotubes, the wrapping of the insulating PVA around the CNTs generated an insulating barrier which decreased the inter-tube contact area, leading to a decreased electrical conductivity of the uncombed CNT/PVA films. In comparison, when the CNTs were combed and had a closer inter-tube distance, CNT strand agglomeration occurred and the PVA molecules were hardly able to penetrate into those highly packed strands. Instead, the PVA matrix might have helped wrap the strands together, maintaining the close contact of the individual nanotubes

against each other. In the combed dry CNT films, the film structure was loose and the contacts between the CNTs were not stable. Therefore, the combed dry CNT films showed slightly lower average electrical conductivity than the combed CNT/PVA films, but larger standard deviation. In this case, CNT strand agglomeration caused by microcombing did not impair the electrical properties of the as-produced composites, but it helped the electron transfer instead.

6.3.3 Mechanical Properties

The mechanical properties of the uncombed and combed CNT/PVA composite films are summarized in Table 6.1. Figure 6.8 displays their typical stress-strain curves. The Young's modulus (60 GPa) and tensile strength (1.3 GPa) of the uncombed composite films were comparable to the reported values of the CNT/PVA films made of the same CNTs [105]. After microcombing, the films' Young's modulus showed about 100% improvement to 119 GPa, and their tensile strength showed about 120% improvement to 2.9 GPa, which were quite significant. Compared to our dry CNT films reported previously (Young's modulus: 172 GPa, tensile strength: 3.2 GPa) [103], the Young's modulus and tensile strength both decreased after adding the PVA matrix. However, the total tensile load of the composite film was actually higher than that of the dry film with similar CNT quantity, but the addition of the matrix increased the thickness of the samples, which in turn resulted in reduced values of Young's modulus and tensile strength, which were normalized by the film thickness. In other words, the lower Young's modulus was caused by lower CNT volume fraction in the CNT/PVA composite sample than in the dry pure CNT films if the void space was taken as

matrix in the latter. Moreover, the PVA was a thermal plastic that could act as lubricant between the CNT strands, which inevitably made the composite films less stiff during deformation. Therefore, the Young's modulus showed a larger degree of decrease than the tensile strength. The mechanical properties of the combed CNT/PVA films were much higher than those reported for CNT/PVA films and yarns [101,105]. Microcombing straightened the wavy CNTs, and packed them denser and more uniformly, which improved their mechanical properties.

Examination of Figure 6.8 also revealed a few interesting phenomena. First, the stress-strain curves of the combed CNT/PVA composites were serrated before failure. In other words, the total stress, which was calculated as the total load divided by the initial cross-sectional area of the sample, had several abrupt drops and slow rises before the final failure. In contrast, no such obvious serrations were on the stress-strain curves of the uncombed CNT/PVA sample. This phenomenon was apparently caused by the successive fracture of individual large CNT strands in the combed sample. When a large CNT strand was broken, the load carried by the strand was suddenly reduced to zero, which caused an abrupt large drop in the total load carried by the sample. This led to an abrupt drop in the apparent stress in the stress-strain curve. The stress continued to increase slowly as the remaining CNT strands were strained further. The above process might repeat itself a few times before the final failure of the composite sample. Such a large abrupt load drop could only be caused by the fracture of large CNT strands. The fracture of individual CNTs or small CNT strands would not lead to observable stress drops because they did not carry high enough load individually. The uncombed CNT/PVA composite samples did not show such serrated stress-

strain curves, indicating that no large CNT strands were formed in the sample. This is another evidence on the promotion of large CNT strands by microcombing, which is consistent with the aforementioned big increase in electrical conductivity by microcombing.

Second, the strains to failure of the CNT/PVA films were larger after microcombing (Figure 6.8), which suggested that during tensile deformation, combed CNTs were more likely to slide against each other than to break. The enhanced tensile strength and strain significantly increased the film toughness by 200% from 17.4 J/cm^3 to 52.4 J/cm^3 (Table 6.1). This is another consequence of formation of large CNT strands promoted by microcombing. Any future studies on the micro-combed CNT composites should take into account this structural feature.

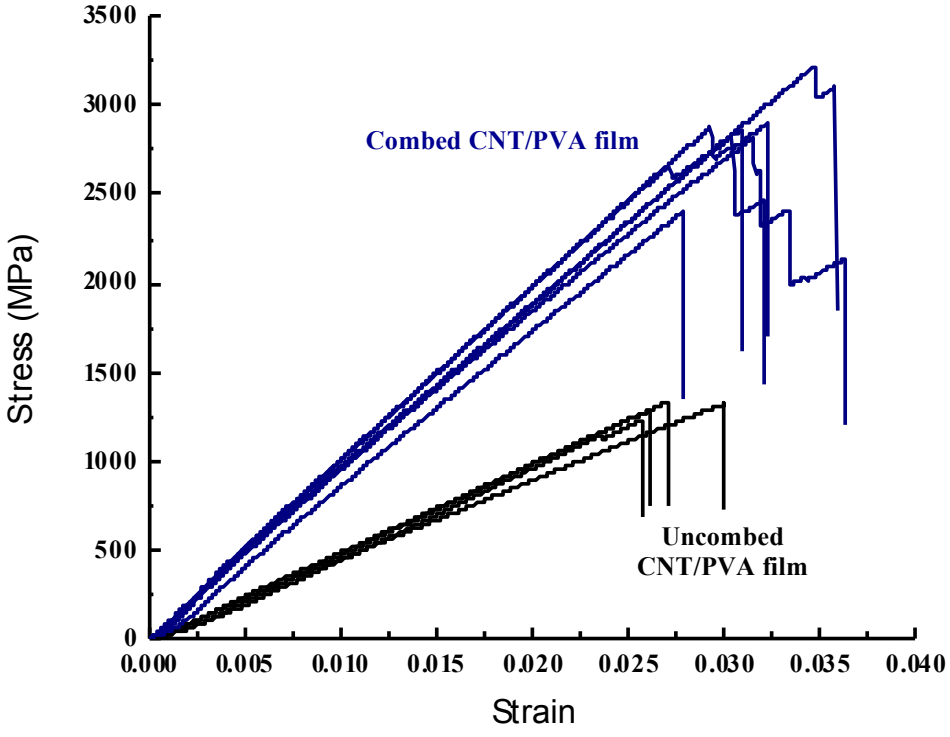

Figure 6.8 Typical stress-strain curves of the uncombed and combed CNT/PVA films.

The simplicity of the microcombing also makes properties of our composites reproducible, which is of great importance since reproducibility has been a challenge in CNT composites fabrication. For several samples we have made, the mechanical behavior of both the uncombed and the combed CNT/PVA composite films are in good consistency, as shown in Figure 6.8. Based on our further studies, which is to be reported in the future, the microcombing approach can be used to make CNT composite with any polymer matrix if the matrix can be dissolved in a solvent to form a dilute polymer solution. It would be interesting to see how the mechanical properties are affected if a stiffer and stronger polymer matrix such as epoxy is used to make micro-combed CNT composite.

It should be noted that this method needs to use high-quality drawable CNT array, which is more difficult to produce in large quantity than CNT powder. On the other hand, CNT powders have so far failed to produce high-strength composites because of their intrinsic limitations in dispersion, length, alignment and volume fraction.

6.4 Conclusions

In this study, it is demonstrated that our recently developed microcombing method can also be used to produce high performance CNT/polymer composite films. By using PVA as a model matrix, we successfully fabricated the CNT/PVA composite films with superior electrical and mechanical properties. The microcombing method provided straightened CNTs, enhanced packing density, and reduced impurities in the composites. The microcombing promoted the formation of CNT strands, but this was found beneficial for enhancing the composite performance. The as-produced CNT/PVA composite films exhibit

an electrical conductivity of 1.84×10^5 S/m, Young's modulus of 119 GPa, tensile strength of 2.9 GPa, and toughness of 52.4 J/cm^3, which represent improvements over those of uncombed samples by 300%, 100%, 120%, and 200%, respectively. While this method is simple, reliable, and reproducible, it is also expected to be applicable to a variety of soluble polymers. In addition, since PVA is a thermal plastic polymer that has relatively low mechanical properties compared with thermoset polymers, we believe that our microcombing method can produce CNT/polymer composites with even better properties if high performance matrix is used.

Acknowledgements

The authors thank Suzhou Institute of Nano-Science and Nano-Biotics for collaboration. The authors acknowledge the use of the Analytical Instrumentation Facility (AIF) at North Carolina State University, which is supported by the State of North Carolina and the National Science Foundation. This work was funded by the US Air Force Office of Scientific Research (Grant No. FA9550-12-1-0088).

Chapter 7

Conclusions and Future Work

7.1 Conclusions

For extensive studies within the recent two decades, it has been proved that carbon nanotubes have the potential to make high-performance products where high-strength and multifunctional properties are desired. Difficulties exist in making the most use of the unprecedented properties of individual CNTs when fabricating macroscopic forms of CNT assemblies. The objectives of the research in this work are to discuss the issues that hinder the performance of dry CNT films and CNT composite materials, and develop an innovative solution to fabricate high-performance and multifunctional CNT films and composites at ease and suitable for scale-up using drawable CNT arrays. The following is a summary of the research outcomes:

- CNTs with different lengths: 230 μm, 300 μm and 360 μm, were used to fabricate dry CNT films by a winding process. The effects of CNT length on the film's structure and mechanical and electrical properties were examined. It was found the films made of 230 μm CNTs exhibited the highest Young's modulus, tensile strength, and electrical conductivity. The mechanical and electrical properties decreased sharply for the films made of 300 μm and 360 μm CNTs. Although shorter CNTs were not good load bearers as longer CNTs, the longer ones were wavier and had more amorphous carbon and structural defects which could not avoid due to the feature of growth process. Therefore, opposite to what has been predicted by theories, in real situation, shorter CNTs resulted

in better performance when made into macro-scale dry films, because the cleaner surfaces of the nanotubes and intrinsic straighter morphology led to a higher degree of CNT alignment and tighter structural packing. It was speculated that if higher CNT arrays could be synthesized in the same quality as the lower ones, then, the dry films made by longer CNTs were expected to have the same CNT alignment degree and structural packing density as those made by shorter CNTs. In this case, the longer CNTs would result in better overall performance of the dry films than the shorter ones.

- A novel microcombing approach was developed to fabricate dry CNT films with ultrahigh mechanical properties and exceptional electrical performances. Principally based on the previously reported winding technique, this approach, for the first time, utilized a pair of sharp surgical blades with microsized features at the blade edges as combs to locally mitigate entangled bundles and straighten the wavy CNTs in the dry-drawn CNT sheet at single-layer level before the formation of densely packed CNT films. The as-combed single layer of CNT sheet exhibited high level of nanotube alignment and straightness with reduced structural defects and enhanced nanotube packing density. The dry CNT films produced by microcombing had a very high Young's modulus of 172 GPa, excellent tensile strength of 3.2 GPa, and unprecedented electrical conductivity of 1.8×10^5 S/m, which were much superior to previously reported CNT films or buckypapers. More importantly, this novel technique required less rigorous process control and could construct CNT films with reproducible properties, which had the potential to be scale-up for industrial mass production.
- Based on the microcombing approach, CNT/PVA composite films were produced in

order to investigate the effect of dispersion of long and aligned CNTs when they were used to make aligned CNT composites at high CNT fractions. High-performance CNT/polymer composites required the CNTs to be well dispersed in order to achieve a good interfacial load transfer with the polymer matrix. However, the greatly improved CNT straightness and packing density by microcombing might cause strand agglomeration in the films, which led to dispersion problems when this kind of CNTs were used to make composites, bringing decreased performance. Nevertheless, based on the study, it was found although microcombing promoted the formation of CNT strands, this was instead beneficial for enhancing the composite performance. When matrix was added, those agglomerated strands were wrapped together which maintained a more stable and better contact between nanotubes than those in the dry films. The as-produced CNT/PVA composite films exhibit an electrical conductivity of 1.84×10^5 S/m, Young's modulus of 119 GPa, tensile strength of 2.9 GPa, and toughness of 52.4 J/cm^3, which represent improvements over those of uncombed samples by 300%, 100%, 120%, and 200%, respectively, demonstrating the effectiveness and reliability of microcombing in producing high-performance CNT/polymer composite films. And more importantly, the dispersion of long and aligned CNTs was not an issue when making aligned CNT composites at high CNT fractions.

7.2 Future Work

7.2.1 Customize Micro-Combs with Desired Features

In Chapter 5 and Chapter 6, microcombing approach was used to straighten wavy CNTs in the dry-drawn CNT sheet, resembling the combing process of fibers in Textile industry. This approach was proved to be very effective in largely improving the properties of the as-produced CNT assemblies. However, the micro-combs used in the research were surgical blades, where the micro-teeth had random and uncontrolled sizes. The researcher found when different kinds of blades were used, such as razor blades, the effect of microcombing was different. In order to further investigate the microcombing mechanism and to obtain an optimum microcombing effect, it is desired to customize the micro-combs with appropriate teeth shapes, widths, depths, and thicknesses.

7.2.2 CNT/Metal Composite Yarns with High Specific Electrical Conductivity

It has been found recently that metals can be incorporated into CNT yarns by electroplating [176,177]. Due to the polymer-like low density and high electrical conductivity of CNTs, the CNT/metal composite yarns are promised to be good substitutes for copper, where there is a metal-like electrical conductivity but lower density. This kind of conductive yarns is suitable for applications as wires and cables used in microelectronics, lightweight conductors, medical implants, and aviation and space applications. The researcher found the microcombing method is also applicable to produce CNT yarns with enhanced mechanical properties and exceptionally high electrical conductivities, which are more desirable materials for electroplating with metal matrix, since high strength is needed

for CNT yarn so that it can exist in the electroplating solution. Figure 7.1 shows a schematic view of the yarn production procedure by microcombing. It is speculated that the CNT/metal composites yarns produced by microcombing and then electroplating have the potential to exceed the electrical conductivity of the metal matrix.

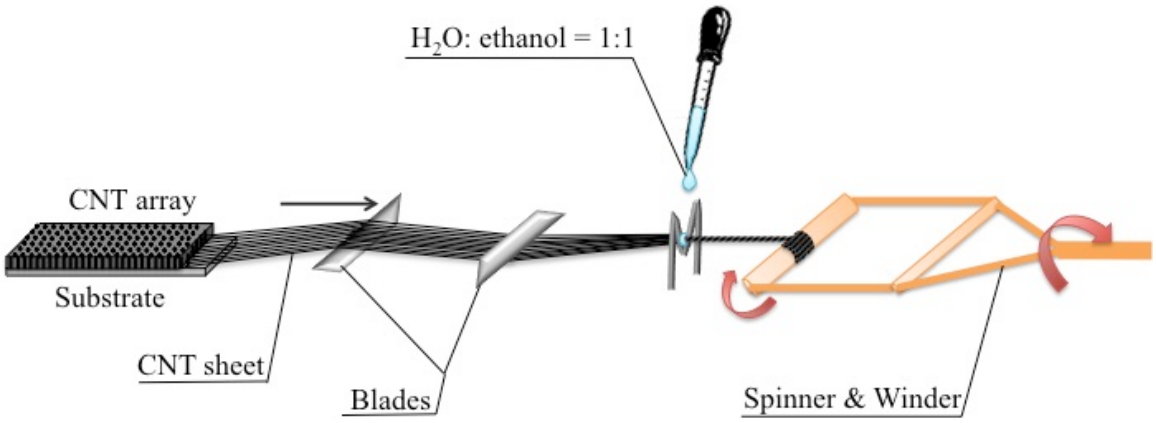

Figure 7.1 Schematic of fabricating CNT yarns by microcombing approach.

7.2.3 Mass Production of High-Performance CNT Products

Drawable SACNT arrays were used as the raw material to fabricate CNT products in the research of this work, which could easily provide highly aligned CNTs that promised to give high properties to the as-produced nanotube products. However, there are problems in mass production of the arrays since the sizes of the substrate and growth furnace were quite limited. The floating catalyst approach is more amenable for scale-up to large-scale production [178]. In this approach, the catalyst particles are dissolved in a solution and directly injected into the growth furnace while carbon source gas also flows through the growth tube which is heated to the CNT growth temperature. Nanotubes grow immediately

and form a continuous sock-like aerogel in the gas flow, and then can be blown out with the carrier gas. This kind of aerogel is finally collected by winding it on a mandrel with certain dimensions to make into macro-scale buckypapers. Figure 7.2 (a) is a schematic illustration of the process and the as-produced buckypapers are presented in Figure 7.2 (b) [157]. The CNTs produced in this approach are centimeter-long and have mainly 2 walls. Although the CNTs in the as-produced buckypapers are quite randomly aligned, with only a little higher degree of alignment in the winding direction than in the width direction. However, studies have found that by stretching and pressing those papers, they can also result in dry CNT films [157] and CNT/polymer composite films [156,179] with superior performance.

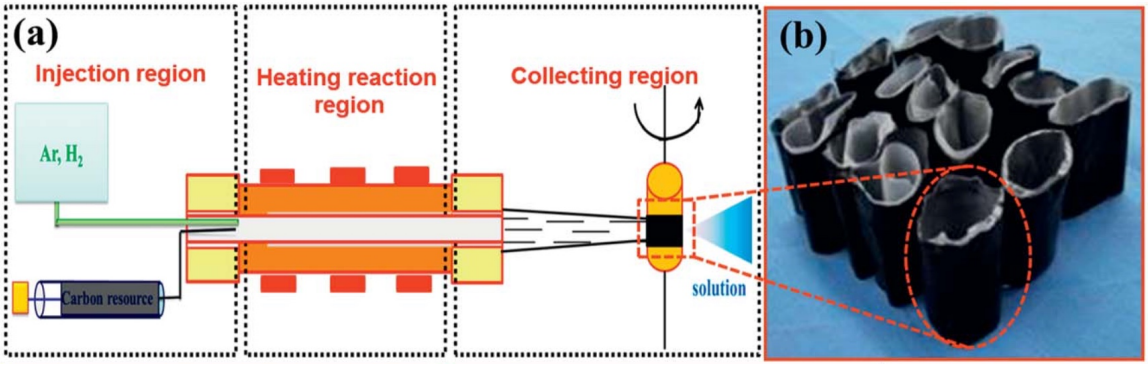

Figure 7.2 (a) Schematic illustration of the floating catalyst approach; (b) The as-produced buckypapers taken off from the winding mandrel [157].

However, all previous work done to improve the performance of the floating catalyst buckypapers were carried out after the formation of the macroscopic assemblies, where multi-layers of CNTs were already densely packed, causing difficulties in stretching process and limiting the stretching ratios. It is proposed that if stretching or microcombing can be done immediately after the CNT aerogel flew out from the furnace before it winds on the

mandrel, there is a high probability to get CNT buckypapers with a higher degree of alignment and/or straightness than those stretched afterward, which will result in better performance when dry films or composite films are fabricated.

REFERENCES

[1] M. Monthioux, V.L. Kuznetsov, Who should be given the credit for the discovery of carbon nanotubes?, Carbon. 44 (2006) 1621–1623. doi:10.1016/j.carbon.2006.03.019.

[2] Z. Ren, Y. Lan, Y. Wang, Aligned carbon nanotubes: physics, concepts, fabrication and devices, Springer, Berlin, 2013.

[3] S. Iijima, Helical microtubules of graphitic carbon, Nature. 354 (1991) 56–58. doi:10.1038/354056a0.

[4] T. Belin, F. Epron, Characterization methods of carbon nanotubes: a review, Mater. Sci. Eng. B. 119 (2005) 105–118. doi:10.1016/j.mseb.2005.02.046.

[5] P.R. Somani, M. Umeno, eds., Carbon nanotubes: multifunctional materials, Applied Science Innovations, Pune, 2009.

[6] M. Meyyappan, ed., Carbon nanotubes: science and applications, CRC Press, Boca Raton, FL, 2005.

[7] C.N.R. Rao, R. Voggu, A. Govindaraj, Selective generation of single-walled carbon nanotubes with metallic, semiconducting and other unique electronic properties, Nanoscale. 1 (2009) 96. doi:10.1039/b9nr00104b.

[8] N. Hamada, S. Sawada, A. Oshiyama, New one-dimensional conductors: graphitic microtubules, Phys. Rev. Lett. 68 (1992) 1579–1581. doi:10.1103/PhysRevLett.68.1579.

[9] R. Saito, M. Fujita, G. Dresselhaus, M.S. Dresselhaus, Electronic structure of graphene tubules based on C 60, Phys. Rev. B. 46 (1992) 1804–1811. doi:10.1103/PhysRevB.46.1804.

[10] J.W.G. Wildoer, L.C. Venema, A.G. Rinzler, R.E. Smalley, C. Dekker, Electronic structure of atomically resolved carbon nanotubes, Nature. 391 (1998) 59–62. doi:10.1038/34139.

[11] Z.W. Pan, S.S. Xie, B.H. Chang, C.Y. Wang, L. Lu, W. Liu, W.Y. Zhou, W.Z. Li, Very long carbon nanotubes, Nature. 394 (1998) 631–632. doi:10.1038/29206.

[12] H.W. Zhu, Direct synthesis of long single-walled carbon nanotube strands, Science. 296 (2002) 884–886. doi:10.1126/science.1066996.

[13] K. Hata, Water-assisted highly efficient synthesis of impurity-free single-walled carbon nanotubes, Science. 306 (2004) 1362–1364. doi:10.1126/science.1104962.

[14] H. Dai, J.H. Hafner, A.G. Rinzler, D.T. Colbert, R.E. Smalley, Nanotubes as nanoprobes in scanning probe microscopy, Nature. 384 (1996) 147–150. doi:10.1038/384147a0.

[15] A.V. Melechko, V.I. Merkulov, T.E. McKnight, M.A. Guillorn, K.L. Klein, D.H. Lowndes, M.L. Simpson, Vertically aligned carbon nanofibers and related structures: controlled synthesis and directed assembly, J. Appl. Phys. 97 (2005) 041301. doi:10.1063/1.1857591.

[16] A. Jorio, G. Dresselhaus, M.S. Dresselhaus, eds., Carbon nanotubes: advanced topics in the synthesis, structure, properties, and applications, Springer, Berlin ; New York, 2008.

[17] N.S. Lee, D.S. Chung, I.T. Han, J.H. Kang, Y.S. Choi, H.Y. Kim, S.H. Park, Y.W. Jin, W.K. Yi, M.J. Yun, J.E. Jung, C.J. Lee, J.H. You, S.H. Jo, C.G. Lee, J.M. Kim, Application of carbon nanotubes to field emission displays, Diam. Relat. Mater. 10 (2001) 265–270. doi:10.1016/S0925-9635(00)00478-7.

[18] P. Liu, L. Liu, Y. Wei, K. Liu, Z. Chen, K. Jiang, Q. Li, S. Fan, Fast high-temperature response of carbon nanotube film and its application as an incandescent display, Adv. Mater. 21 (2009) 3563–3566. doi:10.1002/adma.200900473.

[19] K.L. Jiang, J.P. Wang, Q.Q. Li, L. Liu, C.H. Liu, S.S. Fan, Superaligned carbon nanotube arrays, films, and yarns: a road to applications, Adv. Mater. 23 (2011) 1154–1161. doi:10.1002/adma.201003989.

[20] R.H. Baughman, A.A. Zakhidov, W.A. de Heer, Carbon nanotubes--the route toward applications, Science. 297 (2002) 787–792. doi:10.1126/science.1060928.

[21] E.T. Thostenson, Z. Ren, T.-W. Chou, Advances in the science and technology of carbon nanotubes and their composites: a review, Compos. Sci. Technol. 61 (2001) 1899–1912. doi:10.1016/S0266-3538(01)00094-X.

[22] J.N. Coleman, U. Khan, Y.K. Gun'ko, Mechanical reinforcement of polymers using carbon nanotubes, Adv. Mater. 18 (2006) 689–706. doi:10.1002/adma.200501851.

[23] J.N. Coleman, U. Khan, W.J. Blau, Y.K. Gun'ko, Small but strong: a review of the mechanical properties of carbon nanotube–polymer composites, Carbon. 44 (2006) 1624–1652. doi:10.1016/j.carbon.2006.02.038.

[24] T. Rueckes, Carbon nanotube-based nonvolatile random access memory for molecular computing, Science. 289 (2000) 94–97. doi:10.1126/science.289.5476.94.

[25] G. Gruner, Carbon nanotube transistors for biosensing applications, Anal. Bioanal. Chem. 384 (2005) 322–335. doi:10.1007/s00216-005-3400-4.

[26] M. O'Connell, ed., Carbon nanotubes: properties and applications, CRC/Taylor & Francis, Boca Raton, FL, 2006.

[27] X. Ho, L. Ye, S.V. Rotkin, Q. Cao, S. Unarunotai, S. Salamat, M.A. Alam, J.A. Rogers, Scaling roperties in transistors that use aligned arrays of single-walled carbon nanotubes, Nano Lett. 10 (2010) 499–503. doi:10.1021/nl903281v.

[28] A.D. Franklin, Electronics: the road to carbon nanotube transistors, Nature. 498 (2013) 443–444. doi:10.1038/498443a.

[29] B.K. Kaushik, S. Goel, G. Rauthan, Future VLSI interconnects: optical fiber or carbon nanotube – a review, Microelectron. Int. 24 (2007) 53–63. doi:10.1108/13565360710745601.

[30] R.S. Prasher, Surface chemistry and characteristics based model for the thermal contact resistance of fluidic interstitial thermal interface materials, J. Heat Transf. 123 (2001) 969. doi:10.1115/1.1388301.

[31] T. Tong, Y. Zhao, L. Delzeit, A. Kashani, M. Meyyappan, A. Majumdar, Dense vertically aligned multiwalled carbon nanotube arrays as thermal interface materials, IEEE Trans. Compon. Packag. Technol. 30 (2007) 92–100. doi:10.1109/TCAPT.2007.892079.

[32] A.P. Ottenhouse, ed., Carbon nanotubes: new research, Nova Science Publishers, New York, 2009.

[33] M. Winter, R.J. Brodd, What are batteries, fuel cells, and supercapacitors?, Chem. Rev. 104 (2004) 4245–4270. doi:10.1021/cr020730k.

[34] M.M.J. Treacy, T.W. Ebbesen, J.M. Gibson, Exceptionally high Young's modulus observed for individual carbon nanotubes, Nature. 381 (1996) 678–680. doi:10.1038/381678a0.

[35] M.-F. Yu, B.S. Files, S. Arepalli, R. Ruoff, Tensile loading of ropes of single-wall carbon nanotubes and their mechanical properties, Phys. Rev. Lett. 84 (2000) 5552–5555. doi:10.1103/PhysRevLett.84.5552.

[36] E.W. Wong, Nanobeam mechanics: elasticity, strength, and toughness of nanorods and nanotubes, Science. 277 (1997) 1971–1975. doi:10.1126/science.277.5334.1971.

[37] M.F. Yu, O. Lourie, M.J. Dyer, K. Moloni, T.F. Kelly, R.S. Ruoff, Strength and breaking mechanism of multiwalled carbon nanotubes under tensile load, Science. 287 (2000) 637–640. doi:10.1126/science.287.5453.637.

[38] H.G. Chae, B.A. Newcomb, P.V. Gulgunje, Y. Liu, K.K. Gupta, M.G. Kamath, K.M. Lyons, S. Ghoshal, C. Pramanik, L. Giannuzzi, K. Şahin, I. Chasiotis, S. Kumar, High strength and high modulus carbon fibers, Carbon. 93 (2015) 81–87. doi:10.1016/j.carbon.2015.05.016.

[39] T. Langston, The tensile behavior of high-strength carbon fibers, Microsc. Microanal. 22 (2016) 841–844. doi:10.1017/S143192761601134X.

[40] M.R. Falvo, G.J. Clary, R.M. Taylor, V. Chi, F.P. Brooks, S. Washburn, R. Superfine, Bending and buckling of carbon nanotubes under large strain, Nature. 389 (1997) 582–584. doi:10.1038/39282.

[41] J.P. Lu, Elastic properties of carbon nanotubes and nanoropes, Phys. Rev. Lett. 79 (1997) 1297–1300. doi:10.1103/PhysRevLett.79.1297.

[42] T.W. Ebbesen, H.J. Lezec, H. Hiura, J.W. Bennett, H.F. Ghaemi, T. Thio, Electrical conductivity of individual carbon nanotubes, Nature. 382 (1996) 54–56. doi:10.1038/382054a0.

[43] J. Appenzeller, R. Martel, P. Avouris, H. Stahl, B. Lengeler, Optimized contact configuration for the study of transport phenomena in ropes of single-wall carbon nanotubes, Appl. Phys. Lett. 78 (2001) 3313. doi:10.1063/1.1373413.

[44] A. Javey, J. Guo, Q. Wang, M. Lundstrom, H. Dai, Ballistic carbon nanotube field-effect transistors, Nature. 424 (2003) 654–657. doi:10.1038/nature01797.

[45] M. Zamkov, A.S. Alnaser, B. Shan, Z. Chang, P. Richard, Probing the intrinsic conductivity of multiwalled carbon nanotubes, Appl. Phys. Lett. 89 (2006) 093111. doi:10.1063/1.2340537.

[46] S. Frank, Carbon nanotube quantum resistors, Science. 280 (1998) 1744–1746. doi:10.1126/science.280.5370.1744.

[47] G.-D. Zhan, A.K. Mukherjee, Carbon nanotube reinforced alumina-based ceramics with novel mechanical, electrical, and thermal properties, Int. J. Appl. Ceram. Technol. 1 (2005) 161–171. doi:10.1111/j.1744-7402.2004.tb00166.x.

[48] Y.J. Kim, T.S. Shin, H.D. Choi, J.H. Kwon, Y.-C. Chung, H.G. Yoon, Electrical conductivity of chemically modified multiwalled carbon nanotube/epoxy composites, Carbon. 43 (2005) 23–30. doi:10.1016/j.carbon.2004.08.015.

[49] P. Dinesh, N.M. Renukappa, Siddaramaiah, Impedance and susceptance characterization of multiwalled carbon nanotubes with high density polyethylene-carbon black nanocomposites, Integr. Ferroelectr. 116 (2010) 128–136. doi:10.1080/10584587.2010.503519.

[50] S. Pande, A. Chaudhary, D. Patel, B.P. Singh, R.B. Mathur, Mechanical and electrical properties of multiwall carbon nanotube/polycarbonate composites for electrostatic discharge and electromagnetic interference shielding applications, RSC Adv. 4 (2014) 13839. doi:10.1039/c3ra47387b.

[51] S. Berber, Y.-K. Kwon, D. Tománek, Unusually high thermal conductivity of carbon nanotubes, Phys. Rev. Lett. 84 (2000) 4613–4616. doi:10.1103/PhysRevLett.84.4613.

[52] P. Kim, L. Shi, A. Majumdar, P.L. McEuen, Thermal transport measurements of individual multiwalled nanotubes, Phys. Rev. Lett. 87 (2001). doi:10.1103/PhysRevLett.87.215502.

[53] A. Peigney, C. Laurent, E. Flahaut, R.R. Bacsa, A. Rousset, Specific surface area of carbon nanotubes and bundles of carbon nanotubes, Carbon. 39 (2001) 507–514. doi:10.1016/S0008-6223(00)00155-X.

[54] T.A. Hilder, J.M. Hill, Carbon nanotubes as drug delivery nanocapsules, Curr. Appl. Phys. 8 (2008) 258–261. doi:10.1016/j.cap.2007.10.011.

[55] S.M. Khamis, R.R. Johnson, Z. Luo, A.T. Charlie Johnson, Homo-DNA functionalized carbon nanotube chemical sensors, J. Phys. Chem. Solids. 71 (2010) 476–479. doi:10.1016/j.jpcs.2009.12.015.

[56] K. Chizari, I. Janowska, M. Houllé, I. Florea, O. Ersen, T. Romero, P. Bernhardt, M.J. Ledoux, C. Pham-Huu, Tuning of nitrogen-doped carbon nanotubes as catalyst support for liquid-phase reaction, Appl. Catal. Gen. 380 (2010) 72–80. doi:10.1016/j.apcata.2010.03.031.

[57] C. Journet, P. Bernier, Production of carbon nanotubes, Appl. Phys. Mater. Sci. Process. 67 (1998) 1–9. doi:10.1007/s003390050731.

[58] N.M. Mubarak, E.C. Abdullah, N.S. Jayakumar, J.N. Sahu, An overview on methods for the production of carbon nanotubes, J. Ind. Eng. Chem. 20 (2014) 1186–1197. doi:10.1016/j.jiec.2013.09.001.

[59] Y. Saito, M. Inagaki, Optical emission studies on chemical species in an arc flame of fullerene/metallofullerene generator, Jpn. J. Appl. Phys. 32 (1993) L954–L957. doi:10.1143/JJAP.32.L954.

[60] B.I. Yakobson, R.E. Smalley, Fullerene nanotubes: C1,000,000 and beyond, Am. Sci. 85 (1997) 324.

[61] T. Guo, P. Nikolaev, A. Thess, D.T. Colbert, R.E. Smalley, Catalytic growth of single-walled manotubes by laser vaporization, Chem. Phys. Lett. 243 (1995) 49–54. doi:10.1016/0009-2614(95)00825-O.

[62] T. Guo, P. Nikolaev, A.G. Rinzler, D. Tomanek, D.T. Colbert, R.E. Smalley, Self-assembly of tubular fullerenes, J. Phys. Chem. 99 (1995) 10694–10697. doi:10.1021/j100027a002.

[63] R.T.K. Baker, Catalytic growth of carbon filaments, Carbon. 27 (1989) 315–323. doi:10.1016/0008-6223(89)90062-6.

[64] Z.P. Huang, D.L. Carnahan, J. Rybczynski, M. Giersig, M. Sennett, D.Z. Wang, J.G. Wen, K. Kempa, Z.F. Ren, Growth of large periodic arrays of carbon nanotubes, Appl. Phys. Lett. 82 (2003) 460. doi:10.1063/1.1539299.

[65] R. Zhang, Y. Zhang, Q. Zhang, H. Xie, W. Qian, F. Wei, Growth of half-meter long carbon nanotubes based on Schulz–Flory distribution, ACS Nano. 7 (2013) 6156–6161. doi:10.1021/nn401995z.

[66] X. Wang, Q. Jiang, W.Z. Xu, W. Cai, Y. Inoue, Y. Zhu, Effect of carbon nanotube length on thermal, electrical and mechanical properties of CNT/bismaleimide composites, Carbon. 53 (2013) 145–152. doi:10.1016/j.carbon.2012.10.041.

[67] Y. Homma, Y. Kobayashi, T. Ogino, D. Takagi, R. Ito, Y.J. Jung, P.M. Ajayan, Role of transition metal catalysts in single-walled carbon nanotube growth in chemical vapor deposition, J. Phys. Chem. B. 107 (2003) 12161–12164. doi:10.1021/jp0353845.

[68] S. Hofmann, R. Sharma, C. Ducati, G. Du, C. Mattevi, C. Cepek, M. Cantoro, S. Pisana, A. Parvez, F. Cervantes-Sodi, A.C. Ferrari, R. Dunin-Borkowski, S. Lizzit, L. Petaccia, A. Goldoni, J. Robertson, In situ observations of catalyst dynamics during surface-bound carbon nanotube nucleation, Nano Lett. 7 (2007) 602–608. doi:10.1021/nl0624824.

[69] S. Esconjauregui, C.M. Whelan, K. Maex, The reasons why metals catalyze the nucleation and growth of carbon nanotubes and other carbon nanomorphologies, Carbon. 47 (2009) 659–669. doi:10.1016/j.carbon.2008.10.047.

[70] H. Yoshida, S. Takeda, T. Uchiyama, H. Kohno, Y. Homma, Atomic-scale in-situ observation of carbon nanotube growth from solid state iron carbide nanoparticles, Nano Lett. 8 (2008) 2082–2086. doi:10.1021/nl080452q.

[71] W.D. Zhang, Y. Wen, S. Min Liu, W.C. Tjiu, G. Qin Xu, L. Ming Gan, Synthesis of vertically aligned carbon nanotubes on metal deposited quartz plates, Carbon. 40 (2002) 1981–1989. doi:10.1016/S0008-6223(02)00052-0.

[72] H. Ohno, D. Takagi, K. Yamada, S. Chiashi, A. Tokura, Y. Homma, Growth of vertically aligned single-walled carbon nanotubes on alumina and sapphire substrates, Jpn. J. Appl. Phys. 47 (2008) 1956–1960. doi:10.1143/JJAP.47.1956.

[73] K. Jiang, Q. Li, S. Fan, Nanotechnology: spinning continuous carbon nanotube yarns, Nature. 419 (2002) 801–801. doi:10.1038/419801a.

[74] Q.W. Li, X.F. Zhang, R.F. DePaula, L.X. Zheng, Y.H. Zhao, L. Stan, T.G. Holesinger, P.N. Arendt, D.E. Peterson, Y.T. Zhu, Sustained growth of ultralong carbon nanotube arrays for fiber spinning, Adv. Mater. 18 (2006) 3160–3163. doi:10.1002/adma.200601344.

[75] S. Noda, K. Hasegawa, H. Sugime, K. Kakehi, Z. Zhang, S. Maruyama, Y. Yamaguchi, Millimeter-thick single-walled carbon nanotube forests: hidden role of catalyst support, Jpn. J. Appl. Phys. 46 (2007) L399–L401. doi:10.1143/JJAP.46.L399.

[76] C. Mattevi, C.T. Wirth, S. Hofmann, R. Blume, M. Cantoro, C. Ducati, C. Cepek, A. Knop-Gericke, S. Milne, C. Castellarin-Cudia, S. Dolafi, A. Goldoni, R. Schloegl, J. Robertson, In-situ X-ray photoelectron spectroscopy study of catalyst−support interactions and growth of carbon nanotube forests, J. Phys. Chem. C. 112 (2008) 12207–12213. doi:10.1021/jp802474g.

[77] W.Z. Li, J.G. Wen, Z.F. Ren, Effect of temperature on growth and structure of carbon nanotubes by chemical vapor deposition, Appl. Phys. Mater. Sci. Process. 74 (2002) 397–402. doi:10.1007/s003390201284.

[78] Y. Tu, Z.P. Huang, D.Z. Wang, J.G. Wen, Z.F. Ren, Growth of aligned carbon nanotubes with controlled site density, Appl. Phys. Lett. 80 (2002) 4018. doi:10.1063/1.1482790.

[79] B. Kitiyanan, W.E. Alvarez, J.H. Harwell, D.E. Resasco, Controlled production of single-wall carbon nanotubes by catalytic decomposition of CO on bimetallic Co–Mo catalysts, Chem. Phys. Lett. 317 (2000) 497–503. doi:10.1016/S0009-2614(99)01379-2.

[80] M. Meyyappan, L. Delzeit, A. Cassell, D. Hash, Carbon nanotube growth by PECVD: a review, Plasma Sources Sci. Technol. 12 (2003) 205–216. doi:10.1088/0963-0252/12/2/312.

[81] X. Zhang, K. Jiang, C. Feng, P. Liu, L. Zhang, J. Kong, T. Zhang, Q. Li, S. Fan, Spinning and processing continuous yarns from 4-Inch wafer scale super-aligned carbon nanotube arrays, Adv. Mater. 18 (2006) 1505–1510. doi:10.1002/adma.200502528.

[82] K. Liu, Y. Sun, L. Chen, C. Feng, X. Feng, K. Jiang, Y. Zhao, S. Fan, Controlled growth of super-aligned carbon nanotube arrays for spinning continuous unidirectional sheets with tunable physical properties, Nano Lett. 8 (2008) 700–705. doi:10.1021/nl0723073.

[83] M. Zhang, K.R. Atkinson, R.H. Baughman, Multifunctional carbon nanotube yarns by downsizing an ancient technology, Science. 306 (2004) 1358–1361. doi:10.1126/science.1104276.

[84] M. Zhang, S. Fang, A.A. Zakhidov, S.B. Lee, A.E. Aliev, C.D. Williams, K.R. Atkinson, R.H. Baughman, Strong, transparent, multifunctional, carbon nanotube sheets, Science. 309 (2005) 1215–1219. doi:10.1126/science.1115311.

[85] Y. Inoue, K. Kakihata, Y. Hirono, T. Horie, A. Ishida, H. Mimura, One-step grown aligned bulk carbon nanotubes by chloride mediated chemical vapor deposition, Appl. Phys. Lett. 92 (2008) 213113. doi:10.1063/1.2937082.

[86] S. Zhang, L. Zhu, M.L. Minus, H.G. Chae, S. Jagannathan, C.-P. Wong, J. Kowalik, L.B. Roberson, S. Kumar, Solid-state spun fibers and yarns from 1-mm long carbon nanotube forests synthesized by water-assisted chemical vapor deposition, J. Mater. Sci. 43 (2008) 4356–4362. doi:10.1007/s10853-008-2558-5.

[87] H. Zhao, P.D. Bradford, X. Wang, W. Liu, T.J.M. Luo, Q. Jia, Y. Zhu, F.-G. Yuan, An intermetallic Fe–Zr catalyst used for growing long carbon nanotube arrays, Mater. Lett. 64 (2010) 1947–1950. doi:10.1016/j.matlet.2010.05.045.

[88] O. Yildiz, P.D. Bradford, Aligned carbon nanotube sheet high efficiency particulate air filters, Carbon. 64 (2013) 295–304. doi:10.1016/j.carbon.2013.07.066.

[89] F. Fisher, Fiber waviness in nanotube-reinforced polymer composites—I: Modulus predictions using effective nanotube properties, Compos. Sci. Technol. 63 (2003) 1689–1703. doi:10.1016/S0266-3538(03)00069-1.

[90] B. Vigolo, A. Penicaud, C. Coulon, C. Sauder, R. Pailler, C. Journet, P. Bernier, P. Poulin, Macroscopic fibers and ribbons of oriented carbon nanotubes, Science. 290 (2000) 1331–1334. doi:10.1126/science.290.5495.1331.

[91] A.B. Dalton, S. Collins, E. Muñoz, J.M. Razal, V.H. Ebron, J.P. Ferraris, J.N. Coleman, B.G. Kim, R.H. Baughman, Super-tough carbon-nanotube fibres, Nature. 423 (2003) 703–703. doi:10.1038/423703a.

[92] S.R. Bakshi, D. Lahiri, A. Agarwal, Carbon nanotube reinforced metal matrix composites - a review, Int. Mater. Rev. 55 (2010) 41–64. doi:10.1179/095066009X12572530170543.

[93] C. Daraio, V.F. Nesterenko, S. Jin, Highly nonlinear contact interaction and dynamic energy dissipation by forest of carbon nanotubes, Appl. Phys. Lett. 85 (2004) 5724. doi:10.1063/1.1829778.

[94] Z. Wang, N. Koratkar, L. Ci, P.M. Ajayan, Combined micro-/nanoscale surface roughness for enhanced hydrophobic stability in carbon nanotube arrays, Appl. Phys. Lett. 90 (2007) 143117. doi:10.1063/1.2720761.

[95] J.Y. Hwang, A.R.P. Singh, M. Chaudhari, J. Tiley, Y. Zhu, J. Du, R. Banerjee, Templated growth of hexagonal nickel carbide nanocrystals on vertically aligned carbon nanotubes, J. Phys. Chem. C. 114 (2010) 10424–10429. doi:10.1021/jp102571g.

[96] S. Boncel, K.K.K. Koziol, K.Z. Walczak, A.H. Windle, M.S.P. Shaffer, Infiltration of highly aligned carbon nanotube arrays with molten polystyrene, Mater. Lett. 65 (2011) 2299–2303. doi:10.1016/j.matlet.2011.04.065.

[97] C.J. Hu, Y.H. Lin, C.W. Tang, M.Y. Tsai, W.K. Hsu, H.F. Kuo, ZnO-coated carbon nanotubes: flexible piezoelectric generators, Adv. Mater. 23 (2011) 2941–2945. doi:10.1002/adma.201100358.

[98] K.K.K. Koziol, S. Boncel, M.S.P. Shaffer, A.H. Windle, Aligned carbon nanotube-polystyrene composites prepared by in situ polymerisation of stacked layers, Compos. Sci. Technol. 71 (2011) 1606–1611. doi:10.1016/j.compscitech.2011.07.007.

[99] X. Zhang, Q. Li, T.G. Holesinger, P.N. Arendt, J. Huang, P.D. Kirven, T.G. Clapp, R.F. DePaula, X. Liao, Y. Zhao, L. Zheng, D.E. Peterson, Y. Zhu, Ultrastrong, stiff, and lightweight carbon-nanotube fibers, Adv. Mater. 19 (2007) 4198–4201. doi:10.1002/adma.200700776.

[100] N. Behabtu, C.C. Young, D.E. Tsentalovich, O. Kleinerman, X. Wang, A.W.K. Ma, E.A. Bengio, R.F. ter Waarbeek, J.J. de Jong, R.E. Hoogerwerf, S.B. Fairchild, J.B. Ferguson, B. Maruyama, J. Kono, Y. Talmon, Y. Cohen, M.J. Otto, M. Pasquali,

Strong, light, multifunctional fibers of carbon nanotubes with ultrahigh conductivity, Science. 339 (2013) 182–186. doi:10.1126/science.1228061.

[101] K. Liu, Y.H. Sun, X.Y. Lin, R.F. Zhou, J.P. Wang, S.S. Fan, K.L. Jiang, Scratch-resistant, highly conductive, and high-strength carbon nanotube-based composite yarns, ACS Nano. 4 (2010) 5827–5834. doi:10.1021/nn1017318.

[102] W. Liu, H. Zhao, Z. Yong, G. Xu, X. Wang, F. Xu, D. Hui, Y. Qiu, Improving mechanical and electrical properties of oriented polymer-free multi-walled carbon nanotube paper by spraying while winding, Compos. Part B Eng. 53 (2013) 342–346. doi:10.1016/j.compositesb.2013.05.043.

[103] L.W. Zhang, X. Wang, W.Z. Xu, Y.Y. Zhang, Q.W. Li, P.D. Bradford, Y.T. Zhu, Strong and conductive dry carbon nanotube films by microcombing, Small. 11 (2015) 3830–3836. doi:10.1002/smll.201500111.

[104] X. Wang, P.D. Bradford, W. Liu, H.B. Zhao, Y. Inoue, J.-P. Maria, Q.W. Li, F.-G. Yuan, Y. Zhu, Mechanical and electrical property improvement in CNT/Nylon composites through drawing and stretching, Compos. Sci. Technol. 71 (2011) 1677–1683. doi:10.1016/j.compscitech.2011.07.023.

[105] W. Liu, X.H. Zhang, G. Xu, P.D. Bradford, X. Wang, H.B. Zhao, Y.Y. Zhang, Q.X. Jia, F.-G. Yuan, Q.W. Li, Y.P. Qiu, Y.T. Zhu, Producing superior composites by

winding carbon nanotubes onto a mandrel under a poly(vinyl alcohol) spray, Carbon. 49 (2011) 4786–4791. doi:10.1016/j.carbon.2011.06.089.

[106] W. Liu, H. Zhao, Y. Inoue, X. Wang, P.D. Bradford, H. Kim, Y.P. Qiu, Y.T. Zhu, Poly(vinyl alcohol) reinforced with large-diameter carbon nanotubes via spray winding, Compos. Part Appl. Sci. Manuf. 43 (2012) 587–592. doi:10.1016/j.compositesa.2011.12.029.

[107] X. Wang, Z.Z. Yong, Q.W. Li, P.D. Bradford, W. Liu, D.S. Tucker, W. Cai, H. Wang, F.G. Yuan, Y.T. Zhu, Ultrastrong, stiff and multifunctional carbon nanotube composites, Mater. Res. Lett. 1 (2013) 19–25. doi:10.1080/21663831.2012.686586.

[108] L.W. Zhang, X. Wang, R. Li, Q.W. Li, P.D. Bradford, Y.T. Zhu, Microcombing enables high-performance carbon nanotube composites, Compos. Sci. Technol. 123 (2016) 92–98. doi:10.1016/j.compscitech.2015.12.012.

[109] J.M. Sieben, A. Ansón-Casaos, M.T. Martínez, E. Morallón, Single-walled carbon nanotube buckypapers as electrocatalyst supports for methanol oxidation, J. Power Sources. 242 (2013) 7–14. doi:10.1016/j.jpowsour.2013.05.044.

[110] S.M. Cooper, H.F. Chuang, M. Cinke, B.A. Cruden, M. Meyyappan, Gas permeability of a buckypaper membrane, Nano Lett. 3 (2003) 189–192. doi:10.1021/nl0259131.

[111] J. Wei, H. Zhu, Y. Li, B. Chen, Y. Jia, K. Wang, Z. Wang, W. Liu, J. Luo, M. Zheng, D. Wu, Y. Zhu, B. Wei, Ultrathin single–layered membranes from double–walled carbon nanotubes, Adv. Mater. 18 (2006) 1695–1700. doi:10.1002/adma.200501841.

[112] P.D. Bradford, X. Wang, H.B. Zhao, J.-P. Maria, Q. Jia, Y.T. Zhu, A novel approach to fabricate high volume fraction nanocomposites with long aligned carbon nanotubes, Compos. Sci. Technol. 70 (2010) 1980–1985. doi:10.1016/j.compscitech.2010.07.020.

[113] A.S. Claye, J.E. Fischer, C.B. Huffman, A.G. Rinzler, R.E. Smalley, Solid-state electrochemistry of the Li single wall carbon nanotube system, J. Electrochem. Soc. 147 (2000) 2845. doi:10.1149/1.1393615.

[114] C. Zhou, S. Kumar, C.D. Doyle, J.M. Tour, Functionalized single wall carbon nanotubes treated with pyrrole for electrochemical supercapacitor membranes, Chem. Mater. 17 (2005) 1997–2002. doi:10.1021/cm047882b.

[115] D. Wang, P. Song, C. Liu, W. Wu, S. Fan, Highly oriented carbon nanotube papers made of aligned carbon nanotubes, Nanotechnology. 19 (2008) 075609. doi:10.1088/0957-4484/19/7/075609.

[116] Q. Wu, C. Zhang, R. Liang, B. Wang, Fire retardancy of a buckypaper membrane, Carbon. 46 (2008) 1164–1165. doi:10.1016/j.carbon.2008.03.021.

[117] Z. Wang, Z. Liang, B. Wang, C. Zhang, L. Kramer, Processing and property investigation of single-walled carbon nanotube (SWNT) buckypaper/epoxy resin matrix

nanocomposites, Compos. Part Appl. Sci. Manuf. 35 (2004) 1225–1232. doi:10.1016/j.compositesa.2003.09.029.

[118] S. Wang, Z. Liang, B. Wang, C. Zhang, High-strength and multifunctional macroscopic fabric of single-walled carbon nanotubes, Adv. Mater. 19 (2007) 1257–1261. doi:10.1002/adma.200602140.

[119] G. Xu, Q. Zhang, W. Zhou, J. Huang, F. Wei, The feasibility of producing MWCNT paper and strong MWCNT film from VACNT array, Appl. Phys. A. 92 (2008) 531–539. doi:10.1007/s00339-008-4606-z.

[120] J.T. Di, D.M. Hu, H.Y. Chen, Z.Z. Yong, M.H. Chen, Z.H. Feng, Y.T. Zhu, Q. Li, Ultrastrong, foldable, and highly conductive carbon nanotube film, ACS Nano. 6 (2012) 5457–5464. doi:10.1021/nn301321j.

[121] Y. Wang, M. Li, Y. Gu, X. Zhang, S. Wang, Q. Li, Z. Zhang, Tuning carbon nanotube assembly for flexible, strong and conductive films, Nanoscale. 7 (2015) 3060–3066. doi:10.1039/C4NR06401A.

[122] J.T. Di, X. Wang, Y.J. Xing, Y.Y. Zhang, X.H. Zhang, W.B. Lu, Q.W. Li, Y.T. Zhu, Dry-processable carbon nanotubes for functional devices and composites, Small. 10 (2014) 4606–4625. doi:10.1002/smll.201401465.

[123] W.D. Callister, D.G. Rethwisch, Materials science and engineering: an introduction, 9th edition, Wiley, Hoboken, NJ, 2014.

[124] Q. Cheng, J. Wang, K. Jiang, Q. Li, S. Fan, Fabrication and properties of aligned multiwalled carbon nanotube-reinforced epoxy composites, J. Mater. Res. 23 (2008) 2975–2983. doi:10.1557/JMR.2008.0356.

[125] Q.F. Cheng, J.P. Wang, J.J. Wen, C.H. Liu, K.L. Jiang, Q.Q. Li, S.S. Fan, Carbon nanotube/epoxy composites fabricated by resin transfer molding, Carbon. 48 (2010) 260–266. doi:10.1016/j.carbon.2009.09.014.

[126] X. Zhang, Q. Li, Y. Tu, Y. Li, J.Y. Coulter, L. Zheng, Y. Zhao, Q. Jia, D.E. Peterson, Y. Zhu, Strong carbon-nanotube fibers spun from long carbon-nanotube arrays, Small. 3 (2007) 244–248. doi:10.1002/smll.200600368.

[127] R.S. Ruoff, D.C. Lorents, Mechanical and thermal properties of carbon nanotubes, Carbon. 33 (1995) 925–930. doi:10.1016/0008-6223(95)00021-5.

[128] P.M. Ajayan, J.M. Tour, Materials science: nanotube composites, Nature. 447 (2007) 1066–1068. doi:10.1038/4471066a.

[129] J. Li, Y. Lu, Q. Ye, M. Cinke, J. Han, M. Meyyappan, Carbon nanotube sensors for gas and organic vapor detection, Nano Lett. 3 (2003) 929–933. doi:10.1021/nl034220x.

[130] R.H. Baughman, Carbon nanotube actuators, Science. 284 (1999) 1340–1344. doi:10.1126/science.284.5418.1340.

[131] D. Gendron, G. Bubak, L. Ceseracciu, F. Ricciardella, A. Ansaldo, D. Ricci, Significant strain and force improvements of single-walled carbon nanotube actuator: A metal chalcogenides approach, Sens. Actuators B Chem. 230 (2016) 673–683. doi:10.1016/j.snb.2016.02.116.

[132] R. Allen, G.G. Fuller, Z. Bao, Aligned SWNT films from low-yield stress gels and their transparent electrode performance, ACS Appl. Mater. Interfaces. 5 (2013) 7244–7252. doi:10.1021/am401592v.

[133] A.C. Schmidt, X. Wang, Y. Zhu, L.A. Sombers, Carbon nanotube yarn electrodes for enhanced detection of neurotransmitter dynamics in live brain tissue, ACS Nano. 7 (2013) 7864–7873. doi:10.1021/nn402857u.

[134] A.G. Zestos, C.B. Jacobs, E. Trikantzopoulos, A.E. Ross, B.J. Venton, Polyethylenimine Carbon Nanotube Fiber Electrodes for Enhanced Detection of Neurotransmitters, Anal. Chem. 86 (2014) 8568–8575. doi:10.1021/ac5003273.

[135] K. Wang, S. Luo, Y. Wu, X. He, F. Zhao, J. Wang, K. Jiang, S. Fan, Super-aligned carbon nanotube films as current collectors for lightweight and flexible lithium ion batteries, Adv. Funct. Mater. 23 (2013) 846–853. doi:10.1002/adfm.201202412.

[136] Y. Inoue, Y. Suzuki, Y. Minami, J. Muramatsu, Y. Shimamura, K. Suzuki, A. Ghemes, M. Okada, S. Sakakibara, H. Mimura, K. Naito, Anisotropic carbon nanotube

papers fabricated from multiwalled carbon nanotube webs, Carbon. 49 (2011) 2437–2443. doi:10.1016/j.carbon.2011.02.010.

[137] H.G. Tennent, J.J. Barber, R. Hoch, Constant diameter, free of pyrolytic carbon; reinforcement of structures; enhance electrical or thermal conductivity, US5578543 A, 1996.

[138] J.W.S. Hearle, P. Grosberg, S. Backer, Structural mechanics of fibers, yarns, and fabrics, Wiley-Interscience, New York, 1969.

[139] K.L. Stano, M. Carroll, R. Padbury, M. McCord, J.S. Jur, P.D. Bradford, Conformal atomic layer deposition of alumina on millimeter tall, vertically-aligned carbon nanotube arrays, ACS Appl. Mater. Interfaces. 6 (2014) 19135–19143. doi:10.1021/am505107s.

[140] J.E. Fischer, W. Zhou, J. Vavro, M.C. Llaguno, C. Guthy, R. Haggenmueller, M.J. Casavant, D.E. Walters, R.E. Smalley, Magnetically aligned single wall carbon nanotube films: preferred orientation and anisotropic transport properties, J. Appl. Phys. 93 (2003) 2157. doi:10.1063/1.1536733.

[141] N.R. Raravikar, L.S. Schadler, A. Vijayaraghavan, Y. Zhao, B. Wei, P.M. Ajayan, Synthesis and characterization of thickness-aligned carbon nanotube−polymer composite films, Chem. Mater. 17 (2005) 974–983. doi:10.1021/cm0485254.

[142] J. Ji, G. Sui, Y. Yu, Y. Liu, Y. Lin, Z. Du, S. Ryu, X. Yang, Significant Improvement of Mechanical Properties Observed in Highly Aligned Carbon-Nanotube-Reinforced Nanofibers, J. Phys. Chem. C. 113 (2009) 4779–4785. doi:10.1021/jp8077198.

[143] M.J. Biercuk, M.C. Llaguno, M. Radosavljevic, J.K. Hyun, A.T. Johnson, J.E. Fischer, Carbon nanotube composites for thermal management, Appl. Phys. Lett. 80 (2002) 2767. doi:10.1063/1.1469696.

[144] J. Wang, J.-S. Wang, Carbon nanotube thermal transport: Ballistic to diffusive, Appl. Phys. Lett. 88 (2006) 111909. doi:10.1063/1.2185727.

[145] C. Niu, E.K. Sichel, R. Hoch, D. Moy, H. Tennent, High power electrochemical capacitors based on carbon nanotube electrodes, Appl. Phys. Lett. 70 (1997) 1480. doi:10.1063/1.118568.

[146] K.H. An, W.S. Kim, Y.S. Park, Y.C. Choi, S.M. Lee, D.C. Chung, D.J. Bae, S.C. Lim, Y.H. Lee, Supercapacitors using single-walled carbon nanotube electrodes, Adv. Mater. 13 (2001) 497–500. doi:10.1002/1521-4095(200104)13:7<497::AID-ADMA497>3.0.CO;2-H.

[147] S. Rosenblatt, Y. Yaish, J. Park, J. Gore, V. Sazonova, P.L. McEuen, High performance electrolyte gated carbon nanotube transistors, Nano Lett. 2 (2002) 869–872. doi:10.1021/nl025639a.

[148] H.D. Wagner, Nanocomposites: paving the way to stronger materials, Nat. Nanotechnol. 2 (2007) 742–744. doi:10.1038/nnano.2007.401.

[149] W.J. Ma, L.Q. Liu, Z. Zhang, R. Yang, G. Liu, T.H. Zhang, X.F. An, X.S. Yi, Y. Ren, Z.Q. Niu, J. Li, H. Dong, W. Zhou, P.M. Ajayan, S. Xie, High-strength composite fibers: realizing true potential of carbon nanotubes in polymer matrix through continuous reticulate architecture and molecular level couplings, Nano Lett. 9 (2009) 2855–2861. doi:10.1021/nl901035v.

[150] X. Zhang, T.V. Sreekumar, T. Liu, S. Kumar, Properties and structure of nitric acid oxidized single wall carbon nanotube films, J. Phys. Chem. B. 108 (2004) 16435–16440. doi:10.1021/jp0475988.

[151] U. Dettlaff-Weglikowska, V. Skákalová, R. Graupner, S.H. Jhang, B.H. Kim, H.J. Lee, L. Ley, Y.W. Park, S. Berber, D. Tománek, S. Roth, Effect of $SOCl_2$ treatment on electrical and mechanical properties of single-wall carbon nanotube networks, J. Am. Chem. Soc. 127 (2005) 5125–5131. doi:10.1021/ja046685a.

[152] J.G. Park, J. Smithyman, C.-Y. Lin, A. Cooke, A.W. Kismarahardja, S. Li, R. Liang, J.S. Brooks, C. Zhang, B. Wang, Effects of surfactants and alignment on the physical properties of single-walled carbon nanotube buckypaper, J. Appl. Phys. 106 (2009) 104310. doi:10.1063/1.3255901.

[153] T.V. Sreekumar, T. Liu, S. Kumar, L.M. Ericson, R.H. Hauge, R.E. Smalley, Single-wall carbon nanotube films, Chem. Mater. 15 (2003) 175–178. doi:10.1021/cm020367y.

[154] Z. Špitalský, C. Aggelopoulos, G. Tsoukleri, C. Tsakiroglou, J. Parthenios, S. Georga, C. Krontiras, D. Tasis, K. Papagelis, C. Galiotis, The effect of oxidation treatment on the properties of multi-walled carbon nanotube thin films, Mater. Sci. Eng. B. 165 (2009) 135–138. doi:10.1016/j.mseb.2009.09.019.

[155] A. Kis, G. Csányi, J.-P. Salvetat, T.-N. Lee, E. Couteau, A.J. Kulik, W. Benoit, J. Brugger, L. Forró, Reinforcement of single-walled carbon nanotube bundles by intertube bridging, Nat. Mater. 3 (2004) 153–157. doi:10.1038/nmat1076.

[156] Q. Cheng, J. Bao, J. Park, Z. Liang, C. Zhang, B. Wang, High mechanical performance composite conductor: multi-walled carbon nanotube sheet/bismaleimide nanocomposites, Adv. Funct. Mater. 19 (2009) 3219–3225. doi:10.1002/adfm.200900663.

[157] Q. Liu, M. Li, Y. Gu, Y. Zhang, S. Wang, Q. Li, Z. Zhang, Highly aligned dense carbon nanotube sheets induced by multiple stretching and pressing, Nanoscale. 6 (2014) 4338–4344. doi:10.1039/C3NR06704A.

[158] L. Song, L. Ci, L. Lv, Z. Zhou, X. Yan, D. Liu, H. Yuan, Y. Gao, J. Wang, L. Liu, X. Zhao, Z. Zhang, X. Dou, W. Zhou, G. Wang, C. Wang, S. Xie, Direct synthesis of a

macroscale single-walled carbon nanotube non-woven material, Adv. Mater. 16 (2004) 1529–1534. doi:10.1002/adma.200306393.

[159] W. Ma, L. Song, R. Yang, T. Zhang, Y. Zhao, L. Sun, Y. Ren, D. Liu, L. Liu, J. Shen, Z. Zhang, Y. Xiang, W. Zhou, S. Xie, Directly synthesized strong, highly conducting, transparent single-walled carbon nanotube films, Nano Lett. 7 (2007) 2307–2311. doi:10.1021/nl070915c.

[160] C.A. Lawrence, Fundamentals of spun yarn technology, CRC Press, Boca Raton, Fla, 2003.

[161] L.Q. Liu, W.J. Ma, Z. Zhang, Macroscopic carbon nanotube assemblies: preparation, properties, and potential applications, Small. 7 (2011) 1504–1520. doi:10.1002/smll.201002198.

[162] J.C. Kearns, R.L. Shambaugh, Polypropylene fibers reinforced with carbon nanotubes, J. Appl. Polym. Sci. 86 (2002) 2079–2084. doi:10.1002/app.11160.

[163] J.K.. Sandler, S. Pegel, M. Cadek, F. Gojny, M. van Es, J. Lohmar, W.. Blau, K. Schulte, A.. Windle, M.S.. Shaffer, A comparative study of melt spun polyamide-12 fibres reinforced with carbon nanotubes and nanofibres, Polymer. 45 (2004) 2001–2015. doi:10.1016/j.polymer.2004.01.023.

[164] E.M. Moore, D.L. Ortiz, V.T. Marla, R.L. Shambaugh, B.P. Grady, Enhancing the strength of polypropylene fibers with carbon nanotubes, J. Appl. Polym. Sci. 93 (2004) 2926–2933. doi:10.1002/app.20703.

[165] X. Zhang, T. Liu, T.V. Sreekumar, S. Kumar, V.C. Moore, R.H. Hauge, R.E. Smalley, Poly(vinyl alcohol)/SWNT composite film, Nano Lett. 3 (2003) 1285–1288. doi:10.1021/nl034336t.

[166] J.N. Coleman, M. Cadek, R. Blake, V. Nicolosi, K.P. Ryan, C. Belton, A. Fonseca, J.B. Nagy, Y.K. Gun'ko, W.J. Blau, High performance nanotube-reinforced plastics: understanding the mechanism of strength increase, Adv. Funct. Mater. 14 (2004) 791–798. doi:10.1002/adfm.200305200.

[167] K.P. Ryan, M. Cadek, V. Nicolosi, S. Walker, M. Ruether, A. Fonseca, J.B. Nagy, W.J. Blau, J.N. Coleman, Multiwalled carbon nanotube nucleated crystallization and reinforcement in poly(vinyl alcohol) composites, Synth. Met. 156 (2006) 332–335. doi:10.1016/j.synthmet.2005.12.015.

[168] Z. Wang, P. Ciselli, T. Peijs, The extraordinary reinforcing efficiency of single-walled carbon nanotubes in oriented poly(vinyl alcohol) tapes, Nanotechnology. 18 (2007) 455709. doi:10.1088/0957-4484/18/45/455709.

[169] Y.L. Zhu, Z.J. Du, H. Li, C. Zhang, Preparation and crystallization behavior of multiwalled carbon nanotubes/poly(vinyl alcohol) nanocomposites, Polym. Eng. Sci. 51 (2011) 1770–1779. doi:10.1002/pen.21964.

[170] A.A. Mamedov, N.A. Kotov, M. Prato, D.M. Guldi, J.P. Wicksted, A. Hirsch, Molecular design of strong single-wall carbon nanotube/polyelectrolyte multilayer composites, Nat. Mater. 1 (2002) 190–194. doi:10.1038/nmat747.

[171] P. Podsiadlo, A.K. Kaushik, E.M. Arruda, A.M. Waas, B.S. Shim, J. Xu, H. Nandivada, B.G. Pumplin, J. Lahann, A. Ramamoorthy, N.A. Kotov, Ultrastrong and stiff layered polymer nanocomposites, Science. 318 (2007) 80–83. doi:10.1126/science.1143176.

[172] N.Y. Zhang, J. Xie, V.K. Varadan, Soluble functionalized carbon nanotube/poly(vinyl alcohol) nanocomposite as the electrode for glucose sensing, Smart Mater. Struct. 15 (2006) 123–128. doi:10.1088/0964-1726/15/1/040.

[173] L. Jin, C. Bower, O. Zhou, Alignment of carbon nanotubes in a polymer matrix by mechanical stretching, Appl. Phys. Lett. 73 (1998) 1197. doi:10.1063/1.122125.

[174] M. Huard, F. Roussel, S. Rouzière, S. Patel, M. Pinault, M. Mayne-L'Hermite, P. Launois, Vertically aligned carbon nanotube-based composite: Elaboration and monitoring of the nanotubes alignment, J. Appl. Polym. Sci. 131 (2014) n/a–n/a. doi:10.1002/app.39730.

[175] J.M. Nugent, K.S.V. Santhanam, A. Rubio, P.M. Ajayan, Fast electron transfer kinetics on multiwalled carbon nanotube microbundle electrodes, Nano Lett. 1 (2001) 87–91. doi:10.1021/nl005521z.

[176] L.K. Randeniya, A. Bendavid, P.J. Martin, C.-D. Tran, Composite yarns of multiwalled carbon nanotubes with metallic electrical conductivity, Small. 6 (2010) 1806–1811. doi:10.1002/smll.201000493.

[177] F. Su, X. Lyu, C. Liu, M. Miao, Flexible two-ply yarn supercapacitors based on carbon nanotube/stainless steel core spun yarns decorated with Co3O4 nanoparticles and MnOx composites, Electrochimica Acta. 215 (2016) 535–542. doi:10.1016/j.electacta.2016.08.140.

[178] R. Sen, A. Govindaraj, C.N.R. Rao, Carbon nanotubes by the metallocene route, Chem. Phys. Lett. 267 (1997) 276–280. doi:10.1016/S0009-2614(97)00080-8.

[179] Y. Han, X. Zhang, X. Yu, J. Zhao, S. Li, F. Liu, P. Gao, Y. Zhang, T. Zhao, Q. Li, Bio-inspired aggregation control of carbon nanotubes for ultra-strong composites, Sci. Rep. 5 (2015) 11533. doi:10.1038/srep11533.